

UNIVERSITY OF TOKYO

Simulation of Concrete Cracking Pattern Combining DEF and ASR Expansion

by

YUSHI MENG

A thesis submitted in partial fulfillment for the degree of
Master

Sigiture	Date	Seal
Supervisor		
Co-supervisor		

Faculty of Engineering
Department of Civil Engineering

January 2019

UNIVERSITY OF TOKYO

Abstract

Faculty of Engineering
Department of Civil Engineering

Master

by YUSHI MENG

Nowadays, many concrete structures are exposed to hazardous of expansion, which result in less structural capacity. Meanwhile, as the production process advanced, expansion do occur in those made from some new developed methods, such as high temperature cured precast concrete elements. However, the mechanism and degree of losses strength under various kinds of expansion are still not clear.

Based in the experimental works, it is not easy to understand the behavior due to the delicate influence factors and long term required by the expansion to develop.

This study aims to develop a three dimensional numerical simulation system of concrete expansion, caused by ASR and DEF, for searching the trend in their cracking patterns, and strength capacity remained.

In this study, the expansion behavior of concrete is simulated base on Rigid Body Spring Model(RBSM). To replicate the process of expansion, initial strain is introduced between elements, then the stress propagate from there, leading into changes in the whole concrete structure. Base on the previous study done by REVISE: ADD MORE PREVIOUS STUDY HERE, the ASR and DEF expansion behavior are able to be simulated by the RBSM method, though the details are still required to be improved. New method of strain distribution are introduced into DEF and ASR simulation to improve the similarities in structural behavior with experimental results.

Also, the changing in mechanical properties are also under discussed, which have not be done before. After the expansion behavior is well simulated, its loss in mechanical properties are are also able to be simulated. This gives us a possibility to connect our research the actual deterioration problems on site, for analysis their capability, prediction of structures further usage suffering from expansion.

Further more, in the future, hopefully more features of concrete behavior would be introduced into the system, along with improvement in accuracy by considering more details into the local expansion mechanisms, the simulation of concrete behavior under expansion could finally lead us to undamaged analysis for concrete structures for their residual capacity, life span, and safety factor of serving under different conditions.

Acknowledgements

I would like to express my very great appreciation to Susan Bones for the ...

I would also like to offer my special thanks to Cedric Diggory for...

My special thanks are extended to the staff of the Matron for...

My special thanks goes to Pomona Sprout for taking on this thesis work.

I am particularly grateful for the support and good times given by my friends, for...

To my family, for..., I am particularly grateful.

Advice given by Helga Hufflepuff has been a great help in...

To my beloved Ernie Macmillan for all the...

Contents

Abstract	i
Acknowledgements	iii
List of Figures	vii
List of Tables	xi
Abbreviations	xiii
Physical Constants	xiv
Symbols	xv
1 Introduction	1
1.1 Background and Purpose of Research	2
1.2 Literature Review	3
1.3 Research Objective	8
1.4 Organization of Contents	9
2 Method of Simulation Models	11
2.1 Rigid Body Spring Model (RBSM)	11
2.2 Constitutive Model	15
2.3 Expansion Model	17
2.3.1 ASR Expansion Behavior In Simulation	19
2.3.2 DEF Expansion Behavior In Simulation	20
2.4 Details of Numerical Models for ASR Simulation	21
2.4.1 Geometry of Numerical Models	21
2.4.2 Coarse Aggregate of Numerical Models	22
2.4.3 ASR Reactive Coarse Aggregate Ratio	22
2.4.4 Boundary Conditions	23
2.4.4.1 Boundary Condition During ASR Expansion	23
2.4.4.2 Boundary Conditions During Uni-axial Loading Test	23
2.4.5 Initial Strain Given For ASR Expansion	23
2.5 Details of Numerical Models for DEF Simulation	24
2.5.1 Introduction	24

2.5.2	Geometry of Numerical Models	24
2.5.3	Coarse Aggregate of Numerical Models	25
2.5.4	DEF Intensified Expansion Area of Numerical Models	25
2.5.5	Boundary Conditions	26
2.5.5.1	Boundary Condition During DEF Expansion	26
2.5.5.2	Boundary Conditions During Uni-axial Loading Test	26
2.6	Conclusions	26
3	Simulation of Cracking Pattern Of ASR and DEF Expanded Concrete	28
3.1	General	28
3.2	Cracking Pattern caused by Pure ASR Expansion	29
3.2.1	Single ASR Expansion Simulation	29
3.2.2	Expansion Ratio Related to Behavior of Concrete During ASR Expansion	34
3.2.3	Aggregate Ratio Related to Behavior of Concrete During ASR Expansion	39
3.2.4	Reactive Aggregate Ratio Related to Behavior of Concrete During ASR Expansion	45
3.3	Cracking Pattern caused by Pure DEF Expansion	51
3.3.1	Single DEF Expansion Simulation	51
3.3.2	Expansion Ratio Related to Behavior of Concrete During DEF Expansion	56
3.3.3	Aggregate Ratio Related to Behavior of Concrete During DEF Expansion	62
3.3.4	Expansion Intensified Part Range Related to Behavior of Concrete During DEF Expansion	69
3.3.4.1	Expansion Intensified 75x75x75mm at Center of Model	69
3.3.4.2	Expansion Intensified 100x100X100mm at Center of Model	70
3.4	Comparing Between ASR Expansion and DEF Expansion Simulation Result	78
4	Simulation of Residual Mechanical Capabilities Of ASR and DEF Expanded Concrete	81
4.1	General	81
4.1.1	Overview of Experimental Results of Residual Mechanical Properties After ASR Expansion	83
4.1.2	Overview of Experimental Results of Residual Mechanical Properties After DEF Expansion	83
4.2	Residual Capabilities after Pure ASR Expansion	84
4.3	Residual Capabilities after Pure DEF Expansion	88
4.3.1	Result And Discussion	90
4.4	Residual Capabilities after Combination of ASR and DEF Expansion	91
4.5	Conclusion	91
5	Summary and Conclusions	93
A	ASR-A30-P25	94

B ASR-A30-P75	98
C ASR-A15-P75	103
D DEF-A30-X-1C	107
E DEF-A30-X-5C	111
F DEF-A30-X0C	115
G DEF-A30-X0D	119
H DEF-A15-X0C	123

List of Figures

1.1	Fractured stirrups in ASR-affected bridge piers in Japan [Miyagawa, et al. 2006, Torii, et al. 2008].	2
1.2	Premature cracking of sleepers in Indian Railways[A. Awasthi, 2016].	2
1.3	Results of field measurement of temperature of sleepers during curing process in Indian Railways[A. Awasthi, 2016].	3
1.4	Elastic modulus and compressive strength results for ASR cylinders. [E.R.Giannini, 2012].	4
1.5	Elastic modulus and compressive strength results for DEF cylinders. [E.R.Giannini, 2012].	5
1.6	Crack pattern of horizontally cast concrete prismcontaining Thames Valley sand (mix A) and 15% fused silica (mix B) [Ahmed et al., 2003].	5
1.7	Premature cracking of sleepers in Indian Railways[A. Awasthi, 2016].	6
1.8	Temperature measurement for pre-heating process of Indian Concrete Sleeper [A. Awasthi, 2016].	6
1.9	3D Concrete Model (units: mm) [L.EDDY et al.]	7
1.10	Surface Cracks (Deformation x 10) [L.EDDY et al.]	7
2.1	Rigid Body Spring Model	11
2.2	Constitutive models of concrete	16
2.3	Flow Diagram of Simulation of Expansion Through RBSM	18
2.4	Points Selected For Calculation One-dimensional Expansion	19
2.5	Characteristic Map Cracking Pattern of ASR bu RBSM Simulation, L.EDDY et al. (2016)	19
2.6	Result of Temperature Measurement, A.AWASTHI 2016	20
2.7	Section View of DEF Damaged Concrete Sleeper, A.AWASTHI 2016	21
2.8	50x50x50mm DEF intensified part range	21
2.9	Numerical Model for Expanding Simulation	22
2.10	Coarse Aggregate Percentage	22
2.11	25% and 75% ASR Reactive Aggregate Ratio Model	22
2.12	Top and Bottom Boundary in Loading	23
2.13	DEF intensified part range	25
2.14	Top and Bottom Boundary in Loading	26
3.1	30% Coarse Aggregate	29
3.2	Global Expansion vs. Step	30
3.3	3D Surface Cracks, 0.4223% Expansion (Deformation x 10)	31
3.4	Internal Stress in Each Step for A30 P75 Case 3 (Deformation x 10)	32
3.5	3D Inner Cracking larger than 0.03mm	33

3.6 30% Coarse Aggregate	34
3.7 3D Surface Cracks (Deformation x 10)	35
3.8 3D Surface Cracks (Single Side View, Deformation x 10)	36
3.9 3D Inner Crack Width Larger than 0.03mm	37
3.10 Generation of Internal Stress and Inner Cracks for ASR Expansion to Step 20(Final Expansion Step, Deformation x 10)	38
3.11 Coarse Aggregate Percentage	39
3.12 3D Surface Cracks (Deformation x 10)	40
3.13 3D Surface Cracks (Single Side View, Deformation x 10)	41
3.14 Comparing Between A15 and A30 3D Surface Cracks (Deformation x 10)	42
3.15 3D Inner Crack Width Larger than 0.03mm	43
3.16 Comparing Between A15 and A30 3D Surface Cracks (Deformation x 10)	44
3.17 25% and 75% ASR Reactive Aggregate Ratio Model	45
3.18 3D Surface Cracks (Deformation x 10)	46
3.19 3D Surface Cracks (Single Side View, Deformation x 10)	47
3.20 3D Inner Cracks	48
3.21 Comparing Between A30P25 and A30P75 3D Surface Cracks (Deformation x 10)	49
3.22 Comparing Between A30P25 and A30P75 3D Surface Cracks (Deformation x 10)	49
3.23 DEF intensified part range	51
3.24 50x50x50mm DEF intensified part range	52
3.25 30% Coarse Aggregate	52
3.26 Global Expansion vs. Step	53
3.27 3D Surface Cracks, 0.4223% Expansion (Deformation x 10)	53
3.28 3D Inner Cracks, 0.4223% Expansion	54
3.29 Internal Stress in Each Step for A30 X0C Case 3 (Deformation x 10)	55
3.30 30% Coarse Aggregate	56
3.31 Global Expansion vs. Step	57
3.32 3D Surface Cracks (Deformation x 10)	58
3.33 3D Surface Cracks (Single Side View, Deformation x 10)	59
3.34 3D Inner Cracks Larger than 0.03mm	60
3.35 Generation of Internal Stress and Inner Cracks for DEF Expansion to Step 20(Final Expansion Step, Deformation x 10)	61
3.36 Coarse Aggregate Percentage	62
3.37 Global Expansion vs. Step	63
3.38 3D Surface Cracks	64
3.39 3D Surface Cracks (Single Side View)	65
3.40 3D Inner Cracks Larger than 0.03mm	66
3.41 Comparing Between A15 and A30 3D Cracks	67
3.42 DEF intensified part range	69
3.43 Global Expansion vs. Step	69
3.44 3D Surface Cracks Expansion Intensified 75x75x75mm (Deformation x 10)	70
3.45 3D Surface Cracks (Single Side View) Expansion Intensified 75x75x75mm (Deformation x 10)	71
3.46 3D Inner Cracks Expansion Intensified 75x75x75mm	72
3.47 Global Expansion vs. Step	73

3.48	3D Surface Cracks Expansion Intensified 100x100X100mm (Deformation x 10)	74
3.49	3D Surface Cracks (Single Side View) Expansion Intensified 100x100X100mm (Deformation x 10)	75
3.50	3D Inner Cracks Expansion Intensified 100x100X100mm (Deformation x 10)	76
3.51	Comparing between different DEF Expansion Intensified Cases	77
3.52	Model for DEF Expansion	78
3.53	Cracks Compare Between ASR Expansion and DEF Expansion Simulation Result	79
3.54	Cross Section Compare Between ASR Expansion and DEF Expansion Simulation Result (Deformation x 10)	80
4.1	30% Coarse Aggregate	81
4.2	ASR Loading	82
4.3	DEF Loading	83
4.4	30% Coarse Aggregate	84
4.5	A30 P75 Fix Load-Displacement	84
4.6	A30 P75 Free Load-Displacement	85
4.7	30% Coarse Aggregate	85
4.8	A30 P25 Fix Load-Displacement	86
4.9	15% Coarse Aggregate	86
4.10	A15 P75 Fix Load-Displacement	87
4.11	A30 I50 Fix Load-Displacement	88
4.12	A30 I75 Fix Load-Displacement	88
4.13	A15 I50 Fix Load-Displacement	89
4.14	A15 I50 Fix Load-Displacement	89
4.15	Residual Compressive Strength vs. Total Number of Cracks	90
4.16	Residual Compressive Strength vs. Total Number of Cracks over 0.0005mm	91
4.17	Cracking Pattern Compare	92
A.1	Generation of Internal Stress for Expansion to Step 20(Final Expansion Step)	95
A.2	LOAD-DISPLACEMENT(Fix Boundary Condition)	96
A.3	LOAD-DISPLACEMENT(Fix Boundary Condition)	96
A.4	3D Surface Cracking Pattern	97
B.1	Generation of Internal Stress for Expansion to Step 20(Final Expansion Step)	99
B.2	LOAD-DISPLACEMENT(Fix Boundary Condition)	100
B.3	LOAD-DISPLACEMENT(Free Boundary Condition)	100
B.4	LOAD-DISPLACEMENT(Fix Boundary Condition)	101
B.5	3D Surface Cracking Pattern	102
C.1	Generation of Internal Stress for Expansion to Step 20(Final Expansion Step)	104
C.2	LOAD-DISPLACEMENT(Fix Boundary Condition)	105
C.3	3D Surface Cracking Pattern	106

D.1	Generation of Internal Stress for Expansion to Step 20(Final Expansion Step)	108
D.2	LOAD-DISPLACEMENT(Fix Boundary Condition)	109
D.3	LOAD-DISPLACEMENT(Fix Boundary Condition)	109
D.4	3D Surface Cracking Pattern	110
E.1	Generation of Internal Stress for Expansion to Step 20(Final Expansion Step)	112
E.2	LOAD-DISPLACEMENT(Fix Boundary Condition)	113
E.3	LOAD-DISPLACEMENT(Fix Boundary Condition)	113
E.4	3D Surface Cracking Pattern	114
F.1	Generation of Internal Stress for Expansion to Step 20(Final Expansion Step)	116
F.2	LOAD-DISPLACEMENT(Fix Boundary Condition)	117
F.3	LOAD-DISPLACEMENT(Fix Boundary Condition)	117
F.4	3D Surface Cracking Pattern	118
G.1	Generation of Internal Stress for Expansion to Step 20(Final Expansion Step)	120
G.2	LOAD-DISPLACEMENT(Fix Boundary Condition)	121
G.3	LOAD-DISPLACEMENT(Fix Boundary Condition)	121
G.4	3D Surface Cracking Pattern	122
H.1	Generation of Internal Stress for Expansion to Step 20(Final Expansion Step)	124
H.2	LOAD-DISPLACEMENT(Fix Boundary Condition)	125

List of Tables

1.1	Effect of ASR expansion on compressive strength of concrete [Ahmed et al., 2003].	5
2.1	ASR Models	24
2.2	DEF Intensified Expansion Area	25
3.1	Expansion in Each Step for A30 P75 Case 3	30
3.2	Crack Summarised by width	31
3.3	One Dimensional Expansion Ratio in Single ASR Model Simulation . . .	34
3.4	One Dimensional Expansion Ratio in Single ASR Model Simulation . . .	40
3.5	Expansion in Each Step for A15P75 Case 3 and A30 P75 Case 3	43
3.6	One Dimensional Expansion Ratio in A30P25 and A30P25 ASR Expansion Simulation	45
3.7	Comparing Between A30P25 and A30P25 3D Surface Cracks	48
3.8	Expansion in Each Step for A30 Case 3	52
3.9	Expansion in Each Step for A30 X0C Case 3	54
3.10	One Dimensional Expansion Ratio in Single DEF Model Simulation . . .	56
3.11	One Dimensional Expansion Ratio in Single DEF Model Simulation . . .	62
3.12	Expansion in Each Step for A15P75 Case 3 and A30 P75 Case 3	68
3.13	One Dimensional Expansion Ratio in Expansion Intensified 75x75x75mm at Center of Model DEF Model Simulation	69
3.14	One Dimensional Expansion Ratio in Expansion Intensified 100x100X100mm at Center of Model DEF Model Simulation	70
3.15	Expansion in Each Step for A30 P75 Case 3	80
4.1	One Dimensional Expansion Ratio in Single ASR Model Simulation . . .	84
4.2	One Dimensional Expansion Ratio in Single ASR Model Simulation . . .	91
A.1	Number of Cracked Faces in Different Crack Width	94
B.1	Number of Cracked Faces in Different Crack Width	98
C.1	Number of Cracked Faces in Different Crack Width	103
D.1	Number of Cracked Faces in Different Crack Width	107
E.1	Number of Cracked Faces in Different Crack Width	111
F.1	Number of Cracked Faces in Different Crack Width	115
G.1	Number of Cracked Faces in Different Crack Width	119

H.1 Number of Cracked Faces in Different Crack Width	123
--	-----

Abbreviations

LAH List Abbreviations Here

OWL Ordinary Wizarding Level

Physical Constants

Speed of Light c = $2.997\ 924\ 58 \times 10^8$ ms⁻¹ (exact)

Symbols

a	distance	m
P	power	W (Js ⁻¹)
ω	angular frequency	rads ⁻¹

For/Dedicated to/To my...

Chapter 1

Introduction

Concrete, as one of the oldest and most important structural materials, has been used since ancient Romans times.

The reason why concrete is so widespread is that it is the most suitable material for construction. With its outstanding resistance to compression forces, such a workable and durable material can be formed into variety of shapes and sizes. In addition, concrete also easy to obtain and economically suitable for structure in the largest scale.

The meaning of concrete is “to grow together” which has Latin origin

[Mindess, 1981; Skalny, 1989].

However, concrete structures do suffering from many kinds of deterioration. Those are including freezing and thawing, wetting and drying, temperature changes, wear and abrasion, leaching and efflorescence, sulphate attack, alkali-aggregate reaction, acids and alkali attack, and many other process.

Among so many process of deterioration, Alkali-silica reaction (ASR) and Delayed Ettringite Formation (DEF) are two very common and important deterioration processes seen on concrete structures.

These two processes causes rising in internal pressure, which triggering cracks in concrete structure, has serious effects on the mechanical properties of concrete such as compressive, flexural strength, splitting tension, pullout resistance, and modulus of elasticity in addition to durability of concrete.

1.1 Background and Purpose of Research

Both ASR and DEF has harmful effects on mechanical properties of concrete structure is an apparent issue after many investigations.

Alkali-silica reaction (ASR) and delayed ettringite formation (DEF) are expansive reactions that can lead to the premature deterioration of concrete structures, both have been implicated in the deterioration of numerous structures around the world, including many transportation structures in Japan.

In Japan, deterioration of ASR-affected structures has attracted significant attention. At least 30 cases of fractured bars have been discovered in structures also damaged by ASR (Mikata, et al. 2012). Webb (2011) provides a more extensive review of the rebar fracture problem in Japan and conducted an investigation into the possibility of fracture with steel grades and reinforcement detailing used in the United States.



FIGURE 1.1: Fractured stirrups in ASR-affected bridge piers in Japan [Miyagawa, et al. 2006, Torii, et al. 2008].

Investigation done by A. Awasthi reveals large ettringite deposition in the damaged sleepers of Indian Railways.



FIGURE 1.2: Premature cracking of sleepers in Indian Railways[A. Awasthi, 2016].

The problem of pre-mature cracking is investigated by collecting extensive samples from Indian Railways, studying the manufacturing processes, measured temperature inside

concrete sleepers in the set up of a concrete sleeper plant, and analyzing samples using SEM (Scanning Electron Microscope), EDS (Energy-dispersive X-ray Spectroscopy) and XRF (X-ray Fluorescence).

In this research, EDS analysis confirmed the composition of DEF. Also, field measurement of temperature reveals that sleepers experiences high early age temperature ($\geq 80^{\circ}\text{C}$), which is very critical for DEF problem to occur in future.

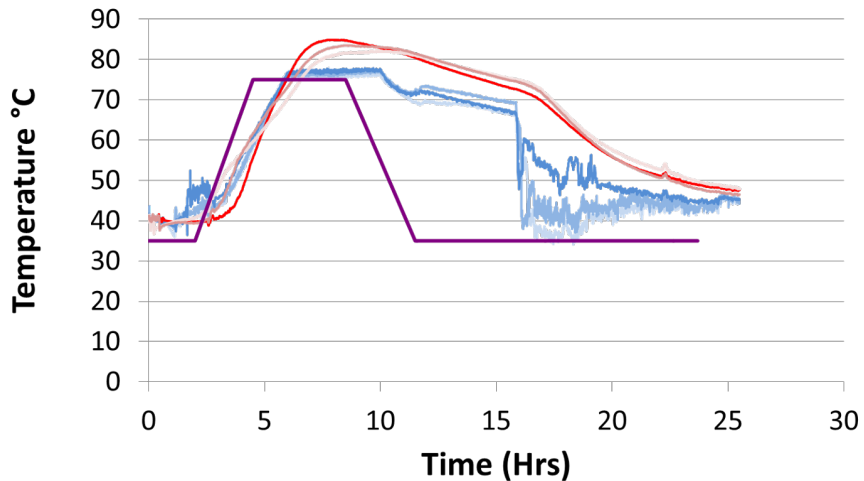


FIGURE 1.3: Results of field measurement of temperature of sleepers during curing process in Indian Railways[A. Awasthi, 2016].

Besides, in many cases, DEF has been accompanied by ASR, and may have been triggered in part by ASR (Folliard et al. 2006).

As a result of considerable research advances, ASR and DEF are now avoidable in new construction, but evaluating and managing the existing stock of structures damaged by these mechanisms remains a challenge.

Therefore, investigating how expansion from ASR and/or DEF affects on mechanical properties of concrete was the principal aim of this study.

In order to reach various expansion result, combinations such as different aggregate volume and different reactive aggregate were tried out by using concrete cube, 100x100x100 mm in size. By expanding the concrete model from 0.? to 1.? percent, the relationship between mechanical properties losses and expansion can also be analyzed.

1.2 Literature Review

- **Evaluation of Concrete Structures Affected by Alkali-Silica Reaction and Delayed Ettringite Formation, E.R.Giannini, 2012**

Four primary types of exposure site specimens were fabricated for this study, including Block, Unreinforced Slab-on grade, Reinforced Column, and Reinforced Bridge Deck.

Aggregate in different level of reactivity are used for the exposure site specimens. Portland cements with high alkali contents were “boosted” with 50% w/w NaOH solution to ensure that all specimens would undergo significant expansions within the time constraints of the project.

		Jobe (F1)						Placitas (C10)						
		Expansion Level (%)						Expansion Level (%)						
		0.009	0.109	0.181	0.272	0.379	0.416	0.429	0.010	0.045	0.074	0.135	0.160	0.177
E (GPa)*	Cyl 1	27.9	20.0	17.6	13.4	13.0	15.8	n/a	29.5	26.3	24.3	23.5	21.8	22.6
	Cyl 2	29.2	21.2	19.3	15.5	12.4	16.7	16.6	30.3	25.6	23.9	22.7	23.1	25.8
	Cyl 3	30.2	19.0	16.6	15.7	13.8	15.4	17.5	29.0	25.2	25.6	25.6	23.0	23.4
	Average	29.1	20.1	17.9	14.9	13.1	16.0	17.1	29.6	25.7	24.6	23.9	22.6	23.9
	Var %	7.9	11.0	15.2	15.4	11.3	7.8	5.3	4.5	4.3	7.2	12.1	5.7	13.4
f'_c (MPa)*	Cyl 1	33.0	35.2	32.2	30.1	28.7	28.9	n/a	35.4	36.0	35.3	39.9	42.2	40.5
	Cyl 2	33.8	34.6	34.8	30.4	29.3	29.6	30.0	36.8	37.2	41.5	39.2	41.0	44.1
	Cyl 3	34.9	36.3	32.8	31.1	28.7	29.6	29.8	35.4	36.7	37.1	40.0	41.5	41.5
	Average	33.9	35.4	33.3	30.6	28.9	29.4	29.9	35.9	36.6	37.9	39.7	41.6	42.0
	Var %	5.4	4.6	7.9	3.3	2.1	2.3	0.7	3.9	3.2	16.4	1.9	2.9	8.6
E, % of predicted by f'_c		105.6	71.3	65.4	56.9	51.3	62.3	66.0	104.5	89.7	84.5	80.1	74.1	78.0

* 1 GPa = 145 ksi; 1 MPa = 145 psi

FIGURE 1.4: Elastic modulus and compressive strength results for ASR cylinders.
[E.R.Giannini, 2012].

Additional procedures were involved to encourage the development of DEF. The cement and aggregates were heated in sealed buckets to 60°C before mixing, while the mixing water was heated to 38°C. The fresh concrete was quickly transported to a 60°C chamber, placed and consolidated in foam-insulated wood forms. The forms were then covered in heavy blankets to minimize heat loss. After twelve hours, the heater for the chamber was turned off. The chamber was opened and the specimen allowed to slowly cool to ambient temperatures. Thermocouples recorded the temperature in the top, middle and base of the specimen. Peak curing temperature were well above the threshold necessary for the development of DEF.

- **The Effect Of Alkali Reactivity On the Mechanical Properties Of Concrete, T. Ahmed et al, 2013**

In this study, T. Ahmed et al. used Thames Valley sand (in Mix A), fused silica (in Mix B) and slowly reactive aggregate (in Mix C) to investigate the effect of ASR expansion on compressive strength of concrete. Specimens in 100x100x100 size were cast and cured with respect to BS 1881 Part 122 [BS, 1881]. After casting and moulding, the cube specimens were cured for 28 days in water at 20°C and then the temperature was increased to 38°C to accelerate alkali-silica reaction. In this temperature, the specimens were stored at water tank until 12 months passed [Ahmed et al., 2003]. After 28-days curing at 20°C and storage at 38°C for 12

		Jobe (F1)							Placitas (C10)						
		Expansion Level (%)							Expansion Level (%)						
		0.000	0.102	0.208	0.344	0.415	0.506	1.011	0.008	0.079	0.179	0.266	0.327	0.454	
E (GPa)*	Cyl 1	22.6	24.4	20.0	8.5	8.4	6.3	6.3	23.1	20.4	16.2	13.4	19.6	8.7	
	Cyl 2	24.6	18.8	10.8	9.1	5.7	7.2	4.6	23.8	21.6	17.5	15.5	20.7	9.5	
	Cyl 3	22.2	16.9	13.5	6.9	8.5	6.6	6.6	23.8	18.4	20.1	19.7	15.5	10.6	
	Average	23.1	20.0	14.8	8.2	7.5	6.7	5.8	23.6	20.1	17.9	16.2	18.6	9.6	
	Var %	10.1	37.3	62.5	26.5	37.1	12.4	34.8	3.1	15.9	21.8	38.6	28.0	19.1	
f'_c (MPa)*	Cyl 1	27.6	33.2	30.7	20.2	20.5	19.1	16.9	32.9	31.9	33.4	28.9	32.7	27.3	
	Cyl 2	27.6	26.1	23.1	20.4	16.5	18.2	14.3	33.9	33.7	30.9	30.4	35.6	25.0	
	Cyl 3	26.9	25.9	24.8	18.4	19.3	17.7	16.6	32.2	33.1	33.0	28.7	30.4	23.1	
	Average	27.3	28.4	26.2	19.7	18.7	18.3	16.0	33.0	32.9	32.5	29.3	32.9	25.2	
	Var %	2.5	25.5	29.2	10.5	21.4	7.9	16.4	5.3	5.4	7.6	5.6	15.9	16.7	
E, % of predicted by f'_c		93.4	79.2	60.3	39.0	36.5	33.1	30.5	86.8	74.2	66.6	63.3	68.3	40.5	

* 1 GPa = 145 ksi; 1 MPa = 145 psi

FIGURE 1.5: Elastic modulus and compressive strength results for DEF cylinders. [E.R.Giannini, 2012].

months, surface cracks are observed (Figure 1.6), and the expansion ratios along with compressive strength are given in Table 1.1.



FIGURE 1.6: Crack pattern of horizontally cast concrete prism containing Thames Valley sand (mix A) and 15% fused silica (mix B) [Ahmed et al., 2003].

Mix	A	B	C
Expansion ratio (mm/mm) for 28-days curing at 20°C	-0.4	0.96	0.05
Compressive Strength (N/mm^2) for 28-days curing at 20°C	50.3	41.0	46.8
Expansion ratio (mm/mm) for 12 months curing at 38°C	4.3	16.86	1.27
Compressive Strength (N/mm^2) for 12 months curing at 38°C	57.0	26.5	65.3

TABLE 1.1: Effect of ASR expansion on compressive strength of concrete [Ahmed et al., 2003].

- Investigation of Premature Cracking of Sleepers in Indian Railways & Evaluation of It's Residual Capacity, A. AWASTHI et al, 2016

In this study, A. Awasthi investigated the damaged premature cracking of sleepers, using the Scanning Electron Microscope (SEM) and Energy-Dispersive X-Ray Spectroscopy(EDS), confirmed the existing of DEF phenomenal in damaged concrete sleepers.



FIGURE 1.7: Premature cracking of sleepers in Indian Railways[A. Awasthi, 2016].

The pre-heating process done on these concrete sleepers in order to achieve a high early strength (in case of Indian concrete sleepers the steam curing temperature is 75 °C) and subsequent exposure to moisture during service lead the formation of delayed ettringite. Temperature measurement was performed in concrete sleeper plant in India both inside and outside of concrete reveals that temperature inside the concrete sleeper is much higher than the outer part, the high temperature over 80°C is a very critical factor for the occurrence of damage due to DEF.



FIGURE 1.8: Temperature measurement for pre-heating process of Indian Concrete Sleeper [A. Awasthi, 2016].

- Mesoscopic analysis of different expansion causes in concrete by 3D Rigid Body Spring Model, L. EDDY, A. AWASTHI, K, MATSUMOTO, K. NAGAI, and S.ASAMOTO, 2017

This study developed the 3 dimensional numerical discrete analysis model using RBSM for mesoscopic analysis of different expansion, including both ASR expansion and DEF expansion.

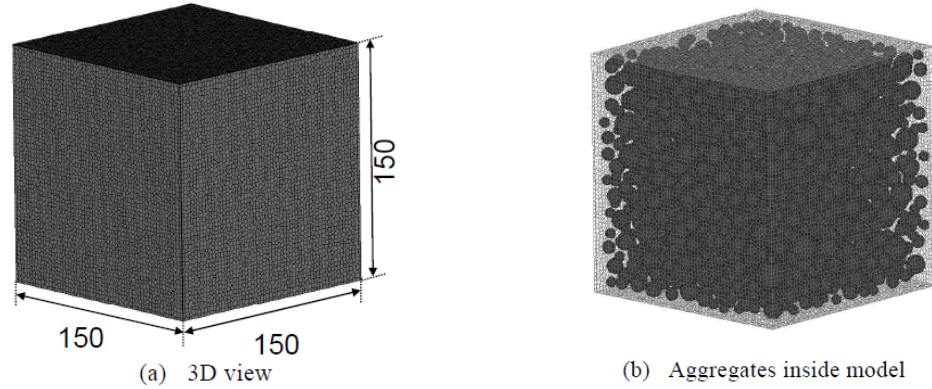


FIGURE 1.9: 3D Concrete Model (units: mm) [L.EDDY et al.]

Fig 1.9 shows the analyzed numerical model. The size of the model is 150x150x150 mm. Aggregate volume is 26% in this research.

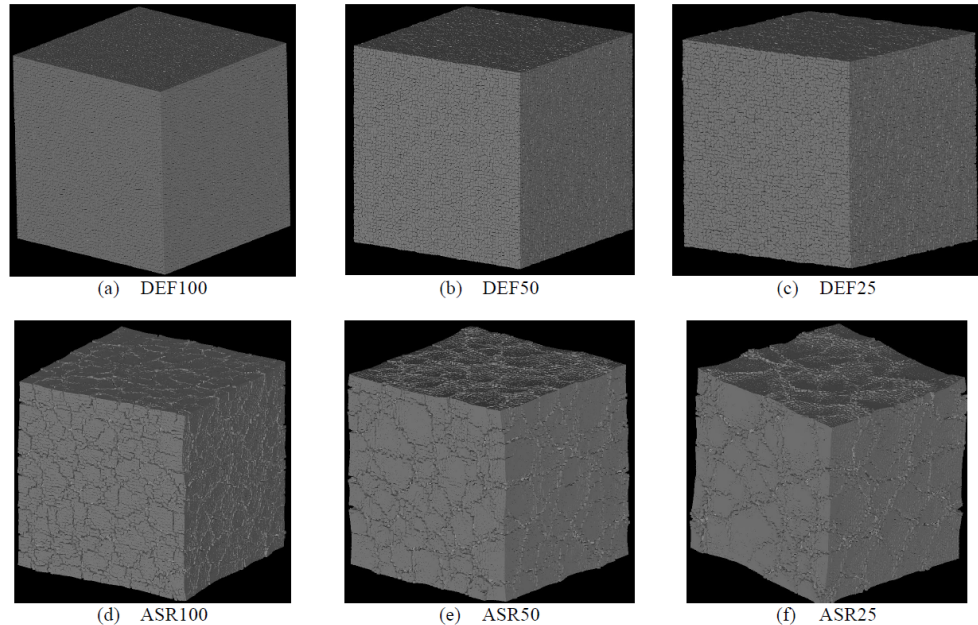


FIGURE 1.10: Surface Cracks (Deformation x 10) [L.EDDY et al.]

In the ASR-type cases, the expansion strain is applied at the mortar-aggregate interfaces to reflect the expansion due to the alkali silicate gel product formed in the aggregates.

Three numerical models, named by ASR100, ASR50, and ASR25 are considered in ASR simulations. ASR100 means that all the mortar-aggregate interfaces expand. ASR50 means that 50% of all springs between mortar-aggregate interfaces

(randomly selected) expand. While ASR25 means that 25% of all springs between mortar-aggregate interfaces (randomly selected) expand.

Stress in the aggregates and mortar decreases because localized cracks in the mortar open. With less percentage of locations of the mortar-aggregate interface expansion, cracks become more localized. These localized cracks in the mortar and the expansion at the mortar-aggregate interfaces are connected to form the map cracks occur in the concrete.

In the cases for DEF-type, the expansion strain is applied in the mortar to represent the paste expansion. However, based on the simulation results, DEF-type cases do not match well with the typical map cracking pattern observed in the real concrete.

Meanwhile, three numerical models, named by DEF100, DEF50, DEF25 are considered in this DEF simulations. DEF100 means that all springs between mortar elements expand. DEF50 means that 50% of all springs between mortar elements (randomly selected) expand. While DEF25 means that 25% of all springs between mortar elements (randomly selected) expand.

E. Liyanto and team proposed that simple model as uniform expansion of paste takes place in DEF could not reproduce the typical cracking pattern of DEF. In order to simulate the DEF appropriately, the simple model in this study needs to be improved because there might be more complex phenomenon occurred.

1.3 Research Objective

The final goal of this research is to develop the simulation system which has ability for revealing the residual capacity of ASR and/or DEF expansion deteriorated structure.

Considering our research group's simulation systems, 3D RBSM was conducted for the quantities evaluation of concrete behavior by directly modeling the shape of aggregates.

Considering the previous study about the expansion of concrete structure in literature review, in order to achieve the final goal, the following objectives are set as the research's goal:

- Develop the simulation of concrete damage from the ASR expansion. Once the ASR expansion occurred, the initial strain will be given at the interfaces between reactive aggregate and mortar. As a result, increasing of tensile stress of concrete around the reactive aggregate will lead to the cracking.
- Develop the simulation of concrete damage from the DEF expansion. Once the DEF expansion occurred, the initial strain will be given at the interfaces between

mortar elements. As a result, increasing of tensile stress of inside concrete paste will lead to the cracking.

- Develop the uni-axial compression test for represent the residual mechanical properties of expanded concrete models. Concrete's behavior under loading and its proprieties such as compressive strength and elastic modulus in macro scale will be obtained.

1.4 Organization of Contents

The development of simulation and mechanical properties test in ASR and/or DEF expanded concrete will be explained in this thesis following structure as shown below:

- Chapter 1 : Introduction.

In this chapter, detailed about research background, statement of problem and objective are explained. Some literature reviews that related to the developing.

- Chapter 2 : Simulation model.

In this chapter, the method in development of each numerical simulation model, related literature review of previous studies, will be described. The development of constitutive model for the expansion will be explained. The method for given expansive strain for simulating the same concrete damage will be explain step by step. The theoretical formulation related in numerical analysis of expanding behaviour are also described in this section.

- Chapter 3: Simulation of Cracking Pattern Of ASR and DEF Expanded Concrete.

In this chapter, details about the surface and cross section cracking pattern results caused by ASR and/or DEF expansion are summarized, comparing between different cases and also with the experimental results.

- Chapter 4: Simulation of Residual Mechanical Capabilities Of ASR and DEF Expanded Concrete.

In this chapter, details about the residual mechanical properties, including residual compressive strength and residual elastic modulus, are summarized. The relationships between residual capacity and expansion behavior due to different expansion causes are also discussed.

- Chapter 5: Conclusions

In this final chapter, several remarks about the capability of ASR and/or DEF expansion simulation are emphasized. Also, some commentaries for further project or improvement are proposed.

Chapter 2

Method of Simulation Models

2.1 Rigid Body Spring Model (RBSM)

The simulations are carried out by the three dimensional RBSM, proposed by Kawai *et al.*(1978). By using 3D RBSM, a concrete model is meshed into rigid bodies, with each consists six degree of freedoms, shown in Figure 2.1.

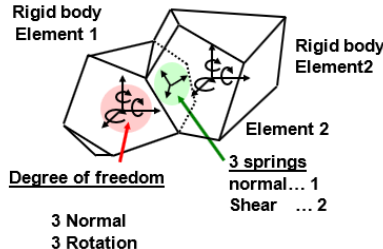


FIGURE 2.1: Rigid Body Spring Model

These six freedoms are three transitional freedoms and three rotational freedoms at the center point within the element.

The computational point (x_c, y_c, z_c) is defined as,

$$\begin{aligned} x_c &= \frac{x_1 + x_2 + \dots + x_i + \dots + x_m}{m} \\ y_c &= \frac{y_1 + y_2 + \dots + y_i + \dots + y_m}{m} \\ z_c &= \frac{z_1 + z_2 + \dots + z_i + \dots + z_m}{m} \end{aligned} \tag{2.1}$$

where m is the number of node composing an element and x_i, y_i and z_i are the coordinates of the nodes in an element.

Three individual springs, which are one normal spring and two shear spring, are set at a point on the face between two elements. This point (x_{cf}, y_{cf}, z_{cf}) is defined as,

$$\begin{aligned} x_{cf} &= \frac{x_1 + x_2 + \cdots + x_j + \cdots + x_n}{n} \\ y_{cf} &= \frac{y_1 + y_2 + \cdots + y_j + \cdots + y_n}{n} \\ z_{cf} &= \frac{z_1 + z_2 + \cdots + z_j + \cdots + z_n}{n} \end{aligned} \quad (2.2)$$

Where m is the number of nodes composing the face and x_j , y_j and z_j are those coordinates.

Since cracks initiate and propagate along the boundary face, the mesh arrangement may affect fracture direction. Random geometry is introduced to avoid the formation of cracks in a certain direction by using a Voronoi diagram **figure**.

In the nonlinear analysis, a stiffness matrix is constructed based on the principle of virtual work (Kawai and Takeuchi 1990), and the Modified Newton-Raphson method is employed for the convergence algorithm.

When an element has small displacement $[u_1, v_1, w_1, \theta_{u1}, \theta_{v1}, \theta_{w1}]$, the springs at a face in an element will be displaced:

$$\begin{aligned} u &= u_1 - \theta_{w1}(y_{cf} - y_{ce1}) + \theta_{v1}(z_{cf} - z_{ce1}) \\ v &= v_1 - \theta_{u1}(z_{cf} - z_{ce1}) + \theta_{w1}(x_{cf} - x_{ce1}) \\ w &= w_1 - \theta_{v1}(x_{cf} - x_{ce1}) + \theta_{u1}(y_{cf} - y_{ce1}) \end{aligned} \quad (2.3)$$

Elongations of normal and shear spring are calculated and expressed as:

$$d = Bu_e \quad (2.4)$$

where $d^T = [\delta_{s1}, \delta_{s2}, \delta_n]$ and $u_e^T = [u_1, v_1, w_1, \theta_{u1}, \theta_{v1}, \theta_{w1}, u_2, v_2, w_2, \theta_{u2}, \theta_{v2}, \theta_{w2}]$

The transformation matrix B is written as:

$$B = \begin{vmatrix} K_{11} & K_{12} & K_{13} & K_{14} & \cdots & K_{19} & K_{110} & K_{111} & K_{112} \\ K_{21} & K_{22} & K_{23} & K_{24} & \cdots & K_{29} & K_{210} & K_{211} & K_{212} \\ K_{31} & K_{32} & K_{33} & K_{34} & \cdots & K_{39} & K_{310} & K_{311} & K_{312} \end{vmatrix} \quad (2.5)$$

where

$$K_{11} = -e_{s1x} \quad K_{21} = -e_{s2x} \quad K_{31} = -e_{nx}$$

$$K_{12} = -e_{s1y} \quad K_{22} = -e_{s1y} \quad K_{32} = -e_{ny}$$

$$K_{13} = -e_{s1z} \quad K_{23} = -e_{s2z} \quad K_{33} = -e_{nz}$$

$$K_{14} = e_{s1y}(z_{cf} - z_{ce1}) - e_{s1z}(y_{cf} - y_{ce1})$$

$$K_{24} = e_{s2y}(z_{cf} - z_{ce1}) - e_{s2z}(y_{cf} - y_{ce1})$$

$$K_{34} = e_{ny}(z_{cf} - z_{ce1}) - e_{nz}(y_{cf} - y_{ce1})$$

$$K_{15} = e_{s1z}(x_{cf} - x_{ce1}) - e_{s1x}(z_{cf} - z_{ce1})$$

$$K_{25} = e_{s2z}(x_{cf} - x_{ce1}) - e_{s2x}(z_{cf} - z_{ce1})$$

$$K_{35} = e_{nz}(x_{cf} - x_{ce1}) - e_{nx}(z_{cf} - z_{ce1})$$

$$K_{15} = e_{s1z}(x_{cf} - x_{ce1}) - e_{s1x}(z_{cf} - z_{ce1})$$

$$K_{25} = e_{s2z}(x_{cf} - x_{ce1}) - e_{s2x}(z_{cf} - z_{ce1})$$

$$K_{35} = e_{nz}(x_{cf} - x_{ce1}) - e_{nx}(z_{cf} - z_{ce1})$$

$$K_{16} = e_{s1x}(y_{cf} - y_{ce1}) - e_{s1y}(x_{cf} - x_{ce1})$$

$$K_{26} = e_{s2x}(y_{cf} - y_{ce1}) - e_{s2y}(x_{cf} - x_{ce1})$$

$$K_{36} = e_{nx}(y_{cf} - y_{ce1}) - e_{ny}(x_{cf} - x_{ce1})$$

$$K_{17} = e_{s1x} \quad K_{27} = e_{s2x} \quad K_{37} = e_{nx}$$

$$K_{18} = e_{s1y} \quad K_{28} = e_{s1y} \quad K_{38} = e_{ny}$$

$$K_{19} = e_{s1z} \quad K_{29} = e_{s2z} \quad K_{39} = e_{nz}$$

$$K_{110} = e_{s1z}(y_{cf} - y_{ce2}) - e_{s1y}(z_{cf} - z_{ce2})$$

$$K_{210} = e_{s2z}(y_{cf} - y_{ce2}) - e_{s2y}(z_{cf} - z_{ce2})$$

$$K_{310} = e_{nz}(y_{cf} - y_{ce2}) - e_{ny}(z_{cf} - z_{ce2})$$

$$K_{111} = e_{s1x}(z_{cf} - z_{ce2}) - e_{s1z}(x_{cf} - x_{ce2})$$

$$K_{211} = e_{s2x}(z_{cf} - z_{ce2}) - e_{s2z}(x_{cf} - x_{ce2})$$

$$K_{311} = e_{nx}(z_{cf} - z_{ce2}) - e_{nz}(x_{cf} - x_{ce2})$$

$$K_{112} = e_{s1y}(x_{cf} - x_{ce2}) - e_{s1x}(y_{cf} - y_{ce2})$$

$$K_{212} = e_{s2y}(x_{cf} - x_{ce2}) - e_{s2x}(y_{cf} - y_{ce2})$$

$$K_{312} = e_{ny}(x_{cf} - x_{ce2}) - e_{nx}(y_{cf} - y_{ce2})$$

where e_{ij} is direction cosine in i axis on j axis.

By applying the principal of virtual work, the local equilibrium relation expressed in global coordinate is:

$$k_e \delta u_e = \delta f_e \quad (2.6)$$

where the stiffness associated with interconnected face k_e is given as:

$$k_e = B^T D B \quad (2.7)$$

where

$$D = \begin{vmatrix} k_{s1} & 0 & 0 \\ 0 & k_{s2} & 0 \\ 0 & 0 & k_3 \end{vmatrix} \quad (2.8)$$

in which k_n , k_{s1} , and k_{s2} are the normal and shear spring stiffness. k_n , k_{s1} , and k_{s2} can be calculated as:

$$\begin{aligned} k_n &= k_{sp} \frac{A}{h_1 + h_2} \\ k_{s1} &= k_{ssp} \frac{A}{h_1 + h_2} \\ k_{s2} &= k_{ssp} \frac{A}{h_1 + h_2} \end{aligned} \quad (2.9)$$

where

$$\begin{aligned} k_{nsp} &= \frac{(1 - \theta_{elem}) E_{elem}}{(1 + \theta_{elem})(1 - 2\theta_{elem})} \\ k_{ssp} &= \frac{E_{elem}}{1 + \theta_{elem}} \end{aligned} \quad (2.10)$$

where h_1 and h_2 are length of perpendicular lines from the element computational point to the face where springs are set.

E_{elem} and ν_{elem} are the modulus of elasticity and poison's ratio, respectively:

$$\begin{aligned} E_{elem} &= \frac{E_{elem1}h_1 + E_{elem2}h_2}{h_1 + h_2} \\ \theta_{elem} &= \frac{\theta_{elem1}h_1 + \theta_{elem2}h_2}{h_1 + h_2} \end{aligned} \quad (2.11)$$

In the convergence process, displacements that cancel the unbalanced force of elements are added to the elements.

The displacements are calculated using the stiffness matrix. Convergence of the model is judged when the ratio of $\sum(\text{Unbalanced force of element in the model})^2$ to $\sum(\text{Applied force to element})^2$ becomes less than 10^5 .

2.2 Constitutive Model

A constitutive model for the concrete part at the mesoscale is used in this research since constitutive model in the macro scale cannot be applied to the mesoscale analysis.

In the analysis, the values of the material properties at the meso level given to the elements are actually different from the material properties where the object is analyzed at the macroscopic scale.

The material properties for the elements were determined to give the correct macroscopic properties. In the discrete analysis done by Nagai et al. in 2005, the shape and fineness of elements do affect the analysis results.

As we concern that the crack direction may affect the crack pattern, size of each concrete elements should be under consideration. Here for small example using 10x10x10mm model, the average diameter of elements is selected to be 0.05mm, while for larger size model in the dimension of 100x100x100mm, the size of each element is approximately 2x2x2mm to 3x3x3mm, almost the size of smallest coarse aggregate introduced. This assumption was made to represent the fracture behavior in concrete in a relatively high fineness and the behavior of both mortar and aggregate can be well presented.

In the elastic analysis, the relationship between macroscopic and mesoscopic Poisson's ratio, the effect of the mesoscopic Poisson's ratio on the macroscopic elastic modulus, are all confirmed by Nagai et al. in 2005, using the same concepts.

$$\begin{aligned}\theta_{elem} &= -24.8\theta^4 + 31.9\theta^3 - 16.4\theta^2 + 4.28\theta \\ E_{elem} &= (-33.7\theta_{elem}^4 + 17.0\theta_{elem}^3 - 4.13\theta_{elem}^2 + 0.327\theta_{elem} + 1)E\end{aligned}\quad (2.12)$$

where E and θ are the macroscopic elastic modulus and Poisson's ratio of the analysis object, respectively.

The material characteristics of each component are presented by means of modeling springs. In normal spring, compressive and tensile stress (σ) are developed. Shear stress(τ) are developed by shear springs.

The elastic modulus of normal sprint(k_{nsp} and k_{ssp}) was presented in the previous chapter. For calculation of shear stress on 3D analysis, a resultant value of strains generated in two shear springs is adopted as shear strain in the constitutive model presented in this chapter. The strains and stress are calculated as follows:

$$\begin{aligned}\varepsilon &= \frac{\delta_n}{h_1 + h_2} \\ \gamma &= \frac{\delta_s}{h_1 + h_2} \\ \sigma &= k_{nsp}\varepsilon \\ \tau &= k_{ssp}\gamma\end{aligned}\quad (2.13)$$

where ε and γ are the strain of normal and shear springs, respectively. δ_n and δ_s are the normal and shear relative displacement of elements of those springs, respectively.

In this study, the constitutive model of the concrete element has been developed based on simulations in material scale level. The constitutive models for the normal and shear springs of the concrete elements are shown in Figure 2.2.

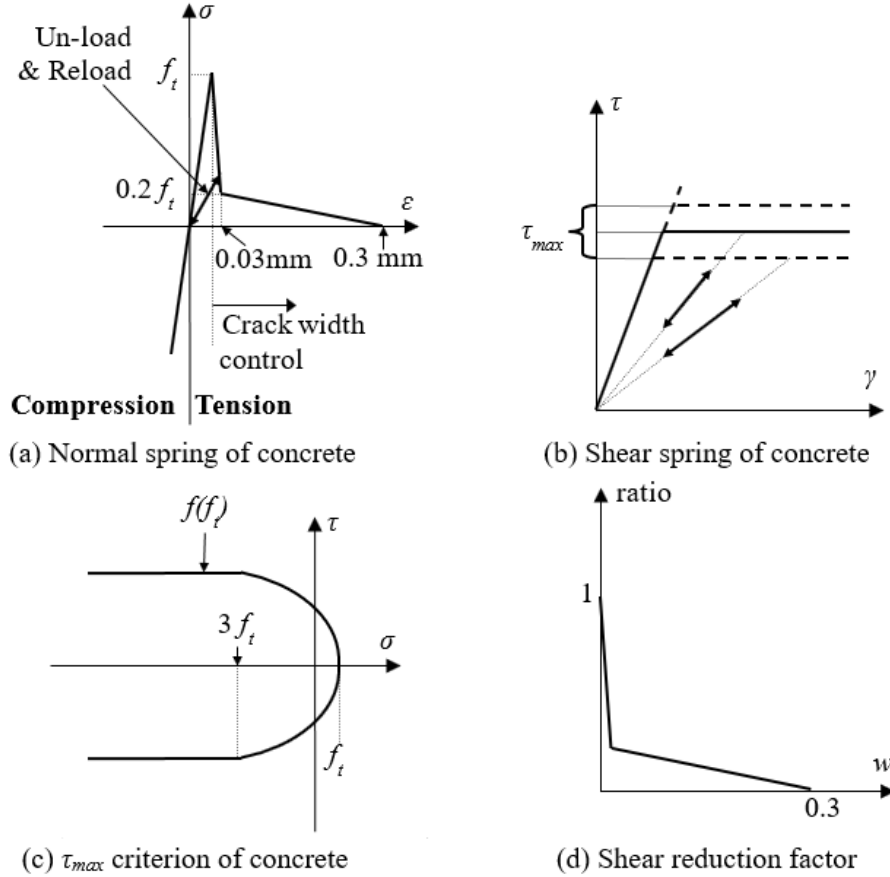


FIGURE 2.2: Constitutive models of concrete

The constitutive models of normal spring and a shear spring of concrete element using in this research are shown in Figure

Basically, the concept of the concrete model is the same as the original simulation development by Nagai et al., 2005, where the compressive failure is not allowed at the

mesoscale. In the tension zone, crack between two rigid bodies occurs only when the tensile stress of the normal spring exceeds the tensile strength of the concrete(f_t). After exceeding the tensile strength(f_t), the tensile stress of a normal spring is assumed to decrease bi-linearly, depending on the crack width, to zero at the maximum crack width(w_{max}), which here is assumed as 0.3mm. An elasto-plastic behavior is also assumed when coming to the shear spring of concrete element with the τ_{max} is calculated based on the following equations:

$$\begin{aligned}\tau_{max} &= \pm(1.6f_{telem}^2(-\sigma + f_{telem})^0.4 + 0.15f_{telem})if(\sigma \geq 3f_{telem}) \\ \tau_{max} &= \pm(1.6f_{telem}^2(-3f_{telem} + f_{telem})^0.4 + 0.15f_{telem})if(\sigma < 3f_{telem})\end{aligned}\quad (2.14)$$

Besides, if fracture occurs in the normal spring, the calculated shear stress will be reduced according to the reduction of the normal stress. As a result, shear spring will now able to carry the stress any longer when the crack width of the normal spring reaches w_{max} .

2.3 Expansion Model

In the expansive behavior of DEF and ASR, the expanse is caused by strains generated from within the concrete when there is no external loading.

One of the similar behavior in previous research is the strength development due to autogenous shrinkage in high strength concrete, which was carried out by Osakabe et al. (2014). The concept of initial strain in RBSM has been successfully utilized in the simulation of the behavior of autogenous shrinkage in high strength concrete.

The same concept of initial strain is utilized in the present of ASR and DEF expanse behavior carried out by L.EDDY et al. in 2016. Characteristic map cracking pattern in ASR simulation was presented successfully, while the DEF simulation results do not match well with the typical map cracking pattern observed in the real concrete.

The concept of the initial strain used in this simulation is based on the case where a specimen expansion occurs without any constraint.

According to 3D RBSM developed by Nagai et al. (2005), the first step is the calculation of actual force, which supposed to be calculated by solving strain, stress and force matrices of all elements in sequence based on input data and boundary condition.

Iteration is then performend until this force under the acceptable limit with an external force. When the convergence condition is reached, the same sequence will be performed for the next step.

In our simulation, one additional step of introducing the initial strain is added here to simulate the behavior of expansion. Then, Stresses due to this initial strain are calculated in the next step, with considering the initial strain added. After the stress is calculated, the initial strain added up earlier will be subtracted, before the forces are calculated.

The illustration of introducing initial strain is shown in the Figure 2.3.

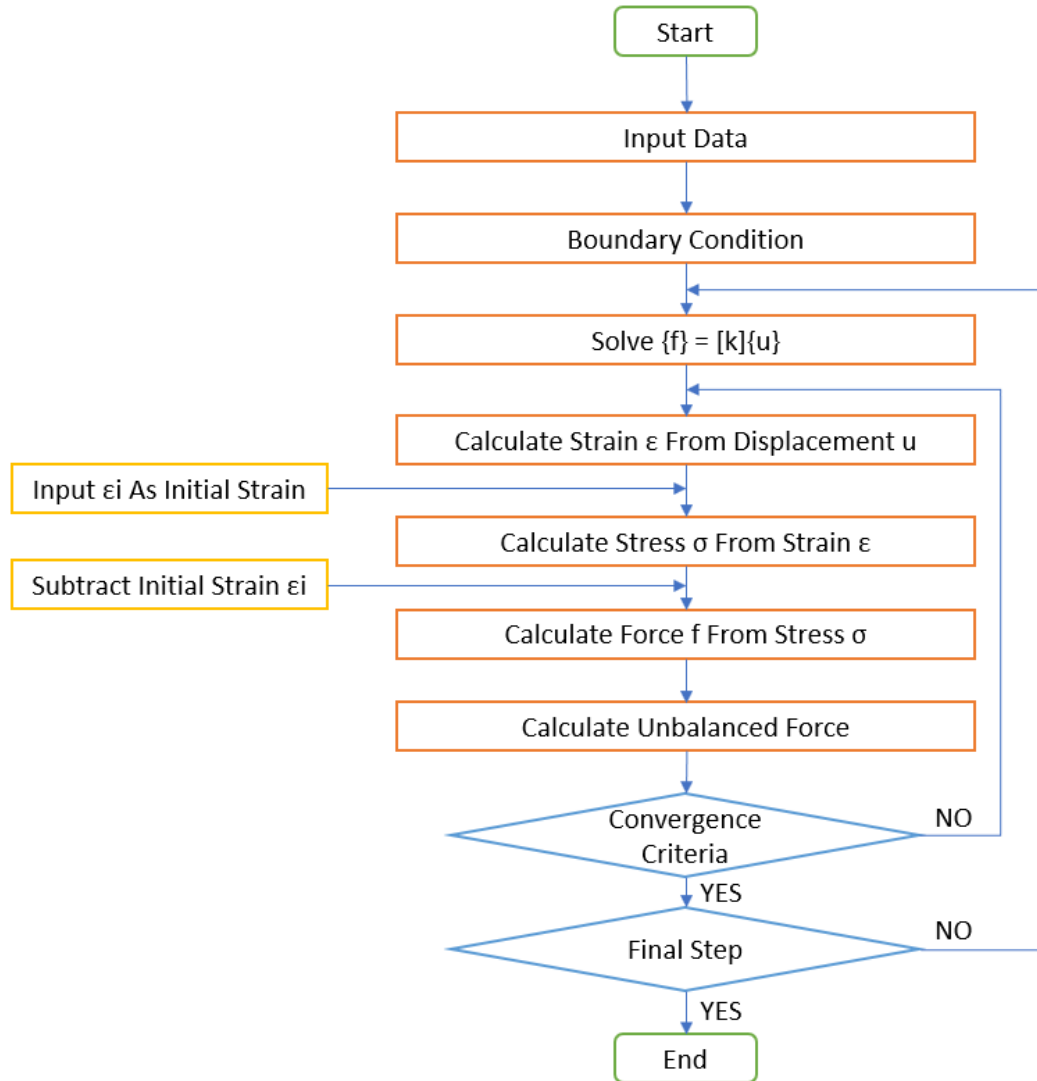


FIGURE 2.3: Flow Diagram of Simulation of Expansion Through RBSM

For ASR and DEF, the initial strains are introduced at different interfaces in concrete.

Expansion is giving to simulative the behavior of model up to 1.3% expansion(in one dimensional).

To calculate the one dimensional expansion, here 2 elements located at center of left and right surface, seperately, are selected, their distant before and after expansion is recorded.

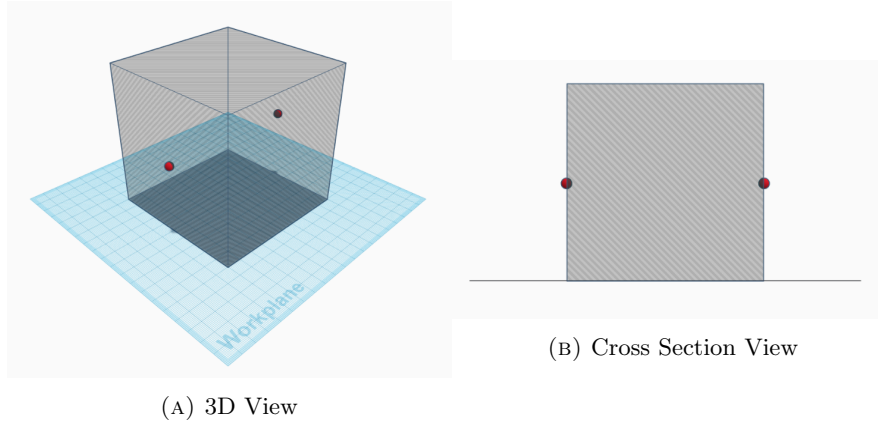


FIGURE 2.4: Points Selected For Calculation One-dimensional Expansion

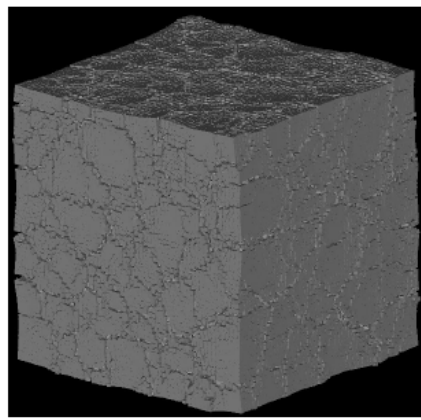


FIGURE 2.5: Characteristic Map Cracking Pattern of ASR bu RBSM Simulation,
L.EDDY et al. (2016)

2.3.1 ASR Expansion Behavior In Simulation

For ASR expansion, the expanse is generated at the location of interfaces between mortar and aggregate. The concept of the initial strain is used here to introduce the expansion.

As we consider the ratio of reactive aggregate may differ the behavior of the model in ASR expansion, cases of different percentage aggregate expanse are simulated and cross-compared. The reactive aggregates are also chosen randomly.

As in the research done by L.EDDY et al. (2016), the desired characteristic map cracking pattern of ASR expansion has already achieved in this method. In this simulation, the discussion is focused on the relationship between cracking pattern with aggregate percentage, reactive aggregate, expanding ratio, also the residual mechanical properties of ASR-damaged concrete.

2.3.2 DEF Expansion Behavior In Simulation

Similar model and mechanism are also applied in the simulation of DEF type expansion. Following the popular theory of expansion in DEF is caused by expansion of paste, initial strain here is given to the interfaces between mortar elements to present the DEF expansion.

According to the previous study done by L.EDDY et al, simple uniformed paste expansion theory need improvement. Whether for cases giving initial strain to 100%, 50% or 25% random faces of mortar chosen to expanse, the surface of expanded concrete does not match with the actual cracking pattern.

It is well established that high early temperature experienced by the concrete is the most important factor inducing DEF in concrete. (Ghorab et al (1980), Ludwig(1987), Sylla(1988), Hanehara & Oyamada(2010), Rasiah and Stephen(2014) etc.)

The research done by Anupam (2016) confirmed the rising of the temperature inside concrete due to combination effect of steam curing and heat of hydration inside the concrete is not uniform. Both the simulation result is done by Astea Macs (FEM based non-linear thermal stress analysis program developed by Research Center of Computational Mechanics, Japan) and the field measurement of temperature rising process inside concrete during steam curing in a concrete plant located in India shows the un-uniformed distribution of maximum temperature experienced. The temperature in the center of the concrete structure is significantly higher than the outer part.

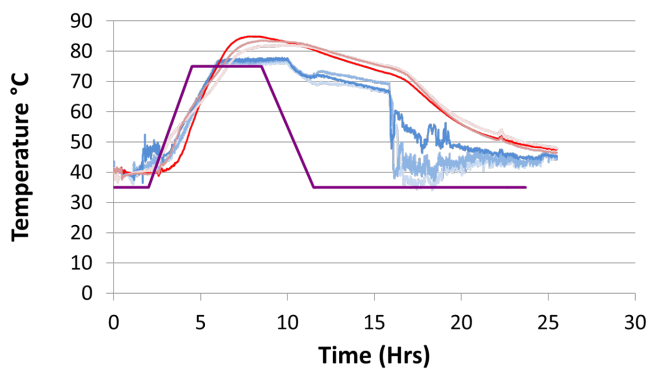


FIGURE 2.6: Result of Temperature Measurement, A.AWASTHI 2016

The cracking pattern in DEF damaged concrete, recorded by Anupam (2016), also suggested the possibility of non-uniformed expansion happens in DEF damaged concrete structure. The cracking concentrated in the outer part of the structure, while the inner part remained undamaged, showing the trend of larger expansion happening in the inner part of the concrete paste.



FIGURE 2.7: Section View of DEF Damaged Concrete Sleeper, A.AWASTHI 2016

Considering the effect of temperature on triggering DEF expansion and its characteristic cracking pattern, for DEF simulation, uniform expansion does not quite fit with the real situation. The expansion inside concrete structure supposes to be much severe than the outer part. For which here in this research non-uniformed expanding is introduced by giving a different amount of DEF initial strain considering the location of element.

The inner part of the model will be giving larger initial strain, present the higher maximum temperature experienced, while the outer part mortar will be giving small or none initial strain.

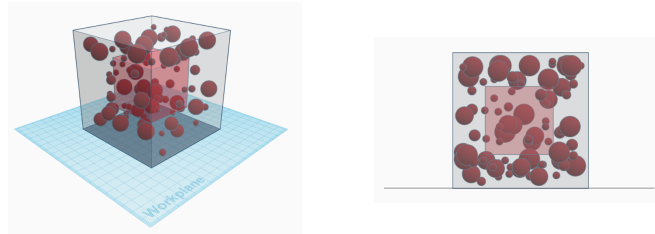
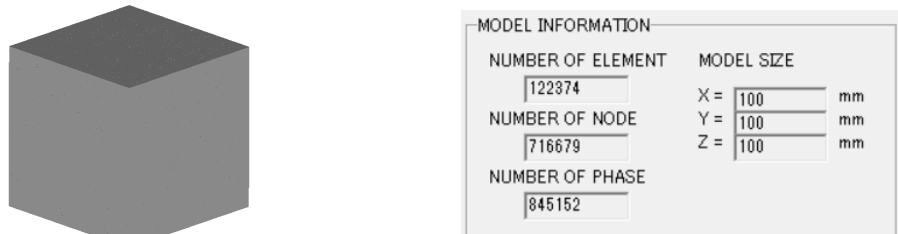


FIGURE 2.8: 50x50x50mm DEF intensified part range

2.4 Details of Numerical Models for ASR Simulation

2.4.1 Geometry of Numerical Models

Figure 2.9 shows the geometry of the model, which is in dimension of 100 x 100 x 100mm. Numbers of elements around 120000. Average diameter of meshed element is around 2mm.



(A) 3D model in dimension 100x100x100mm (B) Model Detail for 30% Coarse Aggregate Case

FIGURE 2.9: Numerical Model for Expanding Simulation

2.4.2 Coarse Aggregate of Numerical Models

To analysis the behavior of concrete with different coarse aggregate volume ratio, 15% coarse aggregate model(Figure 3.52b) and 30% coarse aggregate model(Figure 4.1) are built for simulation.



(A) 15% Coarse Aggregate (B) 30% Coarse Aggregate

FIGURE 2.10: Coarse Aggregate Percentage

2.4.3 ASR Reactive Coarse Aggregate Ratio

To analysis the behavior of concrete with different ASR reactive coarse aggregate ratio, 25% ASR reactive coarse aggregate ratio model and 25% ASR reactive coarse aggregate ratio model are built for 30% aggregate case.



(A) 30% Coarse Aggregate with 75% ASR Reactive Aggregate (B) 30% Coarse Aggregate with 25% ASR Reactive Aggregate

FIGURE 2.11: 25% and 75% ASR Reactive Aggregate Ratio Model

2.4.4 Boundary Conditions

2.4.4.1 Boundary Condition During ASR Expansion

During ASR Expansion, no confinements are added to the boundary elements. Models expand freely in all directions.

2.4.4.2 Boundary Conditions During Uni-axial Loading Test

Figure 2.14 shows the boundary condition of simulation models for uni-axial loading test.

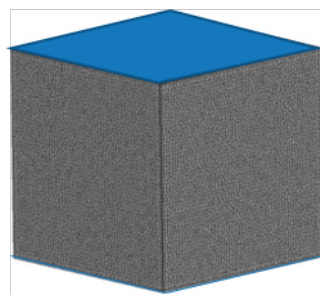


FIGURE 2.12: Top and Bottom Boundary in Loading

In the case of fixed boundary condition, displacement in all directions are assumed as 0 at the bottom. Displacement in horizontal directions are all assumed as 0 at the top, and displacement in vertical direction is increased by 0.02mm downward at each loading step.

In the case of free boundary condition, all boundary elements able to move freely in horizontal direction except 2 center elements in top and bottom are fixed in horizontal direction, to prevent the sliding of whole model during loading. Same as fixed boundary condition cases, displacement in vertical direction is increased by 0.02mm downward at each loading step for top boundary elements.

Loading is applied until the maximum compressive strength is reached.

2.4.5 Initial Strain Given For ASR Expansion

To analysis the relationship of concrete behavior and mechanical properties with expansion amount, initial strain is given between reactive aggregate and mortar.

Aggregate Ratio[%]	Reactive Aggregate Ratio[%]	Boundary Condition	Initial Strain (Each Step)	Expanding Steps
15	11.25	Fix	0	0
15	11.25	Fix	0.0002	20
15	11.25	Fix	0.0005	20
15	11.25	Fix	0.001	20
15	11.25	Fix	0.002	20
15	11.25	Fix	0.003	20
15	11.25	Free	0	0
15	11.25	Free	0.0002	20
15	11.25	Free	0.0005	20
15	11.25	Free	0.001	20
15	11.25	Free	0.002	20
30	22.50	Fix	0	0
30	22.50	Fix	0.0002	20
30	22.50	Fix	0.0005	20
30	22.50	Fix	0.001	20
30	22.50	Fix	0.002	20
30	22.50	Fix	0.003	20
30	22.50	Free	0	0
30	22.50	Free	0.0002	20
30	22.50	Free	0.0005	20
30	22.50	Free	0.001	20
30	22.50	Free	0.002	20
30	7.50	Fix	0	0
30	7.50	Fix	0.001	20
30	7.50	Fix	0.002	20
30	7.50	Fix	0.004	20
30	7.50	Fix	0.006	20

TABLE 2.1: ASR Models

2.5 Details of Numerical Models for DEF Simulation

2.5.1 Introduction

The exactly same model is used for DEF simulation in order to cross compare the cracking patterns and mechanical properties changes under ASR and DEF expansion.

2.5.2 Geometry of Numerical Models

The geometry of the models is exactly the same as models using in ASR simulation, which is in dimension of 100 x 100 x 100mm.

All materials properties are set to be exactly the same.

2.5.3 Coarse Aggregate of Numerical Models

To analysis the behavior of concrete with different coarse aggregate volume ratio, 15% coarse aggregate model(Fig.X) and 30% coarse aggregate model(Fig.X) are built for simulation.

2.5.4 DEF Intensified Expansion Area of Numerical Models

Since DEF is closely related to higher curing temperature, here we choose to intensified the expansion in center part of model.

Here we chooses 3 cases in different expansion intensified area. The **table 2.2** is a list of cases simulated.

Case	Expansion Intensified Depth[mm]	Expansion Intensified Area[%]
1	0	100
2	12.5	56.25
3	25	25

TABLE 2.2: DEF Intensified Expansion Area

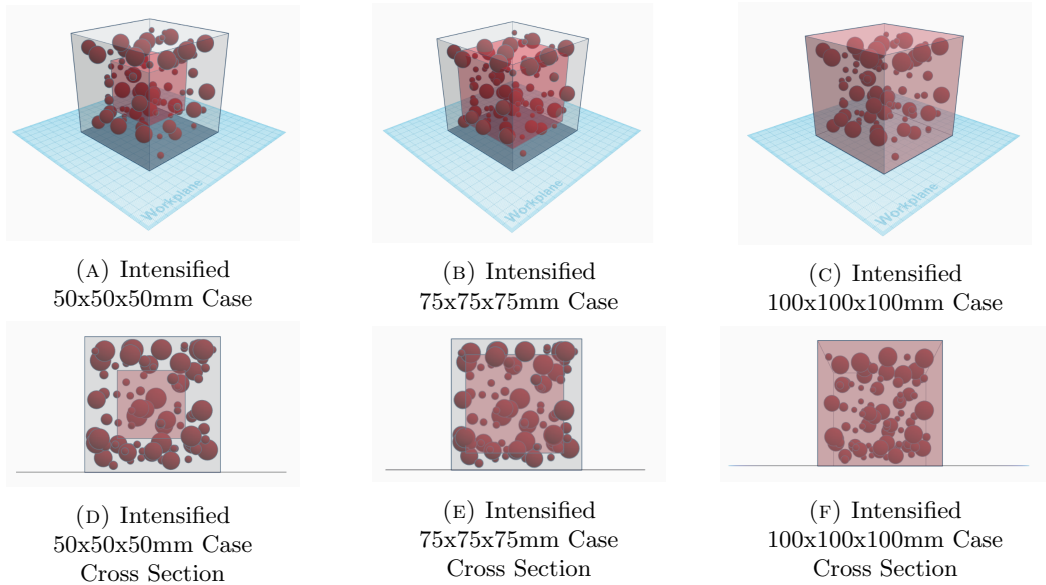


FIGURE 2.13: DEF intensified part range

2.5.5 Boundary Conditions

2.5.5.1 Boundary Condition During DEF Expansion

Same as in ASR expansion, during DEF expansion, no confinements are added to the boundary elements. Models expand freely in all directions.

2.5.5.2 Boundary Conditions During Uni-axial Loading Test

Same as in ASR expansion, Uni-axial Loading Test is applied with both fixed and free boundary conditions.

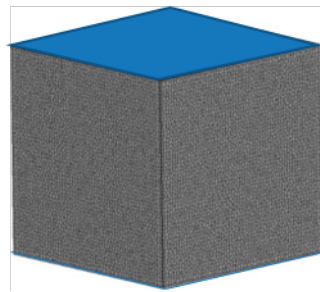


FIGURE 2.14: Top and Bottom Boundary in Loading

In the case of fixed boundary condition, displacement in all directions are assumed as 0 at the bottom. Displacement in horizontal directions are all assumed as 0 at the top, and displacement in vertical direction is increased by 0.02mm downward at each loading step.

In the case of free boundary condition, all boundary elements able to move freely in horizontal direction except 2 center elements in top and bottom are fixed in horizontal direction, to prevent the sliding of whole model during loading. Same as fixed boundary condition cases, displacement in vertical direction is increased by 0.02mm downward at each loading step for top boundary elements.

Loading is applied until the maximum compressive strength is reached.

2.6 Conclusions

In this chapter describe about the numerical simulation system that has been used in this research, RBSM. In the this study, RBSM is used to simulate the deterioration of concrete due to expansion such as expansion crack, then the mechanical properties of expanded concrete will be calculated by using RBSM.

In RBSM, the response of normal spring and shear spring represent the mechanical response of mortar and aggregate member. By giving initial strain, the response of spring changed in the relatively close manner as real expanded structure. Also the cases that will be simulated in later are introduced in this chapter. The details of simulation results from this simulation will be described again in Chapter 3 and 4.

Chapter 3

Simulation of Cracking Pattern Of ASR and DEF Expanded Concrete

3.1 General

In this chapter, three-dimensional expanded simulations are carried out on concrete models in free condition. The purpose of this study is for the prediction of the behavior during the expansion of concrete, especially the cracking pattern and stress distribution.

3.2 Cracking Pattern caused by Pure ASR Expansion

3.2.1 Single ASR Expansion Simulation

In this section, the process of simulated one ASR expansion is present. The expanse is generated at the location of interfaces between mortar and reactive aggregate, to introduce the expansion, as introduced in chapter 2.

For usually the case not all aggregate inside concrete structure are ASR reactive aggregate, here only partial of aggregates are selected to be ASR reactive and will be giving initial strain in expansion steps to simulate ASR expansion.

This single example case has been choosing here use the model in the dimension of 100x100x100mm, with 30% aggregate, of which 75% are ASR reactive. Aggregate in Figure 4.1 in red color is assumed as ASR reactive, while aggregate in blue color is assumed as non-reactive aggregate.

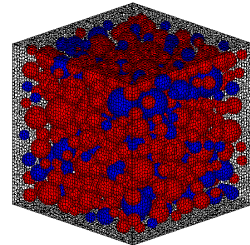


FIGURE 3.1: 30% Coarse Aggregate

Table. Aggregate consistent(if we have it)

To simulate ASR expansion, an initial strain of 0.001mm is given in each step, for totally 20 steps expansion. Before and after expansion, the distance of element between 2 elements is recorded to gauge the global expansion. These two element selected here are the middle element in the left surface of model and the middle element in the right surface of model.

With the increasing of initial strain giving, the global expansion also gradually increasing. After 20 steps of ASR expansion, the model here reached 0.4223% expansion(one-dimensionally). Characteristic ASR map cracking pattern can be seen on the surface of the expanded concrete model in Figure 3.3.

As can be seen in Figure 3.4 the internal stress from step 1 to 20, along with the increasing of giving initial strain, unbalanced force present in the concrete model, compressive stress (in red color) generated and distributed especially in coarse aggregates. Gradually crack

Step	Expansion	Step	Expansion
1	0.000136	11	0.002140
2	0.000314	12	0.002358
3	0.000501	13	0.002582
4	0.000695	14	0.002812
5	0.000894	15	0.003049
6	0.001096	16	0.003278
7	0.001301	17	0.003536
8	0.001507	18	0.003767
9	0.001715	19	0.003989
10	0.001924	20	0.004223

TABLE 3.1: Expansion in Each Step for A30 P75 Case 3

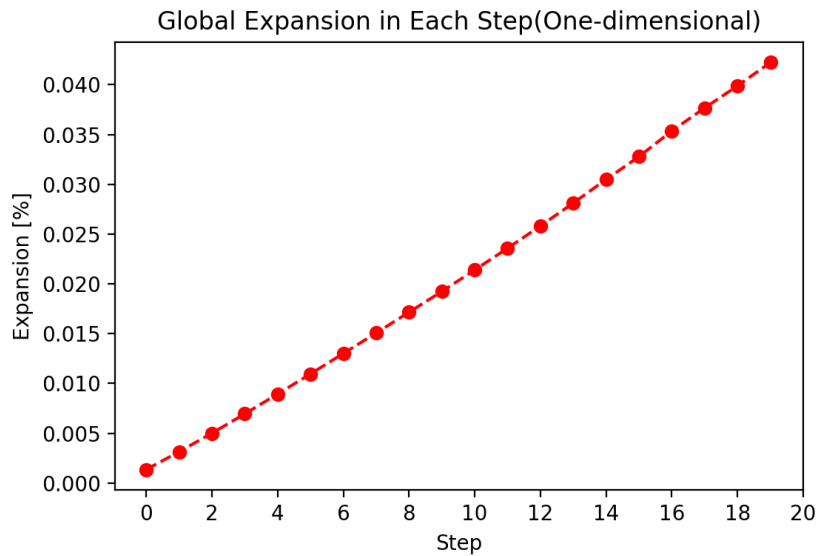


FIGURE 3.2: Global Expansion vs. Step

generated around the aggregate, penetrated and finally linked between aggregates and reached surface of the model.

In Figure 3.5 shows the inner crack distribution right after 20 steps of ASR expansion. The cracked interfaced which larger than 0.03mm are colored in orange, to present the distribution of internal crack three dimensionally. With 0.4223% of one dimensional global expansion, cracks over 0.03mm are distributed relatively uniformed inside the model.

For analyzing the behavior of expansion caused by ASR numerically, cracked interfaces are summarised in different crack width scale, shown in Table 3.15. The maximum crack width, in this case, is in range of 0.01-0.03mm, while most of the cracks are under 0.001mm. The ability of RBSM simulation in numerically analysis distribution of cracked interfaces gives us information that with difficulties to obtain in experimental

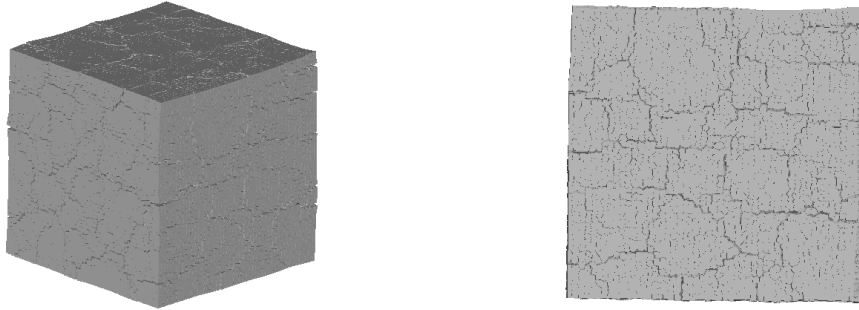


FIGURE 3.3: 3D Surface Cracks, 0.4223% Expansion (Deformation x 10)

tests. These numbers will be compared with simulations given different global expansion ratio, different aggregate consistent, even different mechanism.

Crack Width [mm]	Total Cracked Interfaces
0.00000 - 0.00005	316744
0.00005 - 0.00010	286704
0.00010 - 0.00020	263943
0.00020 - 0.00050	234672
0.00050 - 0.00100	183238
0.00100 - 0.00300	131553
0.00300 - 0.01000	42432
0.01000 - 0.03000	275
0.03000 - 0.10000	0
0.1000+	0

TABLE 3.2: Crack Summarised by width

In Figure 3.5, inner cracking interfaces with over 0.03mm are colored in orange. From this illustration, it can be seen that the cracks are distributed relatively uninformed in the expanded model, which is co-insistent with the condition shown in the 2D inner section.

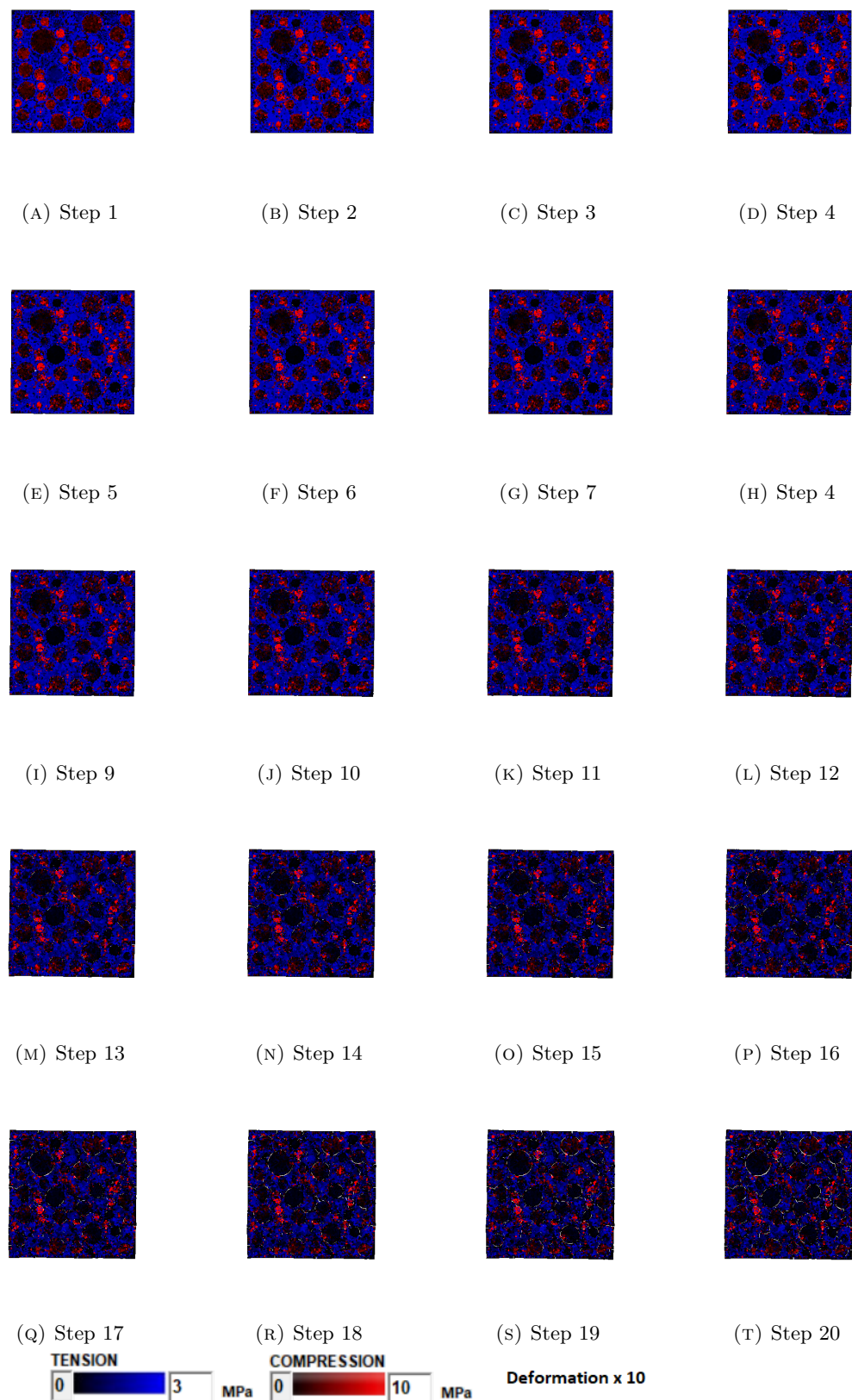


FIGURE 3.4: Internal Stress in Each Step for A30 P75 Case 3 (Deformation x 10)

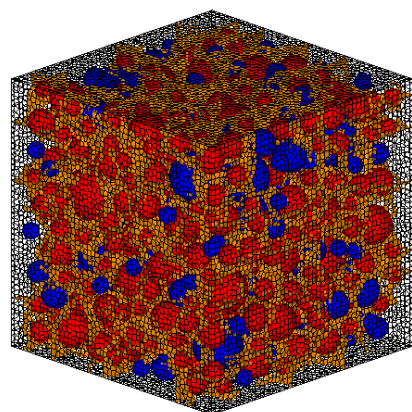


FIGURE 3.5: 3D Inner Cracking larger than 0.03mm

3.2.2 Expansion Ratio Related to Behavior of Concrete During ASR Expansion

In this section, the relationship between given initial strain, final expansion and behavior during expansion is discussed.

Model in size of 100x100x100mm is used, with 30% Aggregate (75% of which is ASR reactive).

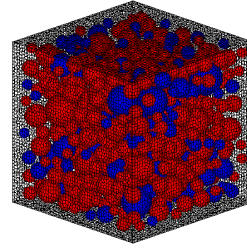


FIGURE 3.6: 30% Coarse Aggregate

Expansion is carried out with initial strain given in each step various from 0 to 0.003. Total expansion steps are set as 20 steps same for all cases. From the Table 4.2 can be seen that with the increasing of giving initial strain in each step, the global expansion reached in step 20 also increased. Non-damage model is used here for compare.

Aggregate Ratio[%]	Reactive Aggregate Ratio[%]	Initial Strain (Each Step)	Expanding Steps	Final Expansion [%]
30	75	0	0	0
30	75	0.0002	20	0.0699
30	75	0.0005	20	0.1936
30	75	0.001	20	0.4223
30	75	0.002	20	0.8832
30	75	0.003	20	1.3224

TABLE 3.3: One Dimensional Expansion Ratio in Single ASR Model Simulation

Figure plot of initial strain vs. global expansion ratio

As shown in Figure 3.7 and Figure 3.8, it is clear that with the increase of global expansion ratio, the cracking can be seen on the surface of concrete model become much significant. However, the map cracking pattern does not change much comparing the expanded models in different expansion ratio.

This also indicated that our simulation can still predict the map cracking behavior for ASR expansion in different deterioration levels.

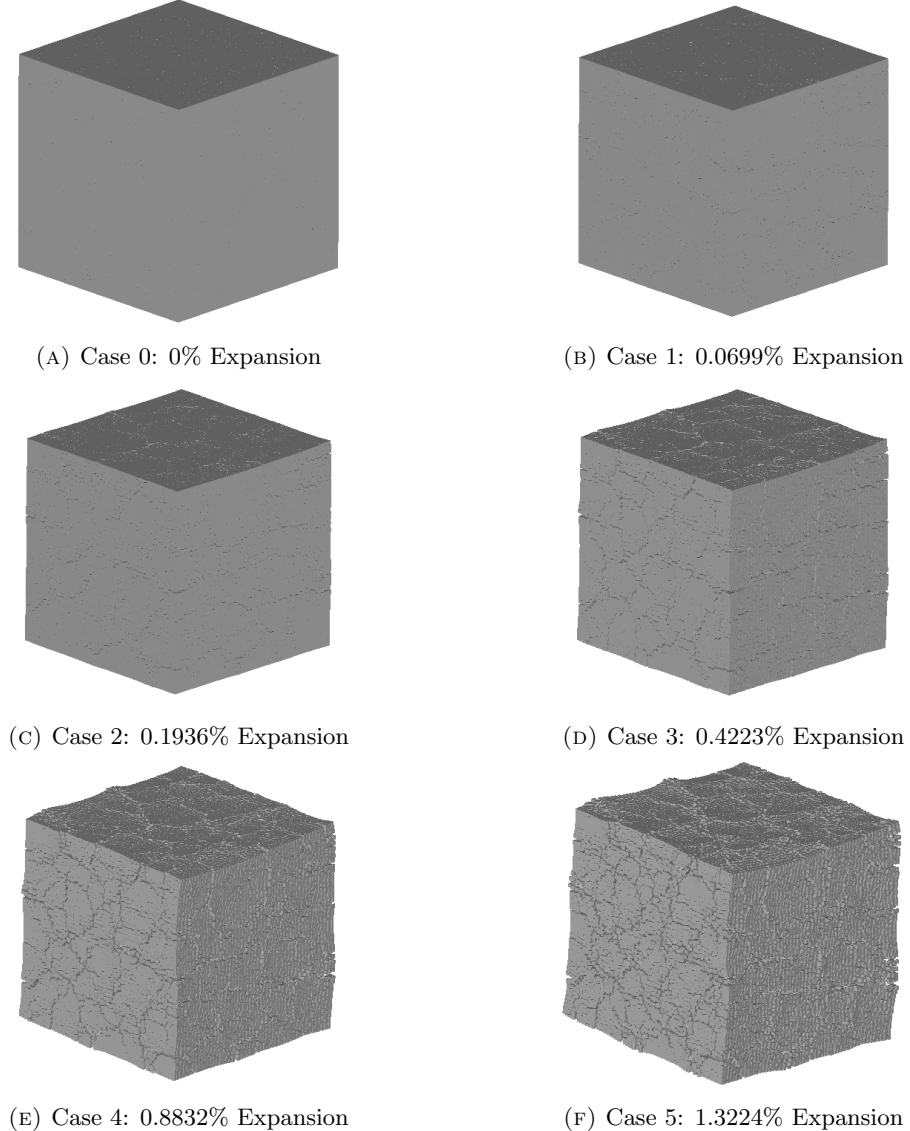


FIGURE 3.7: 3D Surface Cracks (Deformation x 10)

It is possible that the position where large crack generated is determined by other factors, for example, the location of coarse aggregate.

By comparing the inner cracking condition in Figure 3.9, it can be seen that start from 0.1936% of one-dimensional global expansion, cracks larger than 0.03mm are generated and able to be recognizable by the naked eye. With the increase of global expansion ratio, the inner crack generally increases, distributed relatively uniform in all inner part of the expanded model. This cracking pattern will be compared with ASR expansion in different reactive aggregate ratio simulation and also DEF simulations.

In Figure 3.10, the internal stress distribution in some middle step and last expansion step are shown. By increasing the initial strain giving to present ASR expansion in each

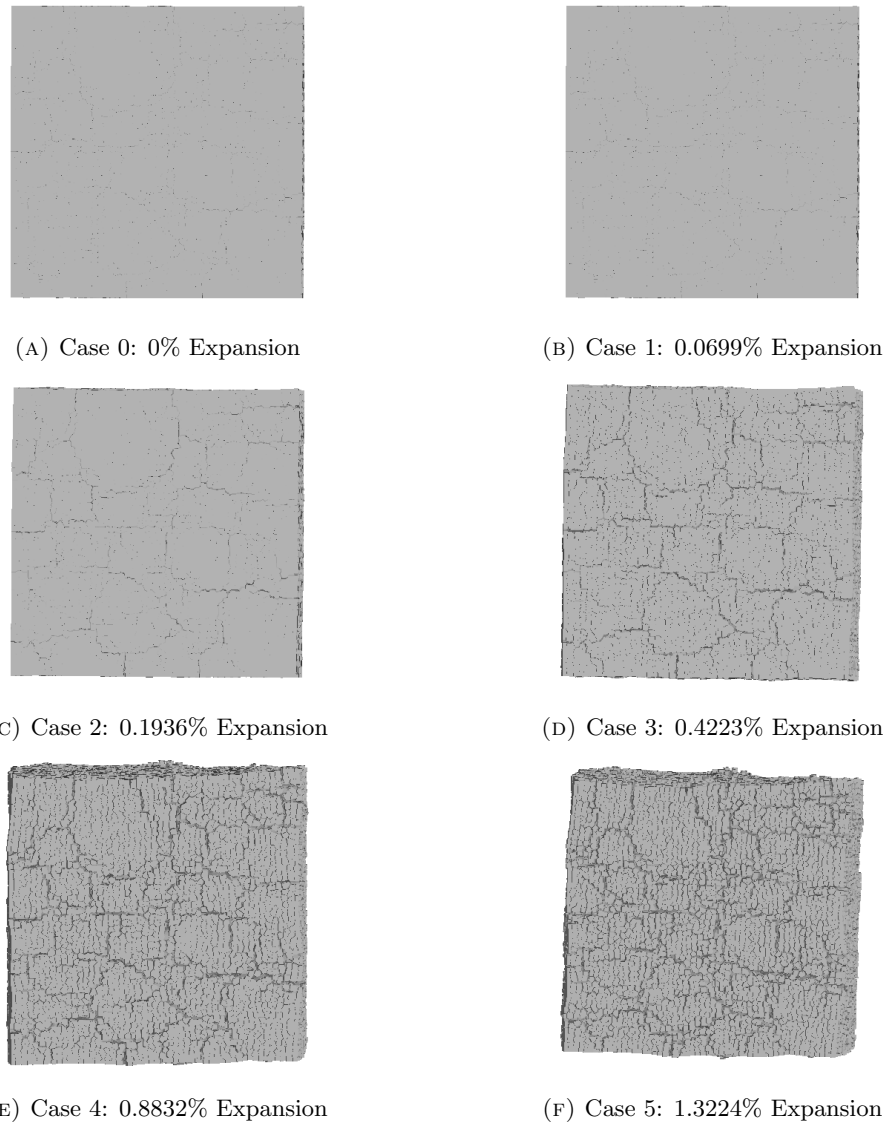


FIGURE 3.8: 3D Surface Cracks (Single Side View, Deformation x 10)

step, the expansion developed more rapidly and more inner cracks generated as well as outer cracks.

This suggests deteration caused by ASR not only causing the aesthetic problem on the surface of the concrete structure but also indicate structually damage inside.

By visualizing the inner crack, we can confirm that the inner part of the ASR-damaged concrete model also deteriorated. As the increasing of global expansion, inner cracks gradually increase its number and volume, in cases over 0.8% global expansion, crack with a width larger than 0.03mm almost covered all inner part of the expanded model.

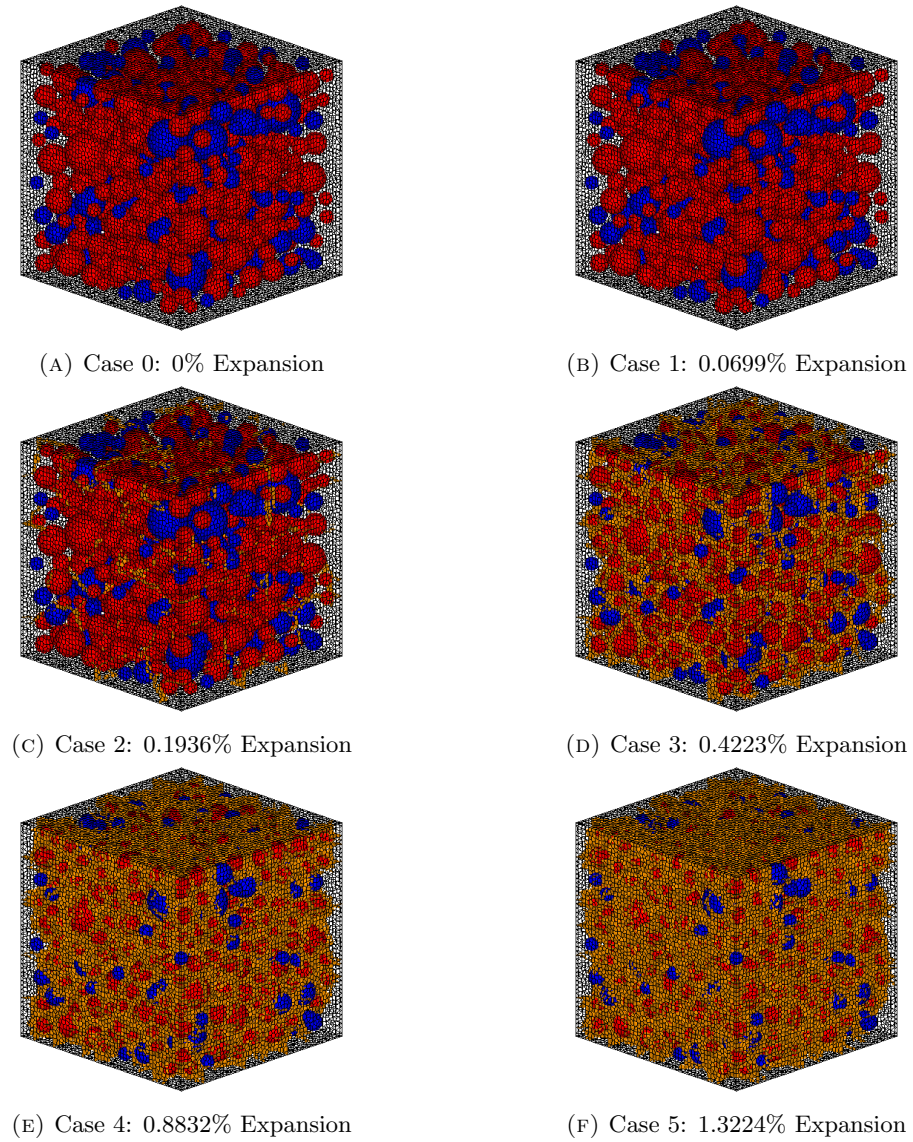


FIGURE 3.9: 3D Inner Crack Width Larger than 0.03mm

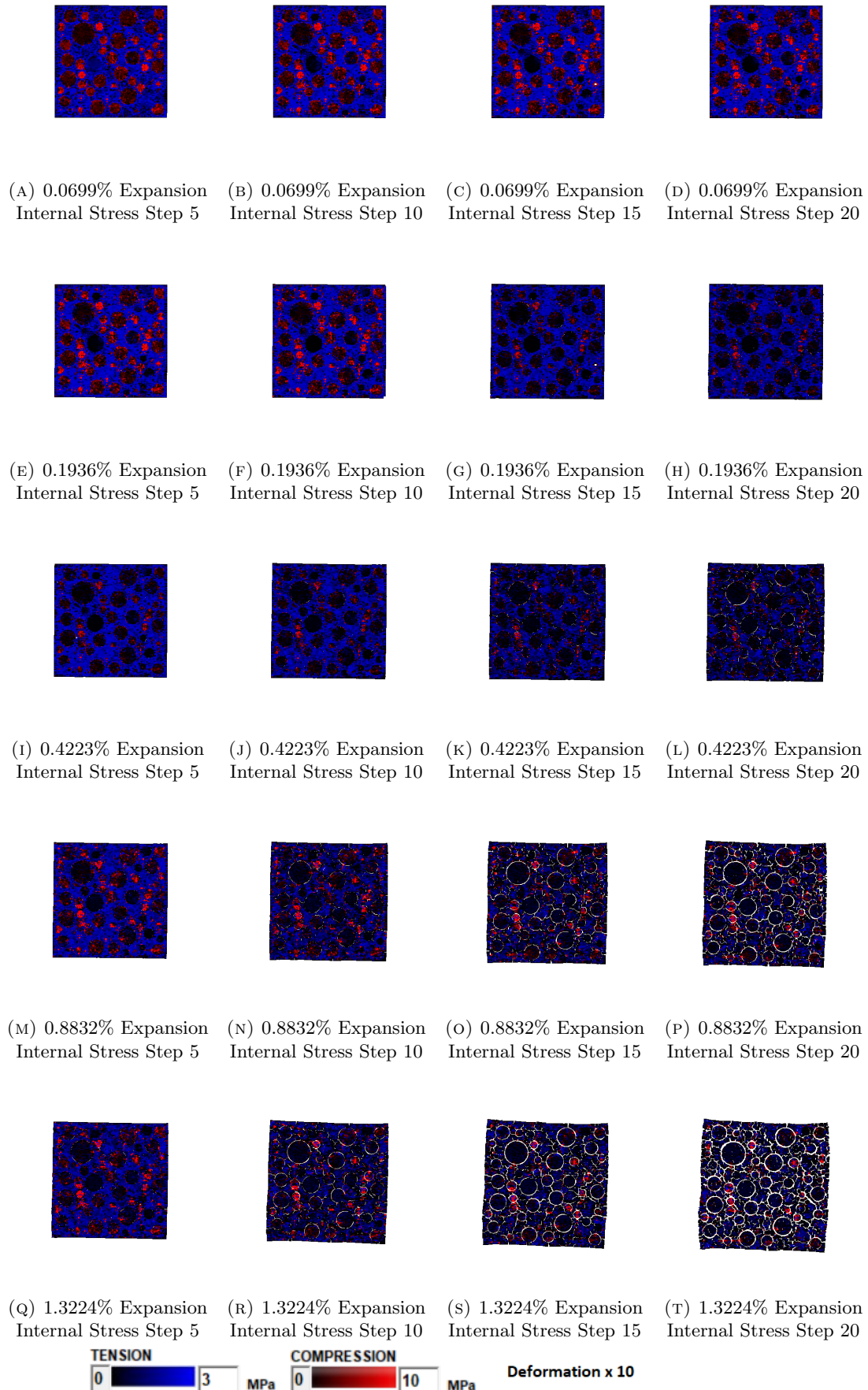


FIGURE 3.10: Generation of Internal Stress and Inner Cracks for ASR Expansion to Step 20(Final Expansion Step, Deformation x 10)

3.2.3 Aggregate Ratio Related to Behavior of Concrete During ASR Expansion

In this section, the relationship between aggregate ratio and behavior during expansion is discussed.

Expansion simulation result between 15% coarse aggregate model and 30% coarse aggregate model is compared here to analysis how the change in aggregate percentage influence the cracking pattern in different expansion ratio.

To eliminate the influence of ASR reactive aggregate percentage, both 15% coarse aggregate model and 30% coarse aggregate model discussed here in this section are set with 75% ASR reactive aggregate and 25% non-reactive aggregate.

ASR reactive coarse aggregate are colored in red, while non-reactive aggregate is colored in blue here. As exactly same model is used, the location of all aggregates are kept exactly the same for different percentage ASR reactive aggregate cases.

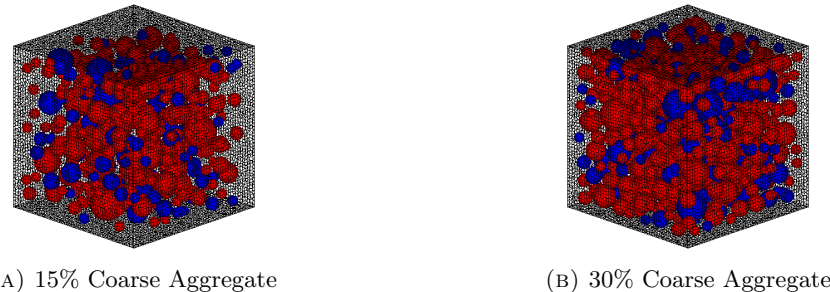


FIGURE 3.11: Coarse Aggregate Percentage

After modeling, similar ASR expansion simulations are carried out in the same way described in the previous section. Initial strain is giving to the interfaces between ASR reactive aggregate and paste, various from 0 to 0.003mm in each step to reach different level of global expansion in step 20.

From Table 3.4 can be seen that with same expansion step and same initial strain given in each step, the global expansion of with more coarse aggregate (A30 cases here) is higher than less coarse aggregate cases (A15 cases here). As coarse aggregate ratio increased, ASR reactive interfaces are also increased, which suggested the reason for achieving larger global expansion in higher coarse aggregate cases.

This difference becomes more significant as the increasing of initial strain in each step, indicate that the amount of global expansion is not only depended on the amount of initial strain giving but also affected by other factors.

Figure, plot of initial strain vs. global expansion ratio

Initial Strain (Each Step)	Expanding Steps	A15 Final Expansion	A30 Final Expansion[%]
0	0	0	0
0.0002	20	0.0699	0.0699
0.0005	20	0.1364	0.1936
0.001	20	0.3051	0.4223
0.002	20	0.6290	0.8832
0.003	20	0.9243	1.3224

TABLE 3.4: One Dimensional Expansion Ratio in Single ASR Model Simulation

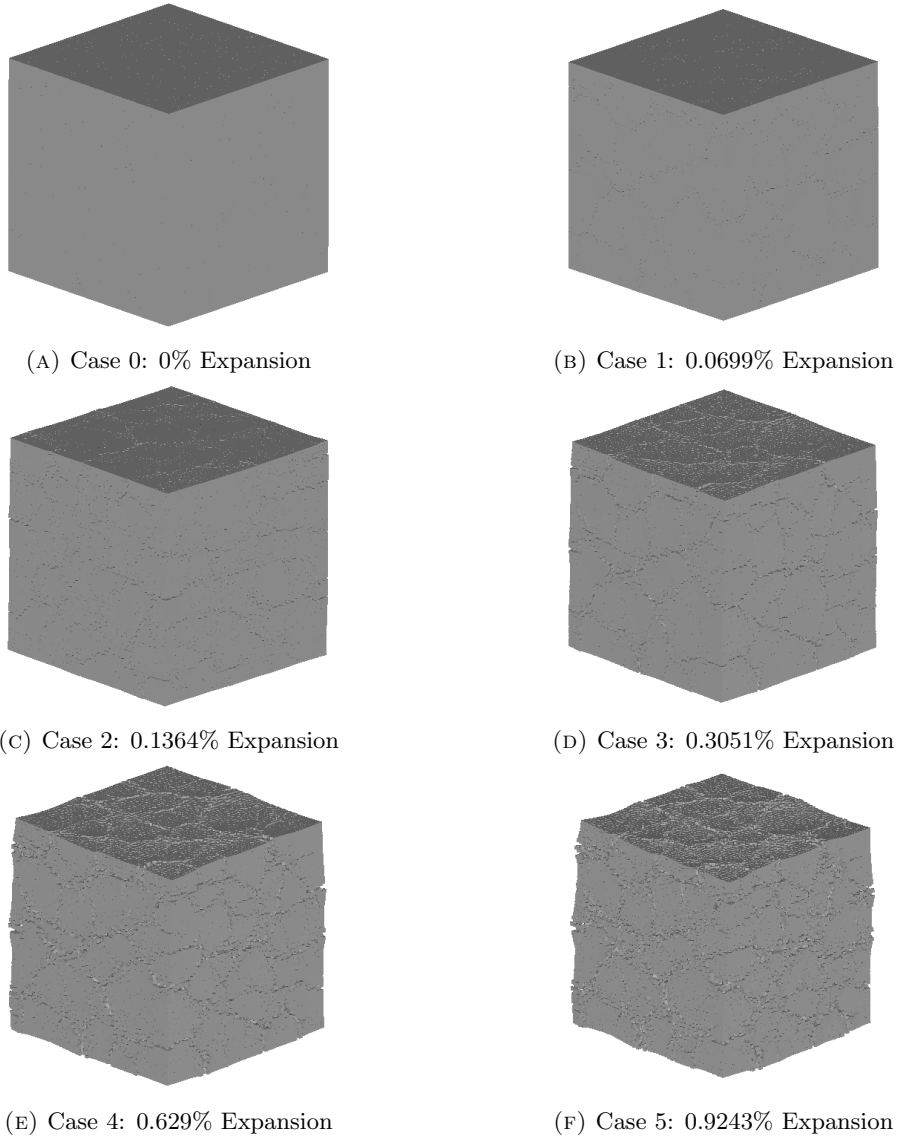


FIGURE 3.12: 3D Surface Cracks (Deformation x 10)

Figure 3.12 and Figure 3.13 show surface crack pattern after ASR expansion of 15% coarse aggregate cases.

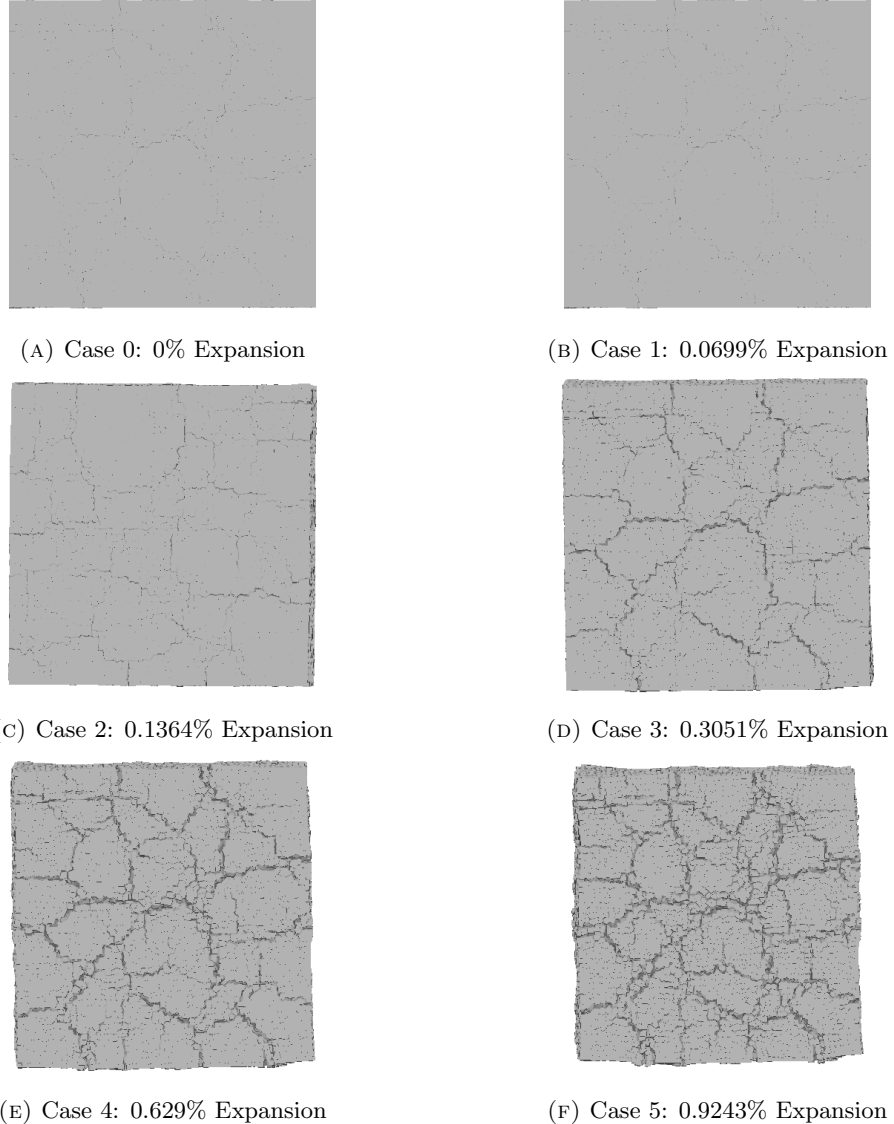


FIGURE 3.13: 3D Surface Cracks (Single Side View, Deformation x 10)

Here 2 cases from 15% coarse aggregate model and 30% coarse aggregate model in relatively close global expansion rate are compared to show the influence of coarse aggregate ratio on cracking pattern.

For the aggregate ratio of 15% model, case 3 is chosen, giving 0.001mm initial strain for ASR reactive interfaces, and reached 0.3051% one-dimensional expansion after 20 steps. And for the aggregate ratio of 30% model, case 3 is chosen, giving 0.001mm initial strain for ASR reactive interfaces and reached 0.4223% one-dimensional expansion after 20 steps.

As can be seen in Figure 3.16, at a relatively close global expansion ratio, the cracks are more concentrated with less coarse aggregate ratio case (aggregate 15% here). This

indicated that the concentration of location generate expansion could result in the concentration of global cracking distribution. Similar trend is also shown when decreasing the ratio of ASR reactive coarse aggregate ratio, which will be discussed later.

Both of the cases show clear characteristic map cracking which normally observed in ASR expanded concrete structures.

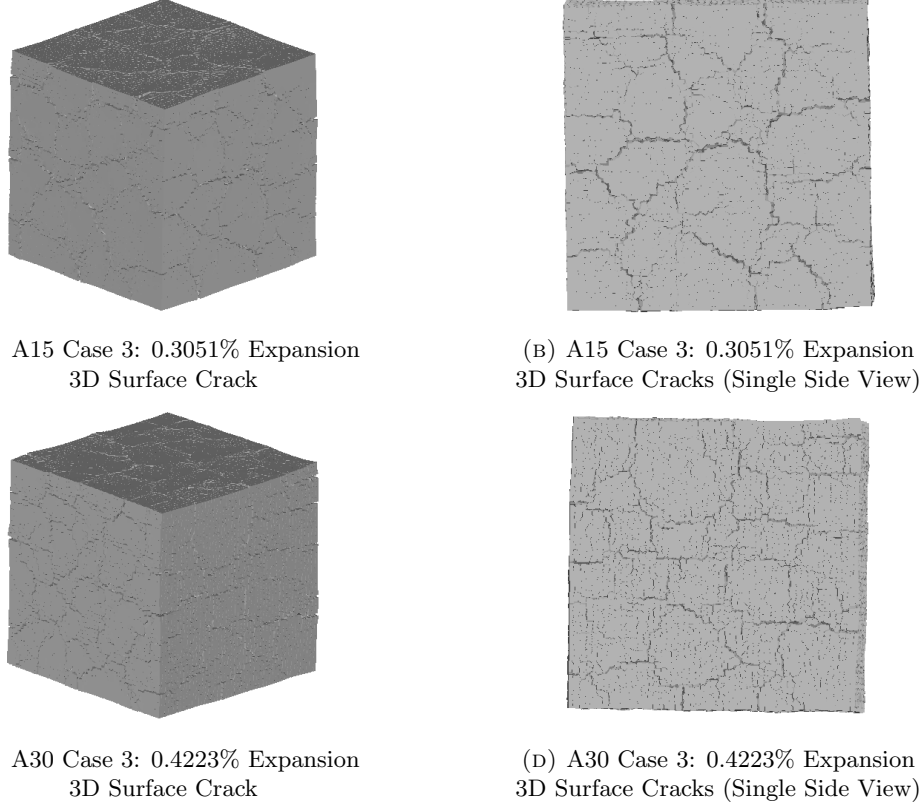


FIGURE 3.14: Comparing Between A15 and A30 3D Surface Cracks (Deformation x 10)

In Figure 3.15, here if compare the inner crack of two cases at a relatively close global expansion ratio, the cracks larger than 0.03mm are generally more with less coarse aggregate ratio case (aggregate 15% here).

If comparing the distribution of cracks summarised by its crack width (Table 3.12), it can be seen that the distribution pattern is relatively close for 15% coarse aggregate case with 0.3051% global expansion and 30% coarse aggregate case with 0.4223% global expansion. The number of cracked faces decrease gradually when increasing the crack width.

However, if compare closer on relatively larger cracks, cracking face number of the case with 15% coarse aggregate is higher. For example, for the number of cracked interfaces larger than 0.003mm, 15% coarse aggregate case is 9.27% higher than 30% coarse aggregate case. And for the number of cracked interfaces larger than 0.01mm,

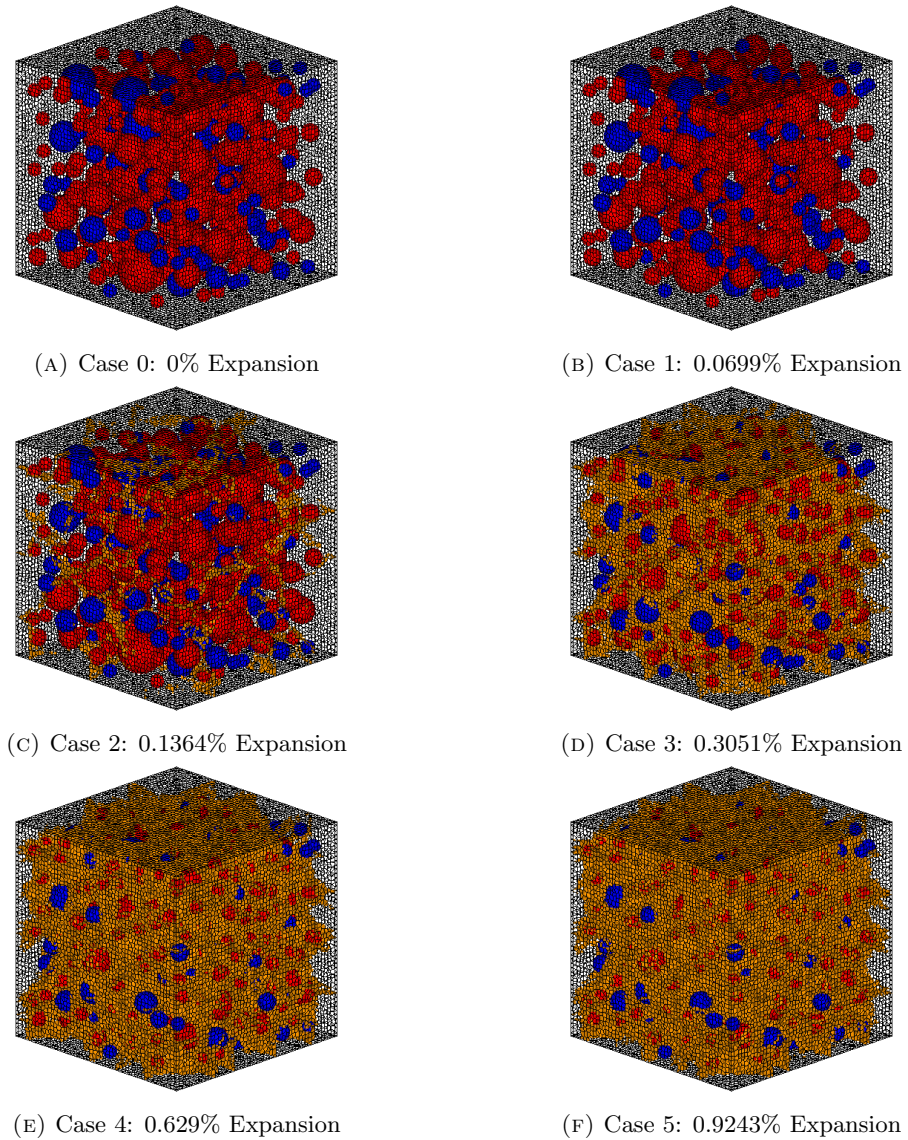
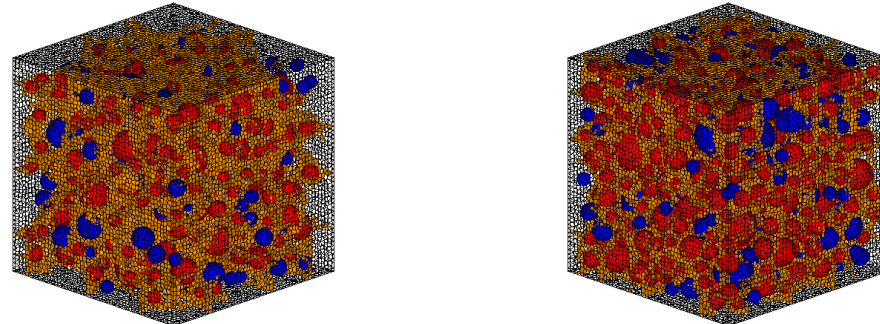


FIGURE 3.15: 3D Inner Crack Width Larger than 0.03mm

Crack Width [mm]	A15 Case 3 Total Cracked Interfaces	A30 Case 3 Total Cracked Interfaces
0.00000 - 0.00005	363340	316744
0.00005 - 0.00010	303804	286704
0.00010 - 0.00020	263111	263943
0.00020 - 0.00050	220320	234672
0.00050 - 0.00100	163316	183238
0.00100 - 0.00300	117764	131553
0.00300 - 0.01000	45969	42432
0.01000 - 0.03000	696	275
0.03000 - 0.10000	0	0
0.1000+	0	0

TABLE 3.5: Expansion in Each Step for A15P75 Case 3 and A30 P75 Case 3

15% coarse aggregate case is 2.53 times of 30% coarse aggregate case. Those larger cracks having more significant influence when the global cracking patterns are compared and should distribute more when considering the damage on the concrete structure.



(A) A15 Case 3: 0.3051% Expansion
3D Inner Crack

(B) A30 Case 3: 0.4223% Expansion
3D Inner Cracks

FIGURE 3.16: Comparing Between A15 and A30 3D Surface Cracks (Deformation x 10)

3.2.4 Reactive Aggregate Ratio Related to Behavior of Concrete During ASR Expansion

In this section, the relationship between ASR reactive aggregate ratio and behavior during expansion is discussed.

Expansion simulation result of 30% coarse aggregate model is used here, and different ASR reactive ratio (25% of total coarse aggregate and 75% of total coarse aggregate) is given, to analyze how the change in ASR reactive aggregate percentage influence the cracking pattern.

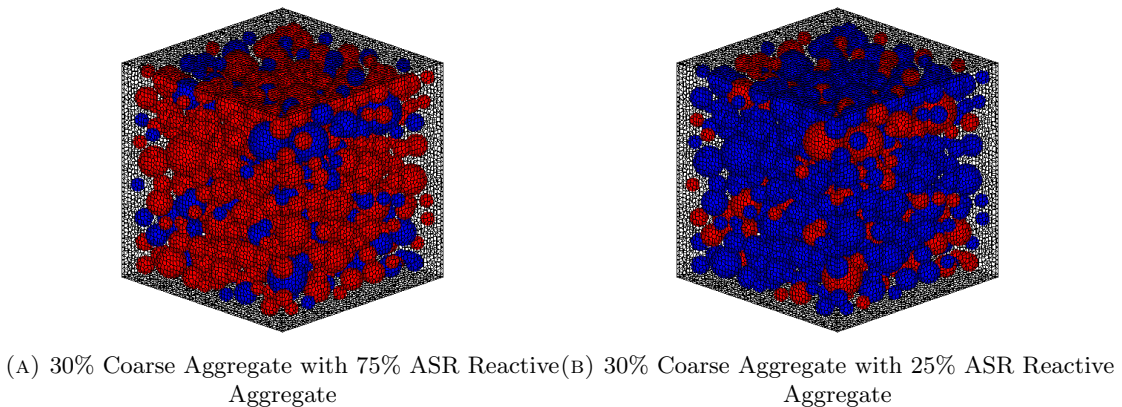


FIGURE 3.17: 25% and 75% ASR Reactive Aggregate Ratio Model

Table 3.6 summarized the giving initial strain in each step and the total step of expansion giving in the two models compared in this section. Relatively larger initial strains are given to the less ASR reactive coarse aggregate cases (25% ASR reactive aggregate cases here) to reach relatively closer global expansion ratio for comparing.

Aggregate Ratio[%]	Reactive Aggregate Ratio[%]	Initial Strain (Each Step)	Expanding Steps	Final Expansion [%]
30	75	0	0	0
30	75	0.0002	20	0.0699
30	75	0.0005	20	0.1936
30	75	0.001	20	0.4223
30	75	0.002	20	0.8832
30	75	0.003	20	1.3224
30	25	0	0	0
30	25	0.001	20	0.1651
30	25	0.002	20	0.3606
30	25	0.004	20	0.7024
30	25	0.006	20	1.0201

TABLE 3.6: One Dimensional Expansion Ratio in A30P25 and A30P25 ASR Expansion Simulation

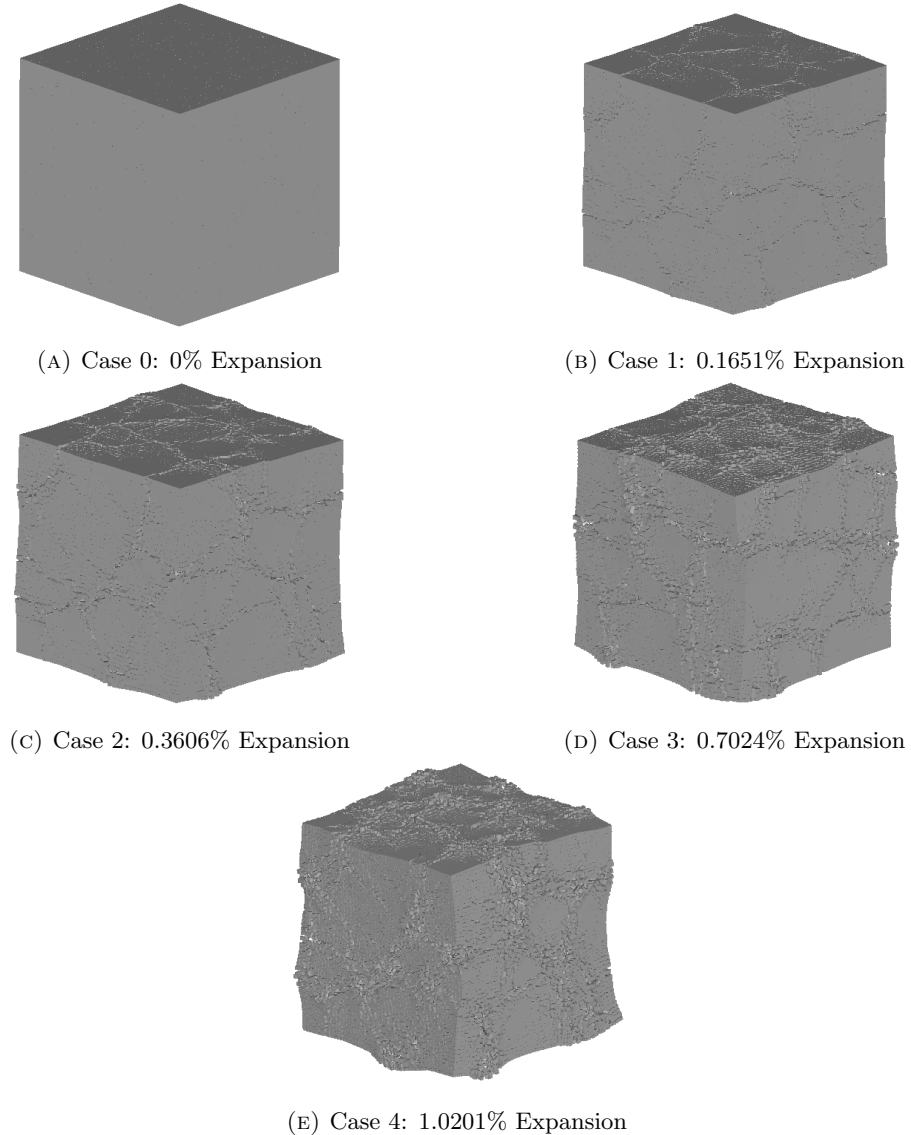


FIGURE 3.18: 3D Surface Cracks (Deformation x 10)

Figure 3.18 and Figure 3.19 show surface crack pattern after ASR expansion of 30% coarse aggregate cases with 25% of the coarse aggregate inside are ASR reactive.

Here 2 cases from 25% ASR reactive coarse aggregate in 30% total coarse aggregate model and 75% ASR reactive coarse aggregate in 30% total coarse aggregate model in relatively close global expansion rate are compared to show the influence of ASR reactive coarse aggregate ratio on cracking pattern.

For the reactive aggregate ratio of 25% model, case 2 is chosen, giving 0.002mm initial strain for ASR reactive interfaces in each step, and reached 0.3606% one-dimensional expansion after 20 steps. And for the reactive aggregate ratio of 75% model, case 3 is chosen, giving 0.001mm initial strain for ASR reactive interfaces and reached 0.4223% one-dimensional expansion after 20 steps.

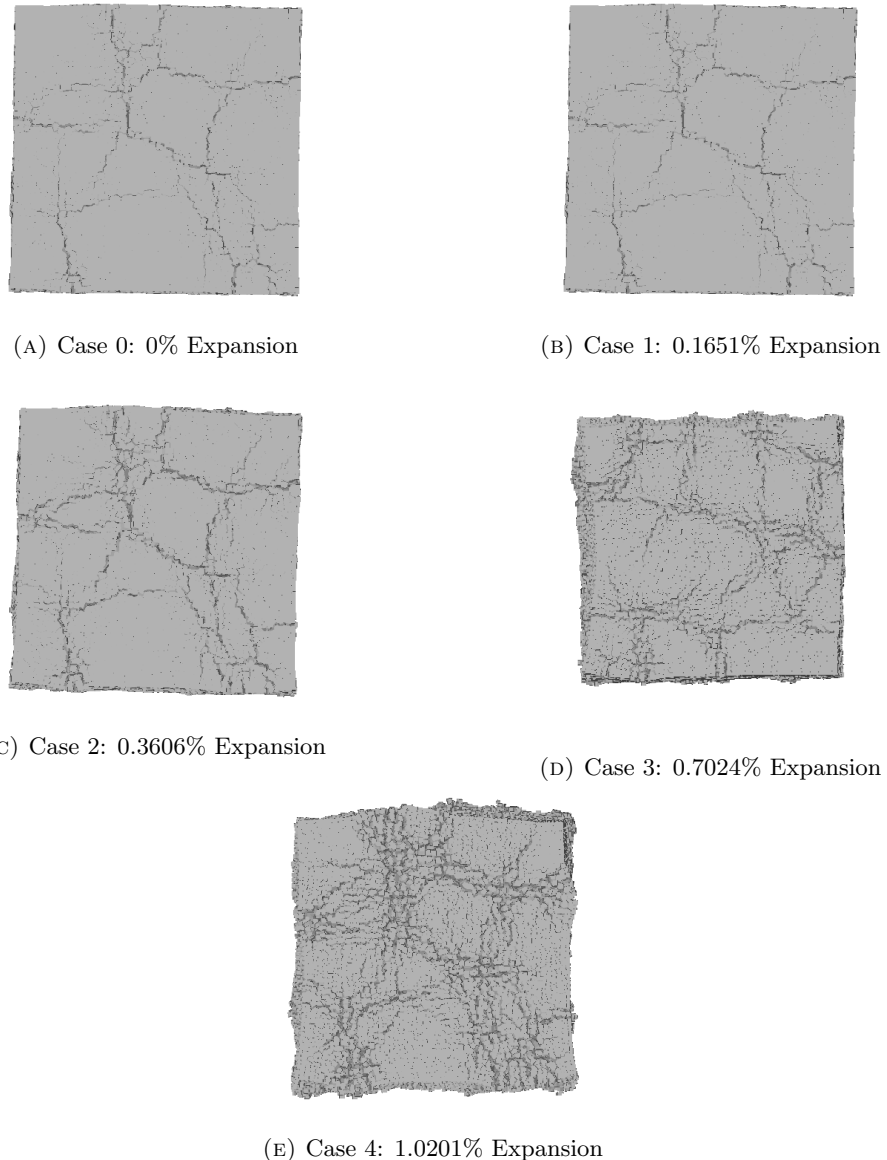


FIGURE 3.19: 3D Surface Cracks (Single Side View, Deformation x 10)

As can be seen in Figure 3.21, at a relatively close global expansion ratio, the cracks are more concentrated with less reactive coarse aggregate ratio case (reactive aggregate ratio of 25% cases here). This indicated that the concentration of location generate expansion could result in the concentration of global cracking distribution, which consists with the previous cases when the total aggregate percentage is decreased.

Still, both of the cases show clear characteristic map cracking which observed in typical ASR expanded concrete structures.

And from Figure 3.22, the inner cracking distribution of 2 cases are also compared. It can be seen that the case with less reactive coarse aggregate ratio (15% ASR reactive aggregate) is having less distributed cracks (larger than 0.03mm).

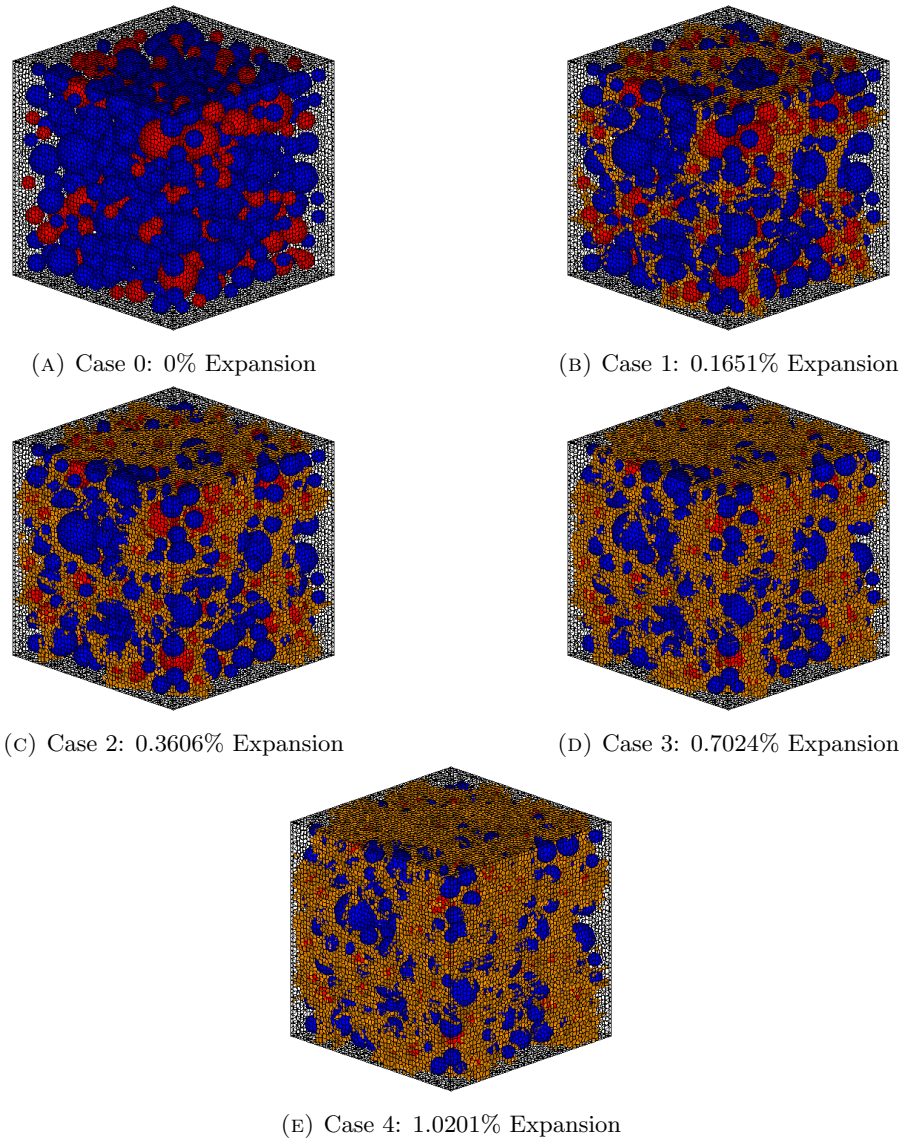


FIGURE 3.20: 3D Inner Cracks

Crack Width [mm]	A30P25 Case 2 Total Cracked Interfaces	A30P75 Case 3 Total Cracked Interfaces
0.00000 - 0.00005	327828	316744
0.00005 - 0.00010	280821	286704
0.00010 - 0.00020	256125	263943
0.00020 - 0.00050	229235	234672
0.00050 - 0.00100	189533	183238
0.00100 - 0.00300	154639	131553
0.00300 - 0.01000	85126	42432
0.01000 - 0.03000	6584	275
0.03000 - 0.10000	0	0
0.1000+	0	0

TABLE 3.7: Comparing Between A30P25 and A30P75 3D Surface Cracks

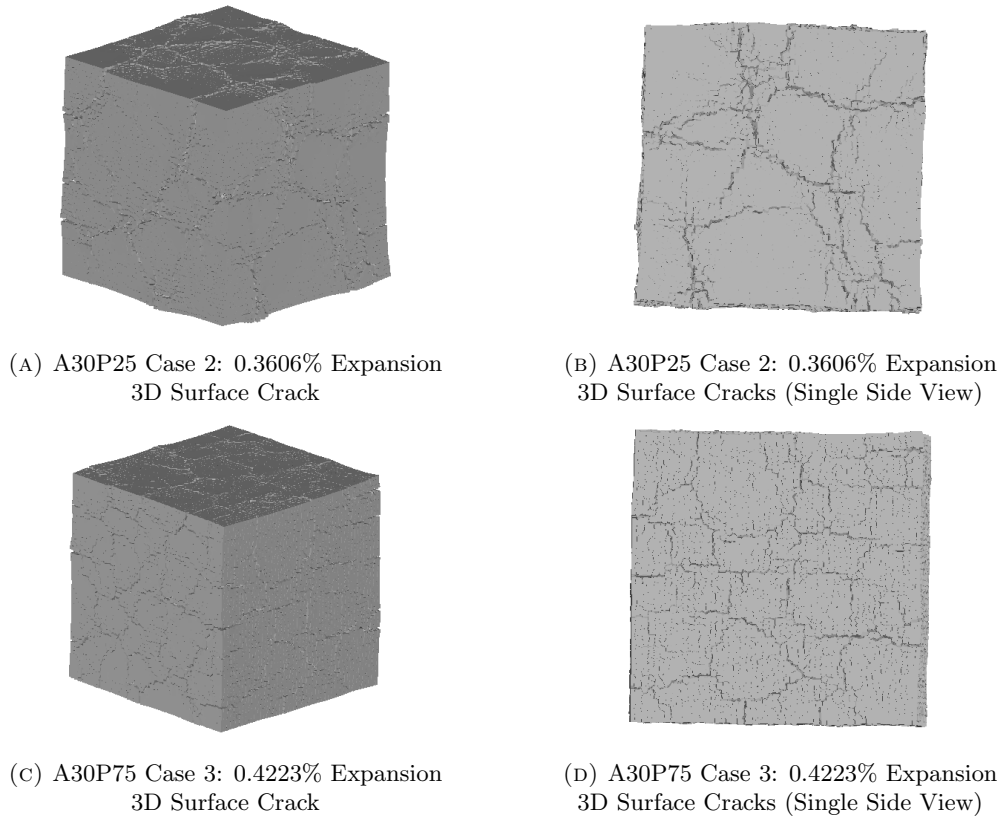


FIGURE 3.21: Comparing Between A30P25 and A30P75 3D Surface Cracks (Deformation x 10)

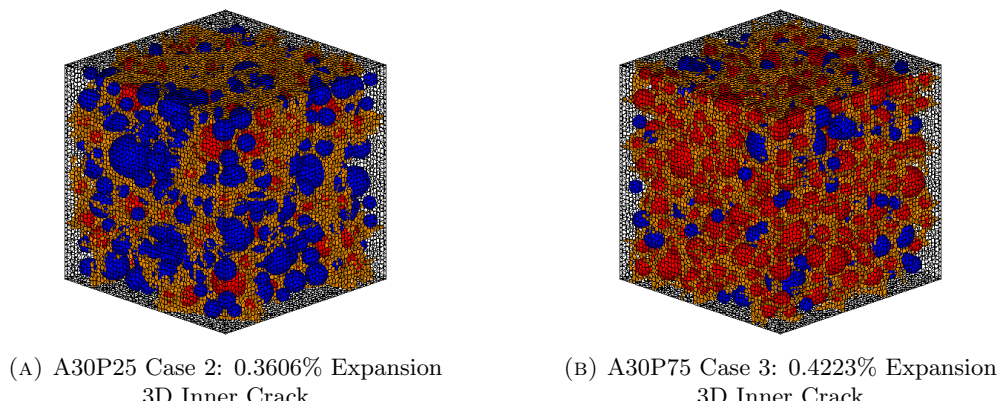


FIGURE 3.22: Comparing Between A30P25 and A30P75 3D Surface Cracks (Deformation x 10)

When numerically comparing their crack distribution summarised by its crack width (Table 3.7), it can be seen that cracking face number of larger cracks the case with 25% ASR reactive coarse aggregate is significantly higher, even when the global expansion ratio in 25% ASR reactive coarse aggregate is slightly smaller than 75% ASR reactive coarse aggregate case.

For the number of cracked interfaces larger than 0.003mm, 25% ASR reactive coarse

aggregate case is 2.15 times of 75% ASR reactive coarse aggregate case. And for the number of cracked interfaces larger than 0.01mm, 25% ASR reactive coarse aggregate case is 23.94 times of 75% ASR reactive coarse aggregate case.

This significant difference in crack distribution indicates consistsit with the global cracking patterns, suggest severe damage when considering the deterioration of the concrete structure.

3.3 Cracking Pattern caused by Pure DEF Expansion

3.3.1 Single DEF Expansion Simulation

In this section, the relationship between DEF intensified part range and concrete behavior during DEF expansion is simulated. The expanse is generated at the location of interfaces between paste element, to introduce the DEF expansion, as introduced in chapter 2.

For DEF expansion is highly related to the curing temperature concrete experienced, it is reasonable to considerate the inner part of the concrete structure should present more severe expansion comparing with outer part, due to its higher maximum experienced temperature during steam curing.

For surrounding part of the model, cases of non-expansion and gradually decreasing expansion are considered.

In this section, 100x100x100mm model is using. For comparison, 3 different cases are simulated, which are intensified 50x50x50mm at the center of the model, intensified 75x75x75mm at the center of the model, and intensified all part of the model (100x100x100mm).

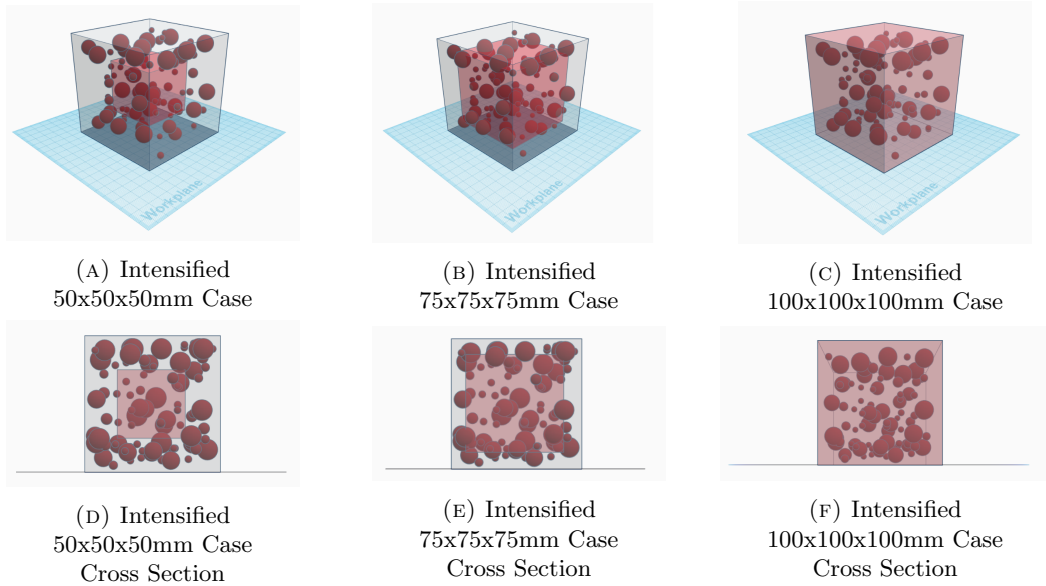


FIGURE 3.23: DEF intensified part range

This single example case showing here as an example has been choosing here use the model in the dimension of 100x100x100mm, with 30% aggregate, of which center 50x50x50mm have intensified DEF reactive, and the expanding giving to the model gradually decrease to 0 in the surrounded part.

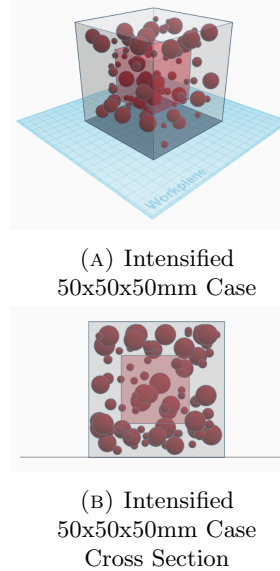


FIGURE 3.24: 50x50x50mm DEF intensified part range

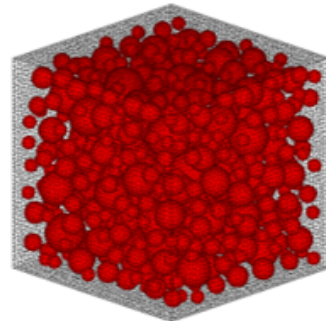


FIGURE 3.25: 30% Coarse Aggregate

Table. Aggregate consistent(if we have it)

To simulate DEF expansion, an initial strain of 0.0004mm is given in intensified DEF expanding area in each step, and the initial strain gradually decrease to 0 for surrounded parts, for totally 20 steps expansion.

Step	Expansion	Step	Expansion
1	0.000235	11	0.003061
2	0.000506	12	0.003355
3	0.000776	13	0.003650
4	0.001051	14	0.003949
5	0.001329	15	0.004249
6	0.001615	16	0.004555
7	0.001900	17	0.004865
8	0.002188	18	0.005175
9	0.002478	19	0.005487
10	0.002768	20	0.005795

TABLE 3.8: Expansion in Each Step for A30 Case 3

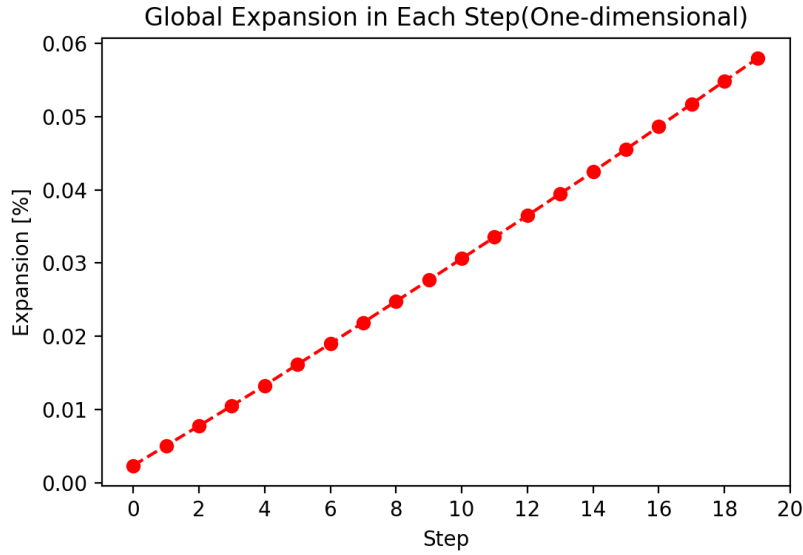


FIGURE 3.26: Global Expansion vs. Step

With the increasing of initial strain giving, the global expansion also gradually increasing. After 20 steps of DEF expansion, the model here reached 0.5795% expansion(one-dimensionally). Characteristic DEF map cracking pattern can be seen on the surface of the expanded concrete model in Figure 3.27.

In Figure ??, the inner distribution of cracked interface with width greater than 0.03mm is presented. It can be seen that the cracks are located with very clear patterns, concentrated in the inner part of the model. This inner cracking distribution pattern is very different with the cases ASR expansion.

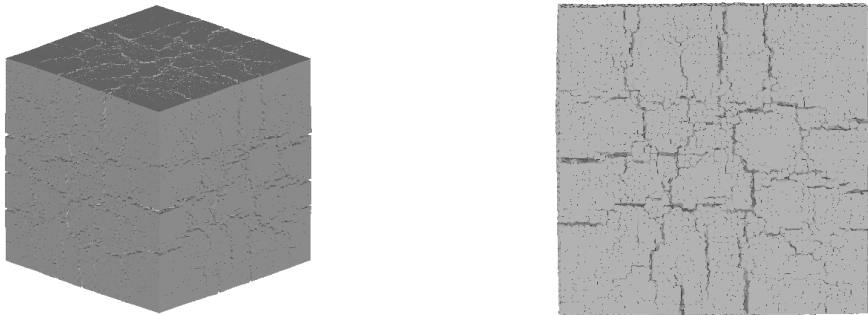


FIGURE 3.27: 3D Surface Cracks, 0.4223% Expansion (Deformation x 10)

As can be seen in Figure 3.29 the compressive stress (in red color) first concentrated in the part where initial strain is intensified given, and from step 1 to 20, unbalanced force penetrated in the concrete model, crack generated gradually around the aggregate and the surrounding part of the model.

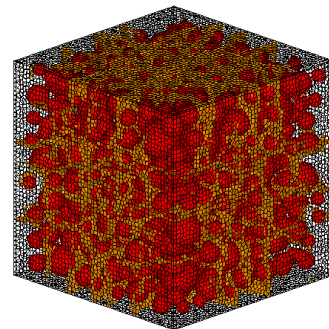


FIGURE 3.28: 3D Inner Cracks, 0.4223% Expansion

Same as previous in ASR expansion simulation, cracked interfaces are summarised in different crack width scale, shown in Table 3.9. The maximum crack width, in this case, is in range of 0.01-0.03mm, while most of the cracks still under 0.001mm. The number of cracked interfaces gradually decreases with the increase of crack width.

Crack Width [mm]	Total Cracked Interfaces
0.00000 - 0.00005	367538
0.00005 - 0.00010	328471
0.00010 - 0.00020	294472
0.00020 - 0.00050	251035
0.00050 - 0.00100	186058
0.00100 - 0.00300	133854
0.00300 - 0.01000	57421
0.01000 - 0.03000	1736
0.03000 - 0.10000	0
0.1000+	0

TABLE 3.9: Expansion in Each Step for A30 X0C Case 3

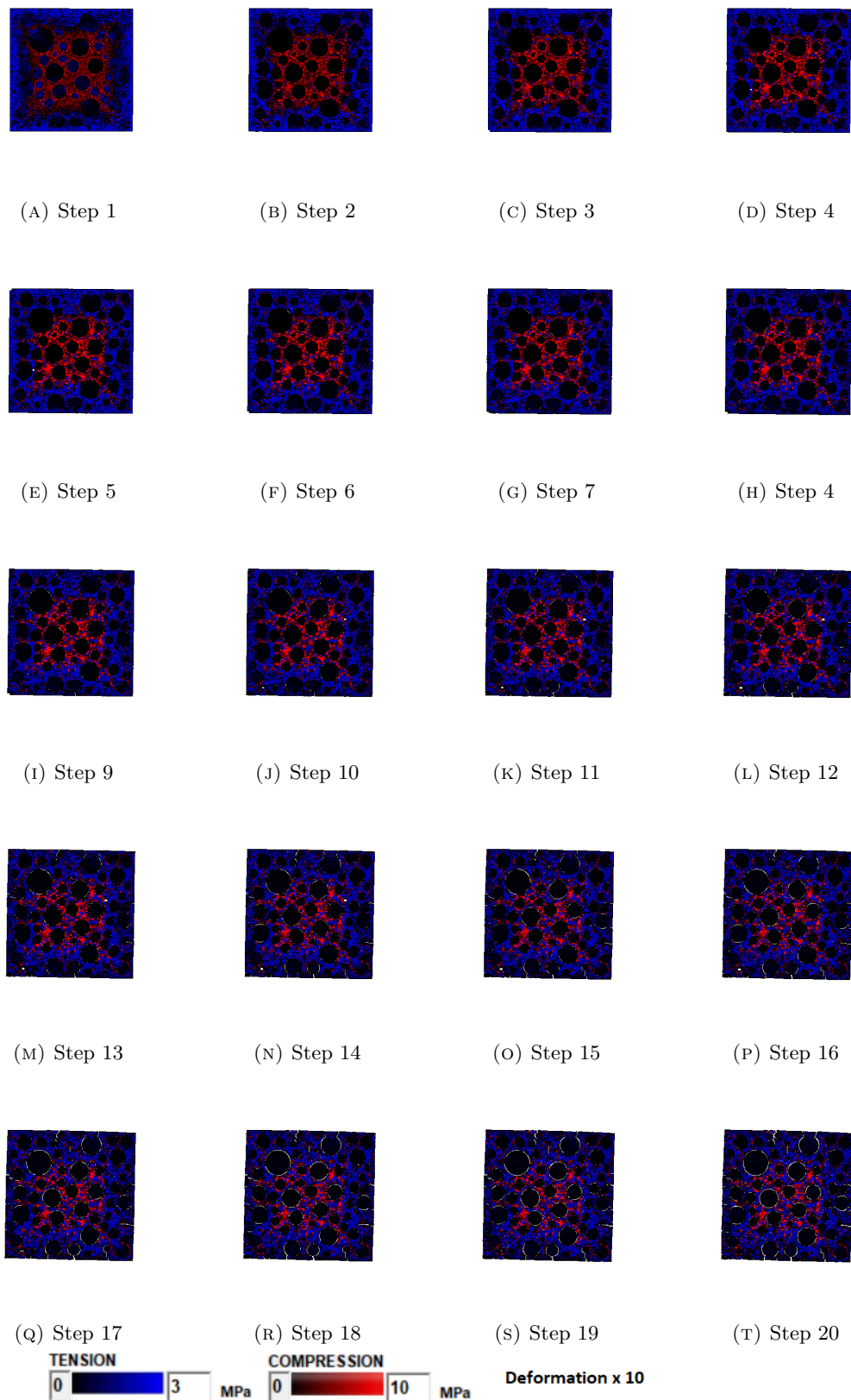


FIGURE 3.29: Internal Stress in Each Step for A30 X0C Case 3 (Deformation x 10)

3.3.2 Expansion Ratio Related to Behavior of Concrete During DEF Expansion

In this section, the relationship between given initial strain, final expansion and behavior during expansion is discussed.

Model in size of 100x100x100mm is used, with 30% Aggregate, and 25% area have intensified DEF reaction, while the expanding giving to the model gradually decrease to 0 in the surrounded part.

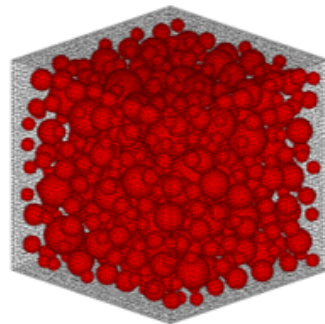


FIGURE 3.30: 30% Coarse Aggregate

Expansion is carried out with initial strain given in each step for intensified zone various from 0 to 0.0006mm. Initial strain given to the surrounding part of paste gradually decreasing to 0. Total expansion step are set as 20 steps same for all cases. From the Table 3.10 can be seen that with the increasing of giving initial strain in each step, the global expansion reached in step 20 also increased.

Aggregate Ratio[%]	Intensified DEF Reacting Area[%]	Initial Strain (Intensified Area, Each Step)	Expanding Steps	Final Expansion [%]
30	25	0	0	0
30	25	0.0001	20	0.1379
30	25	0.0002	20	0.2873
30	25	0.0004	20	0.5795
30	25	0.0006	20	0.8789

TABLE 3.10: One Dimensional Expansion Ratio in Single DEF Model Simulation

As shown in Figure 3.32 and Figure 3.33, it is clear that with the increase of global expansion ratio, the cracking can be seen on the surface of concrete model become much significant. However, the map cracking pattern does not change much comparing the expanded models in different expansion ratio.

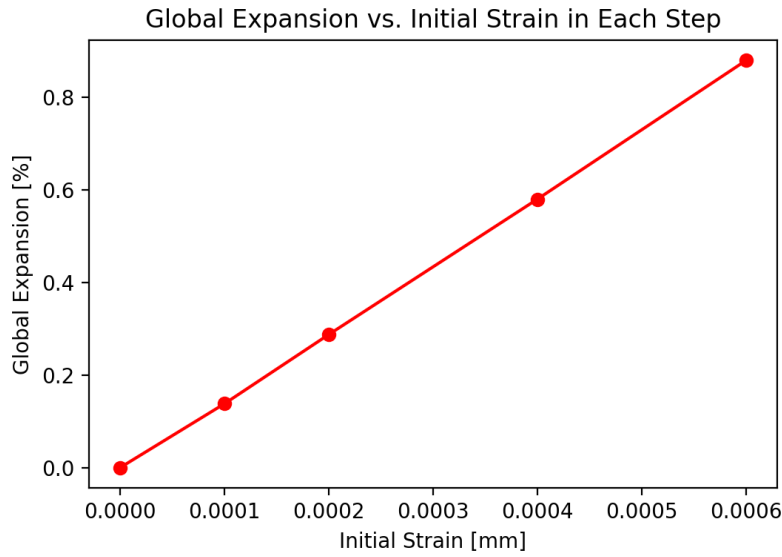


FIGURE 3.31: Global Expansion vs. Step

And in Figure 3.34, the internal cracking distribution in different global expansion cases are presented. It can be seen that the cross pattern of internal cracks gradually generate and penetrated, but still the pattern of its distribution dose not change in much. At small ratio of global exoansion, cracks are concentrated in the center of each surface, then penetrated to larger range with increasing of global expansion ratio.

This indicated that our simulation can still predict the map cracking behavior for DEF expansion in different deterioration levels.

In Figure 3.35, the internal stress distribution in some middle step and last expansion step are shown. By increasing the initial strain giving to present DEF expansion in each step, the expansion developed more rapidly and more cracks generated especially on the outside part of concrete sturcture. This result is consistent with the 3D cracking pattern presented earlier in this section, where cracks are generated in the surrounding part of the model.

This pattern of crack development is very different from ASR cases, and may suggests deterioration caused by DEF may not suffering severe inner structually damage inside as it looks from the surface.

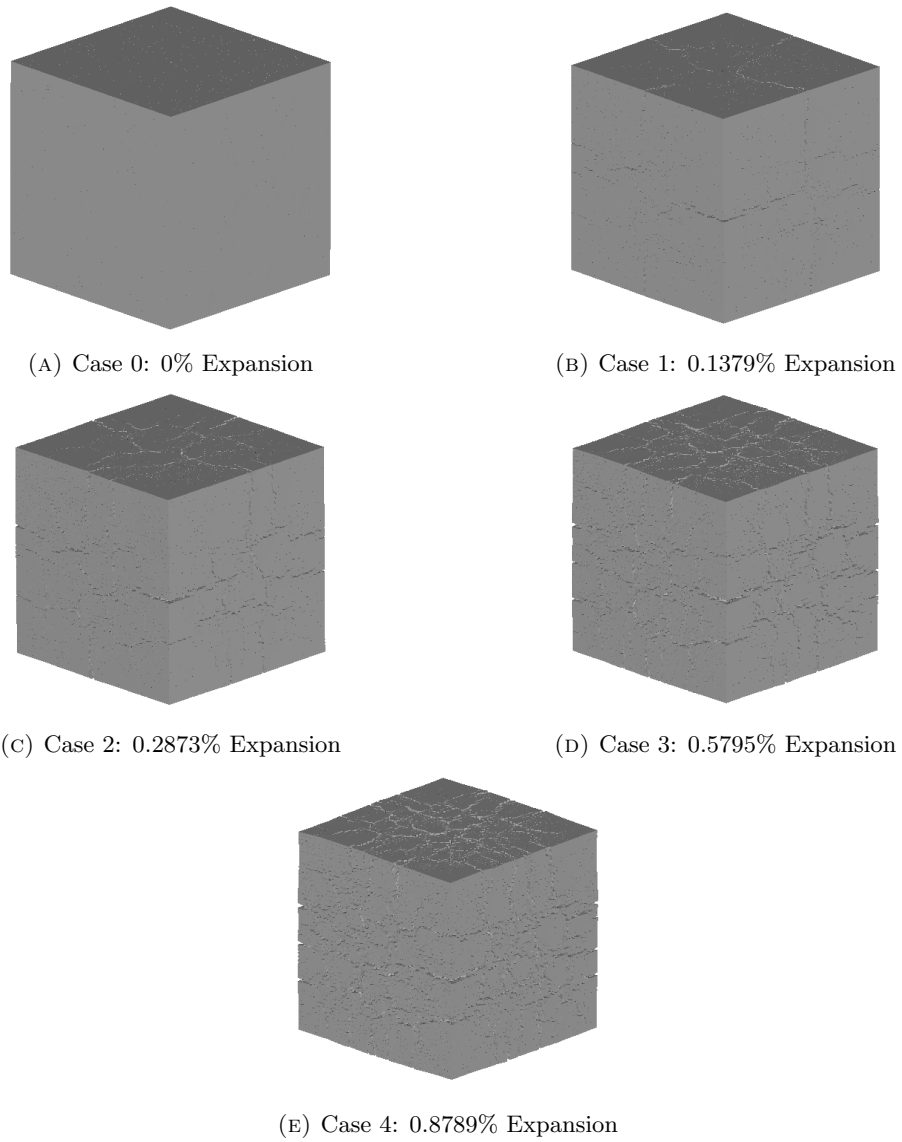
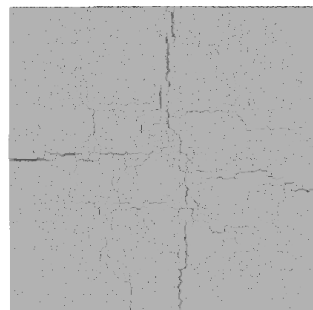
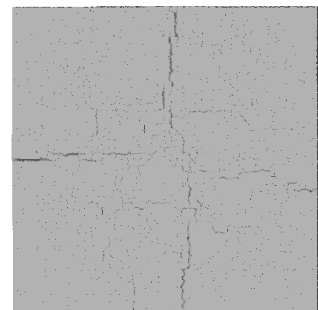


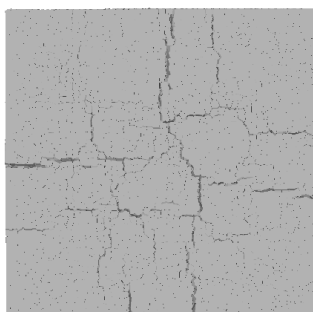
FIGURE 3.32: 3D Surface Cracks (Deformation x 10)



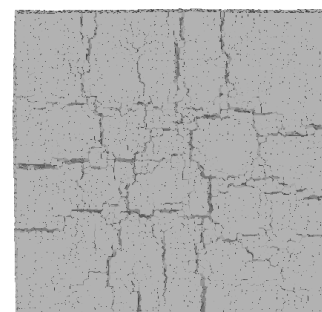
(A) Case 0: 0% Expansion



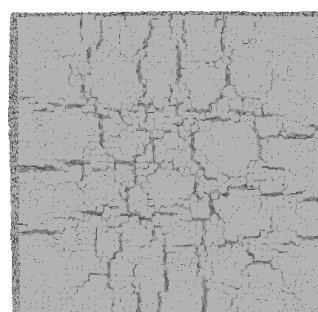
(B) Case 1: 0.1379% Expansion



(C) Case 2: 0.2873% Expansion



(D) Case 3: 0.5795% Expansion



(E) Case 4: 0.8789% Expansion

FIGURE 3.33: 3D Surface Cracks (Single Side View, Deformation x 10)

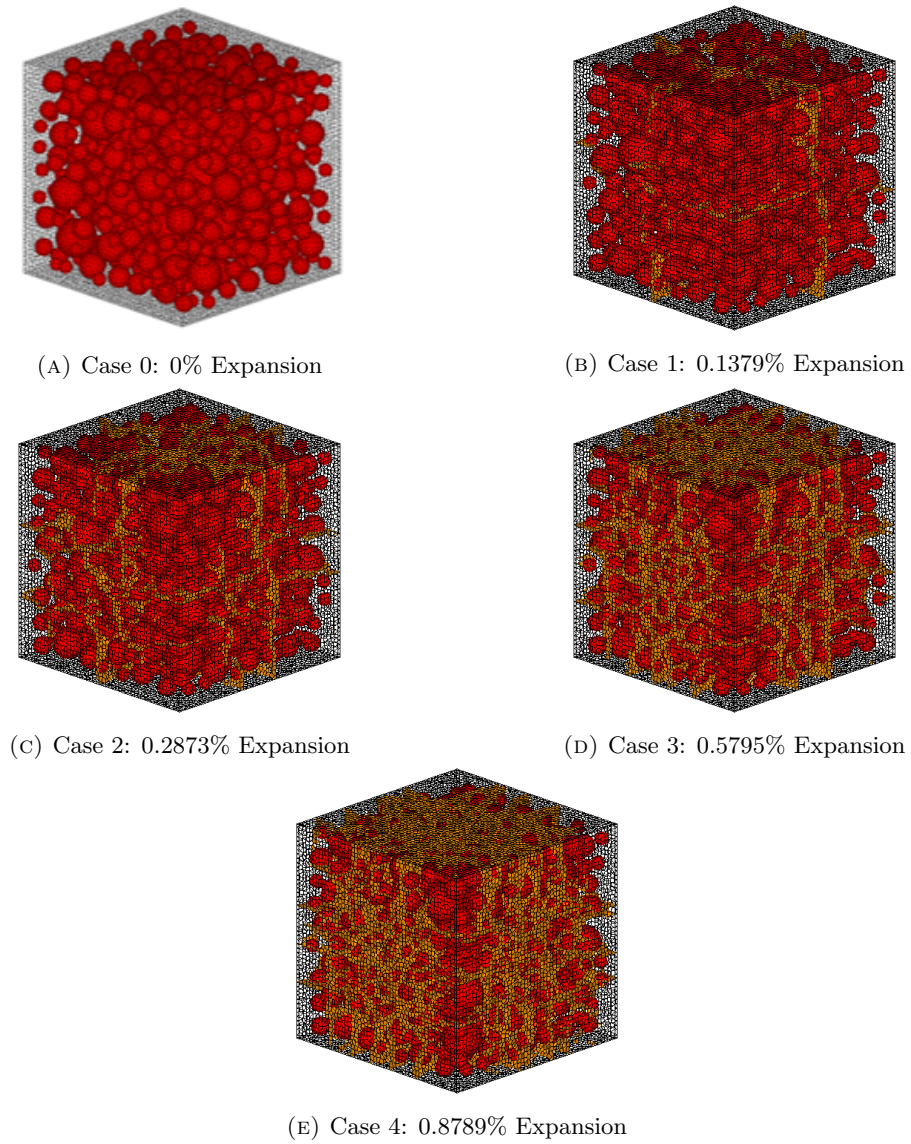


FIGURE 3.34: 3D Inner Cracks Larger than 0.03mm

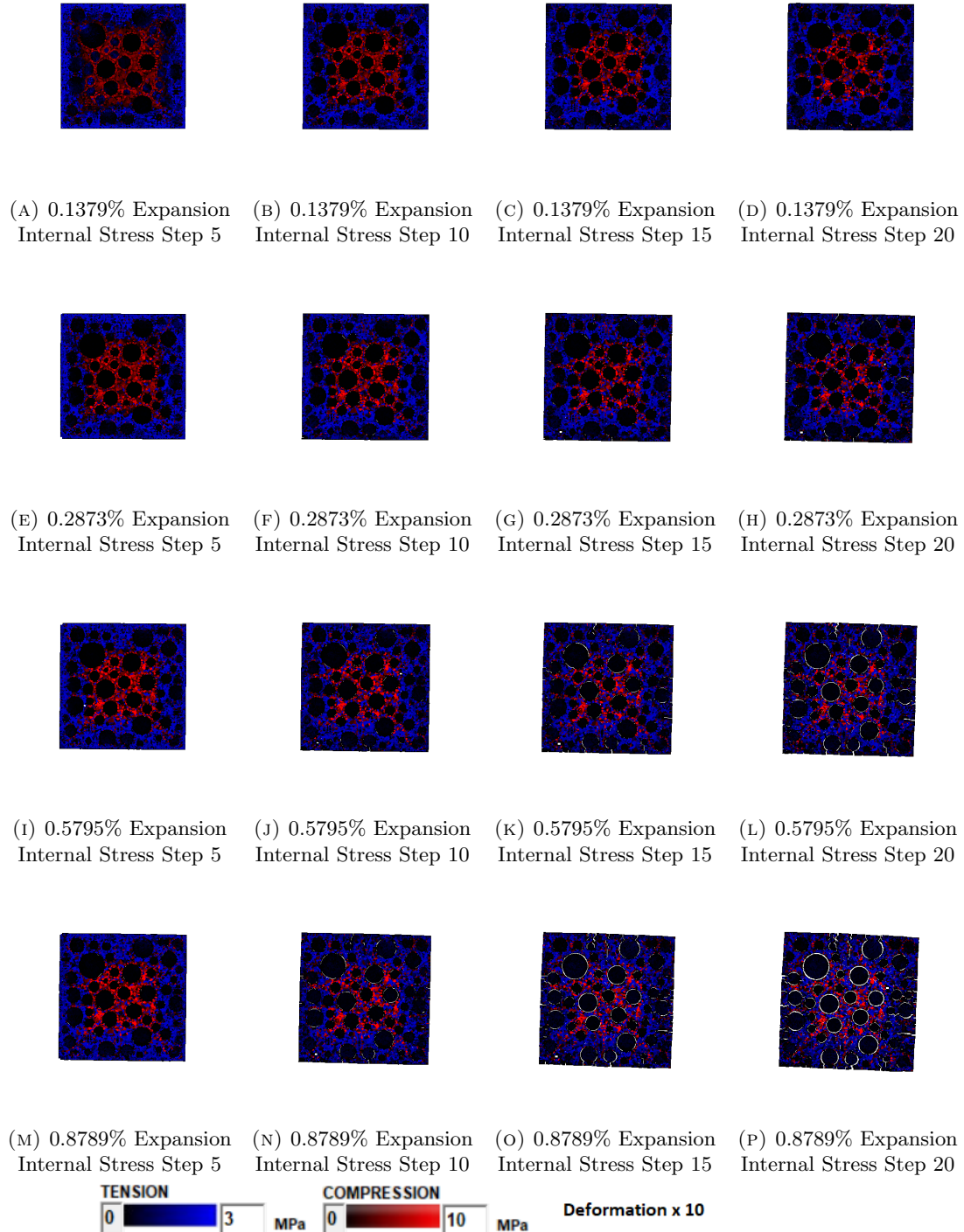


FIGURE 3.35: Generation of Internal Stress and Inner Cracks for DEF Expansion to Step 20(Final Expansion Step, Deformation x 10)

3.3.3 Aggregate Ratio Related to Behavior of Concrete During DEF Expansion

In this section, the relationship between aggregate ratio and behavior during expansion is discussed.

Expansion simulation result between 15% coarse aggregate model and 30% coarse aggregate model is compared here to analysis how the change in aggregate percentage influence the cracking pattern in different expansion ratio.



FIGURE 3.36: Coarse Aggregate Percentage

From Table 3.11 can be seen that with same expansion step and same initial strain given in each step, the global expansion of with less coarse aggregate (A15 cases here) is higher than less coarse aggregate cases (A30 cases here). As coarse aggregate ratio increased, DEF reactive interfaces decrease, which suggested the reason for achieving smaller global expansion in higher coarse aggregate cases.

Initial Strain (Each Step)	Expanding Steps	A15 Final Expansion	A30 Final Expansion[%]
0	0	0	0
0.001	20	0.1645	0.1379
0.002	20	0.3413	0.2873
0.004	20	0.6631	0.5795
0.006	20	0.9587	0.8785

TABLE 3.11: One Dimensional Expansion Ratio in Single DEF Model Simulation

Figure 3.38 and Figure ?? show surface crack pattern after DEF expansion of 15% coarse aggregate cases.

Here 2 cases from 15% coarse aggregate model and 30% coarse aggregate model in relatively close global expansion rate are compared to show the influence of coarse aggregate ratio on cracking pattern.

For the aggregate ratio of 15% model, case 3 is chosen, giving 0.0004mm initial strain for intensified DEF reactive interfaces, and reached 0.6631% one-dimensional expansion

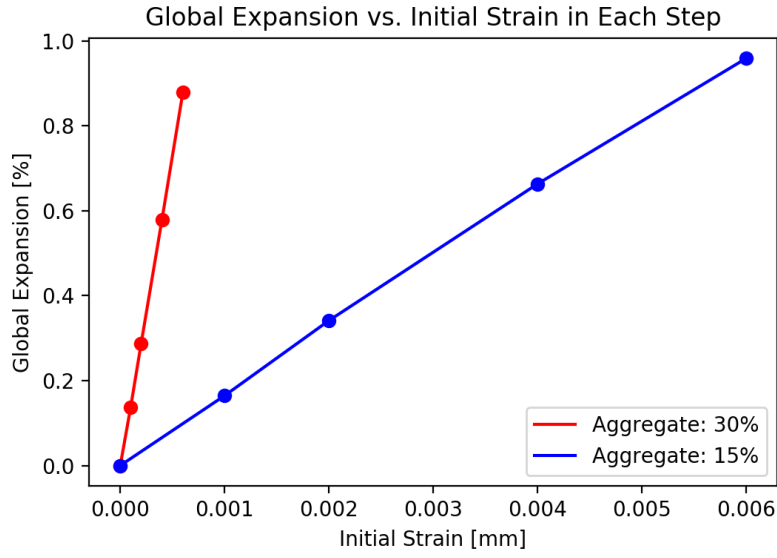


FIGURE 3.37: Global Expansion vs. Step

after 20 steps. And for the aggregate ratio of 30% model, case 3 is chosen, giving 0.004mm initial strain for DEF reactive interfaces and reached 0.5795% one-dimensional expansion after 20 steps.

If plot the global expansion with initial strain given in each step to simulate DEF expansion, it can be seen that model with higher percentage of aggregate reach higher global expansion in the same initial strain giving comparing to to lower aggregate content one.

This may caused by more complicated interaction between expanded pastes and aggregate.

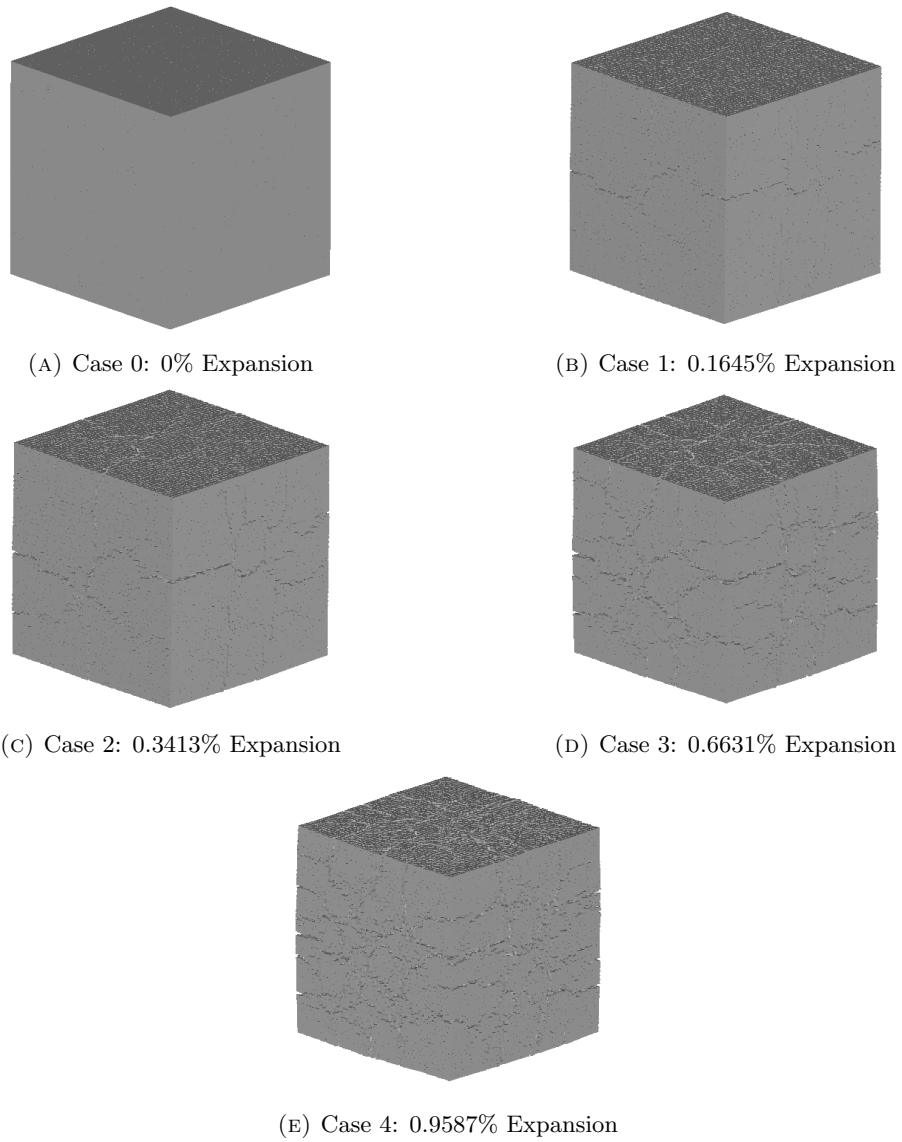


FIGURE 3.38: 3D Surface Cracks

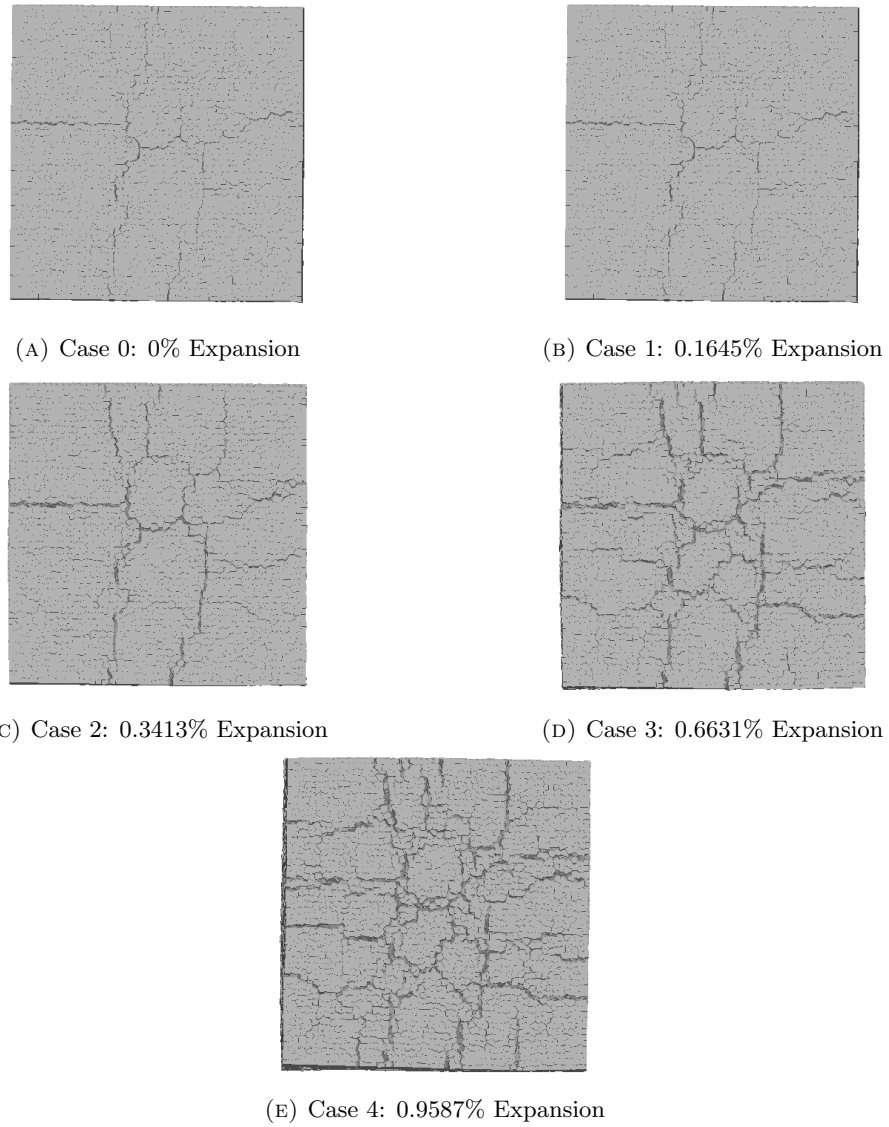


FIGURE 3.39: 3D Surface Cracks (Single Side View)

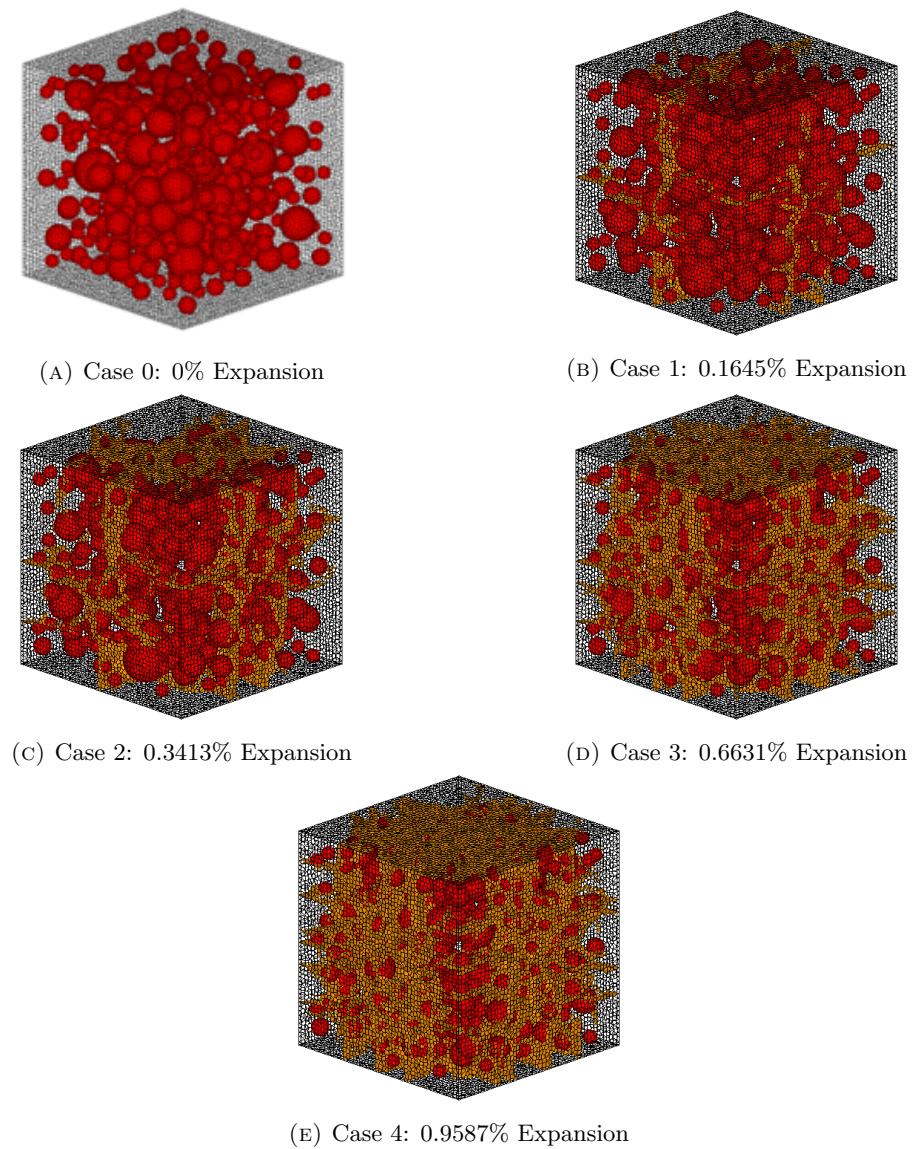


FIGURE 3.40: 3D Inner Cracks Larger than 0.03mm

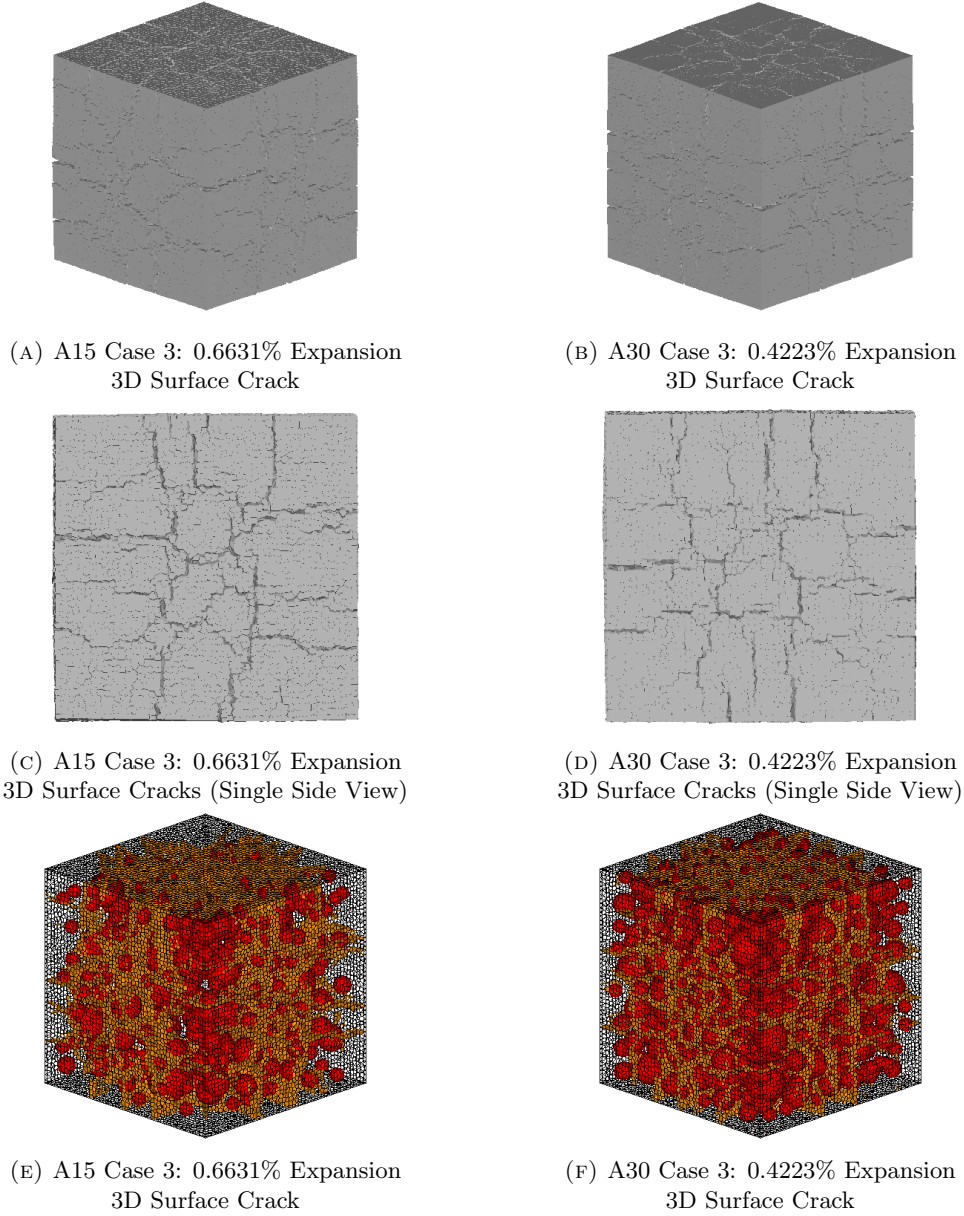


FIGURE 3.41: Comparing Between A15 and A30 3D Cracks

As can be seen in Figure 3.41, at a relatively close global expansion ratio, the crack pattern on the surface of the expanded model are also very similar. This indicated that aggregate ratio does not influence the behavior of DEF expansion so obviously as it does in ASR cases.

Clear characteristic map cracking which normally observed in DEF expanded concrete structures is presented in both cases.

Also, in Figure 3.41, the inner crack distribution of 2 cases are compared. Though it is difficult to tell the difference by naked eyes, if comparing the distribution of cracks

Crack Width [mm]	A15 Case 3 Total Cracked Interfaces	A30 Case 3 Total Cracked Interfaces
0.00000 - 0.00005	396456	367538
0.00005 - 0.00010	344516	328471
0.00010 - 0.00020	294996	294472
0.00020 - 0.00050	231816	251035
0.00050 - 0.00100	151693	186058
0.00100 - 0.00300	105939	133854
0.00300 - 0.01000	3983	57421
0.01000 - 0.03000	696	1736
0.03000 - 0.10000	0	0
0.1000+ 0.1000+	0	0

TABLE 3.12: Expansion in Each Step for A15P75 Case 3 and A30 P75 Case 3

numerically summarised by its crack width (Table 3.12), it can be seen that the distribution pattern is very close for 15% coarse aggregate case with 0.6631% global expansion and 30% coarse aggregate case with 0.5795% global expansion. The number of cracked faces decrease gradually when increasing the crack width.

However, if compare closer on relatively larger cracks, cracking face number of the case with 30% coarse aggregate is higher. For example, for the number of cracked interfaces larger than 0.003mm, 15% coarse aggregate case is 12.64 times of 30% coarse aggregate case. And for the number of cracked interfaces larger than 0.01mm, 30% coarse aggregate case is 2.49 times of 15% coarse aggregate case. Those larger cracks having more significant influence when the global cracking patterns are compared and should distribute more when considering the damage on the concrete structure. Though it is difficult to distinguish by naked eye, the cracking pattern in 30% coarse aggregate case is confirmed to be more concentrate with more large cracks in scale.

3.3.4 Expansion Intensified Part Range Related to Behavior of Concrete During DEF Expansion

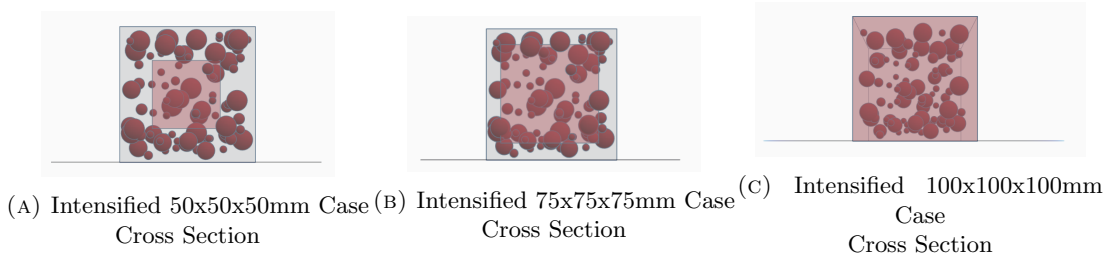


FIGURE 3.42: DEF intensified part range

In this section, DEF expansion simulation result of intensified center 75x75x75mm and uniformly expansion for all part (intensified center 100x100x100mm) is presented.

3.3.4.1 Expansion Intensified 75x75x75mm at Center of Model

Initial Strain (Each Step)	Expanding Steps	Final Expansion[%]
0	0	0
0.001	20	0.1671
0.002	20	0.3380
0.003	20	0.5118
0.005	20	0.8577

TABLE 3.13: One Dimensional Expansion Ratio in Expansion Intensified 75x75x75mm at Center of Model DEF Model Simulation

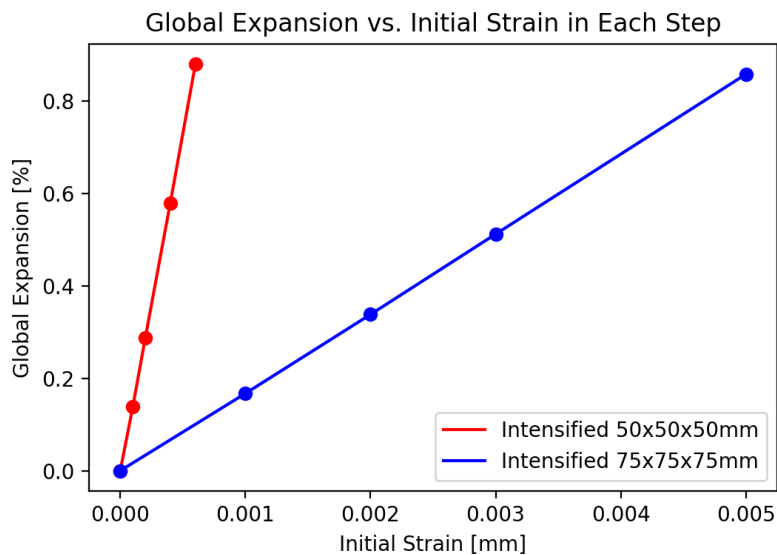


FIGURE 3.43: Global Expansion vs. Step

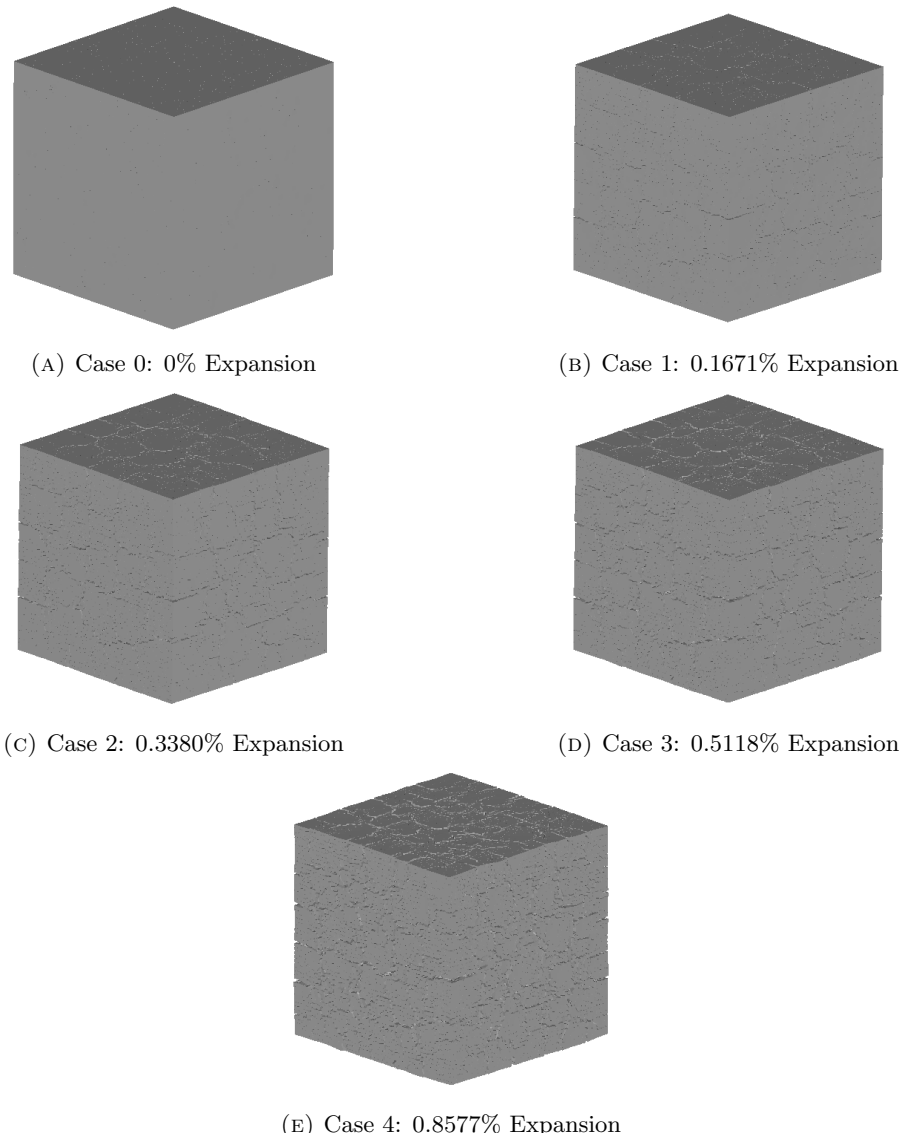


FIGURE 3.44: 3D Surface Cracks Expansion Intensified 75x75x75mm (Deformation x 10)

3.3.4.2 Expansion Intensified 100x100X100mm at Center of Model

Initial Strain (Each Step)	Expanding Steps	Final Expansion[%]
0	0	0
0.001	20	0.2
0.002	20	0.4087
0.004	20	0.6191
0.006	20	1.0454

TABLE 3.14: One Dimensional Expansion Ratio in Expansion Intensified 100x100X100mm at Center of Model DEF Model Simulation

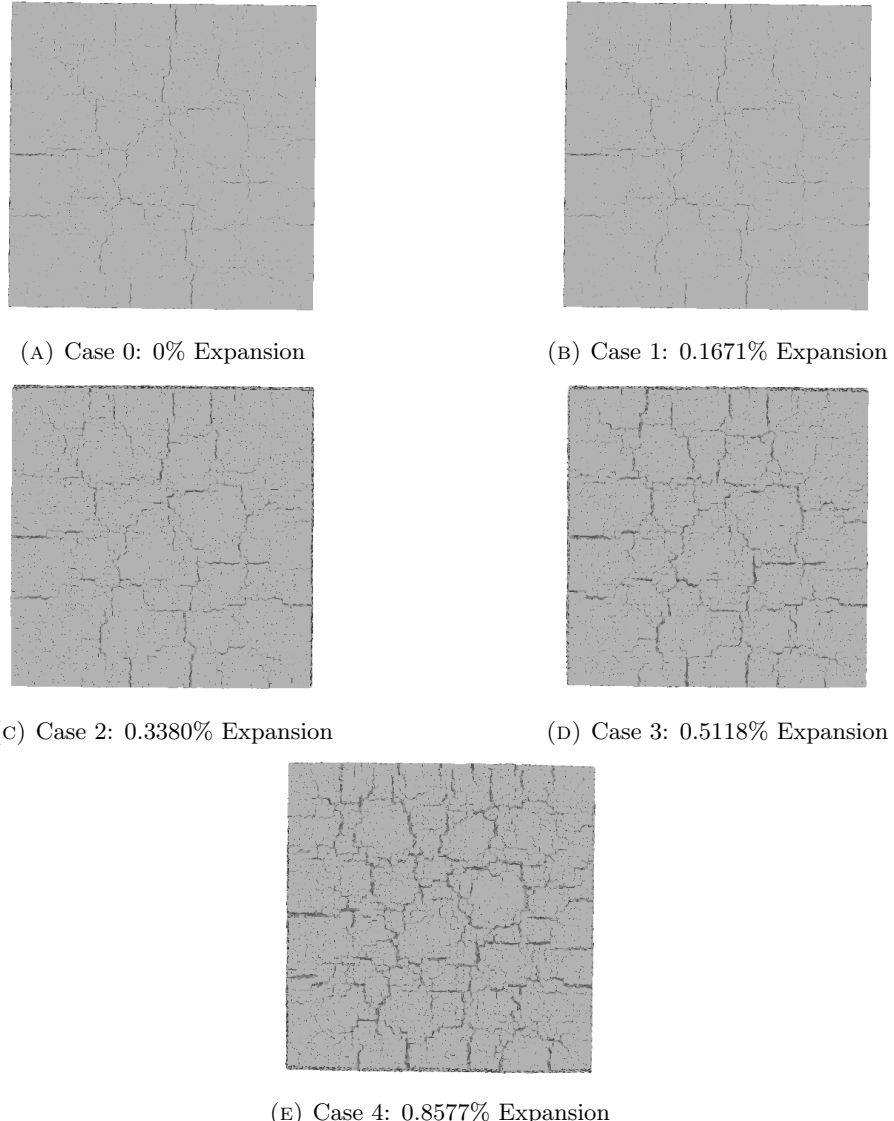


FIGURE 3.45: 3D Surface Cracks (Single Side View) Expansion Intensified 75x75x75mm (Deformation x 10)

From Figure ??, Figure 3.45, Figure ?? and Figure 3.49, it can be seen that when intensified the DEF expansion at the center 75x75x75mm, still the characteristic map cracking pattern can be achieved, which is similar to 50x50x50mm case.

However, when comparing to uniformed overall expansion (DEF expansion at the center 75x75x75mm), the increasing of the concrete volume is achieved without generating significant surface cracks. This simulation result is correlated with the research result done by L.Eddy et.al., 2016, concluded as the simply uniformed paste expansion does not present DEF simulation well as it behaves in reality.

When examined closely of the intersection, it can be seen that no inner crack is happening in the paste for the uniformed expanding case, separation only happens between the

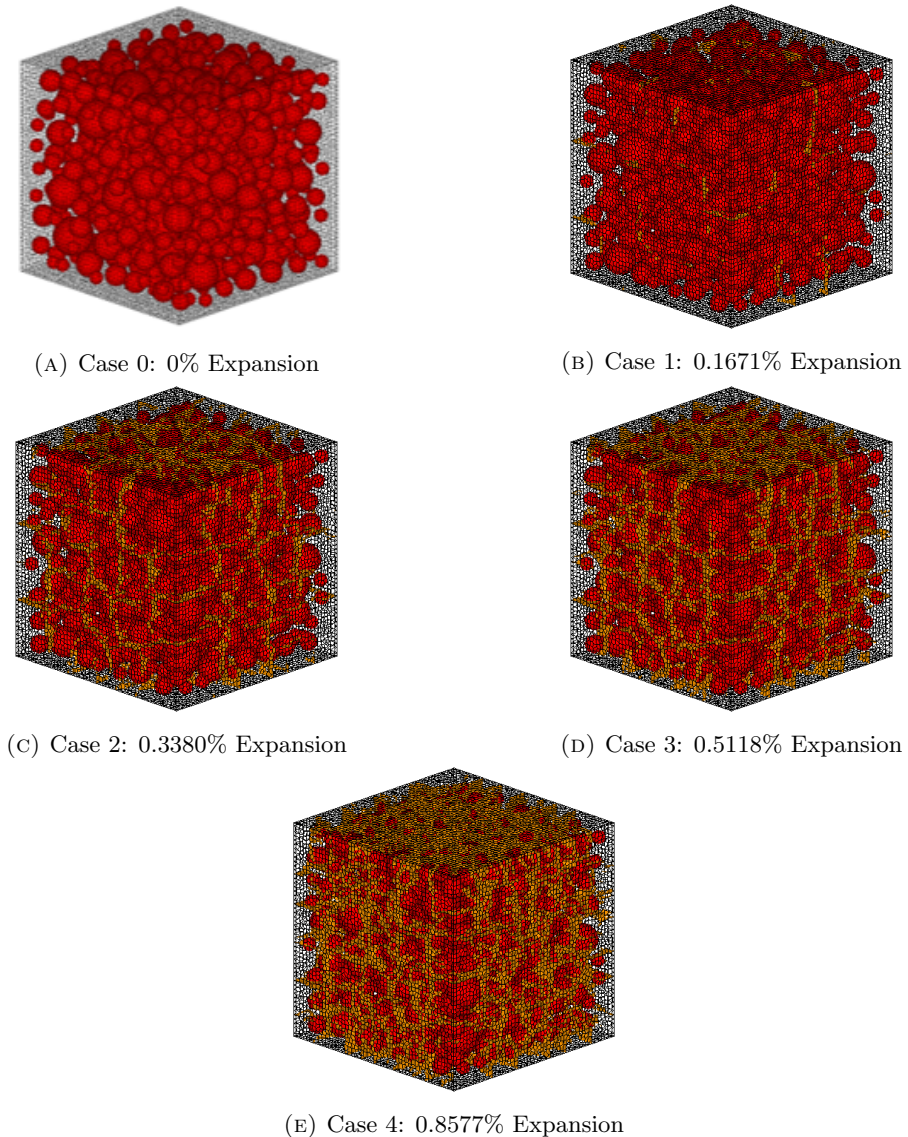


FIGURE 3.46: 3D Inner Cracks Expansion Intensified 75x75x75mm

surface of aggregate and paste, which is different with other 2 cases.

With expansion intensified in the inner part of concrete model, the compressive force concentrated in the inner part of the model, while outer parts are under tension. This unbalanced force generates cracks at the surrounding part of the concrete, preset as map cracking pattern at the surface view. This cracking pattern is also correlated with the observation form A.Awasthi in his investigation of DEF deteriorated Indian concrete sleeper in 2016.

Figure here.

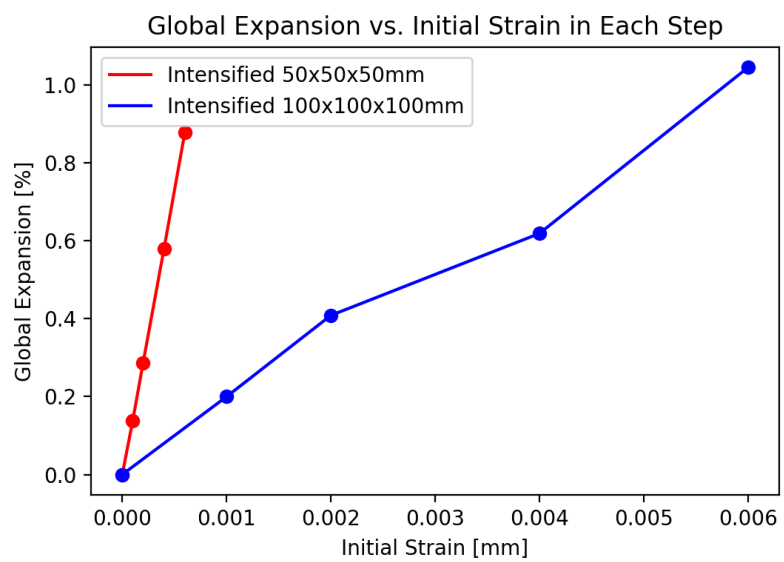


FIGURE 3.47: Global Expansion vs. Step

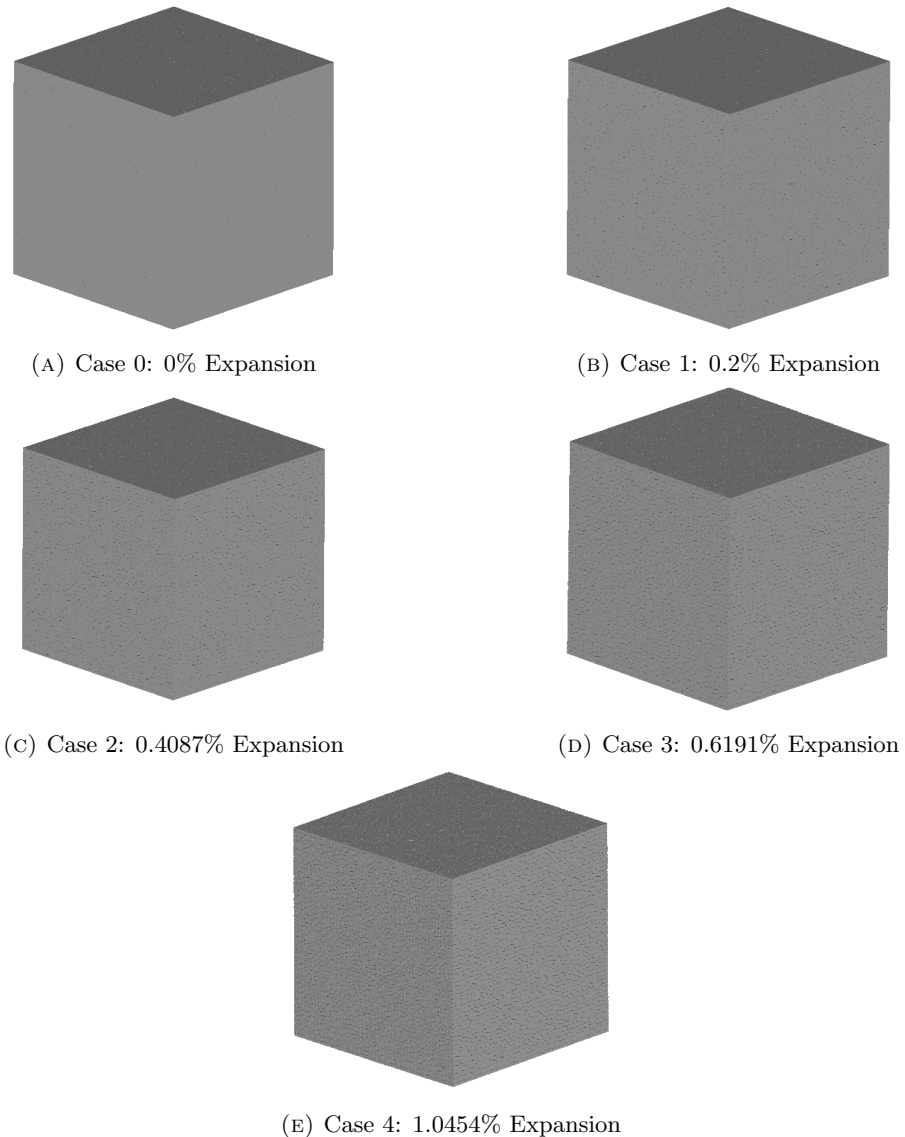


FIGURE 3.48: 3D Surface Cracks Expansion Intensified 100x100X100mm (Deformation x 10)

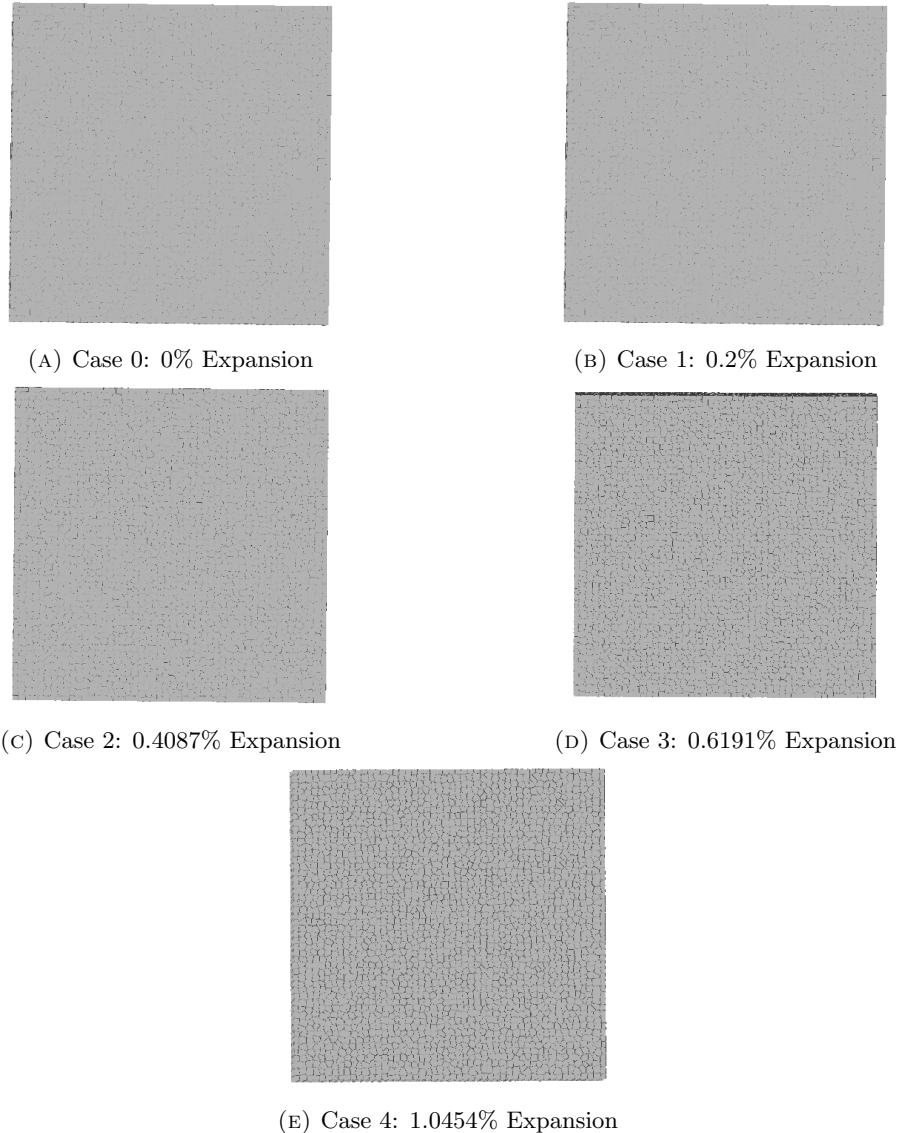


FIGURE 3.49: 3D Surface Cracks (Single Side View) Expansion Intensified
100x100X100mm (Deformation x 10)

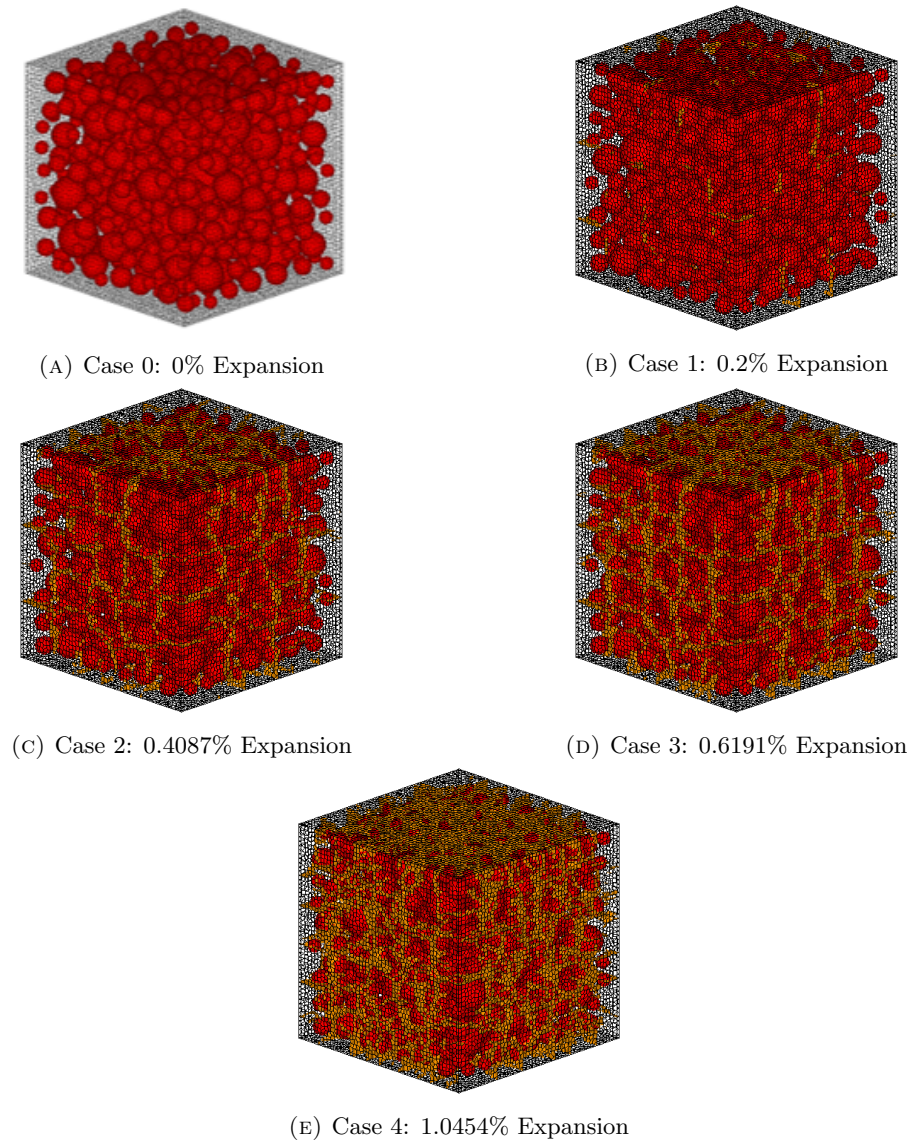


FIGURE 3.50: 3D Inner Cracks Expansion Intensified 100x100X100mm (Deformation x 10)

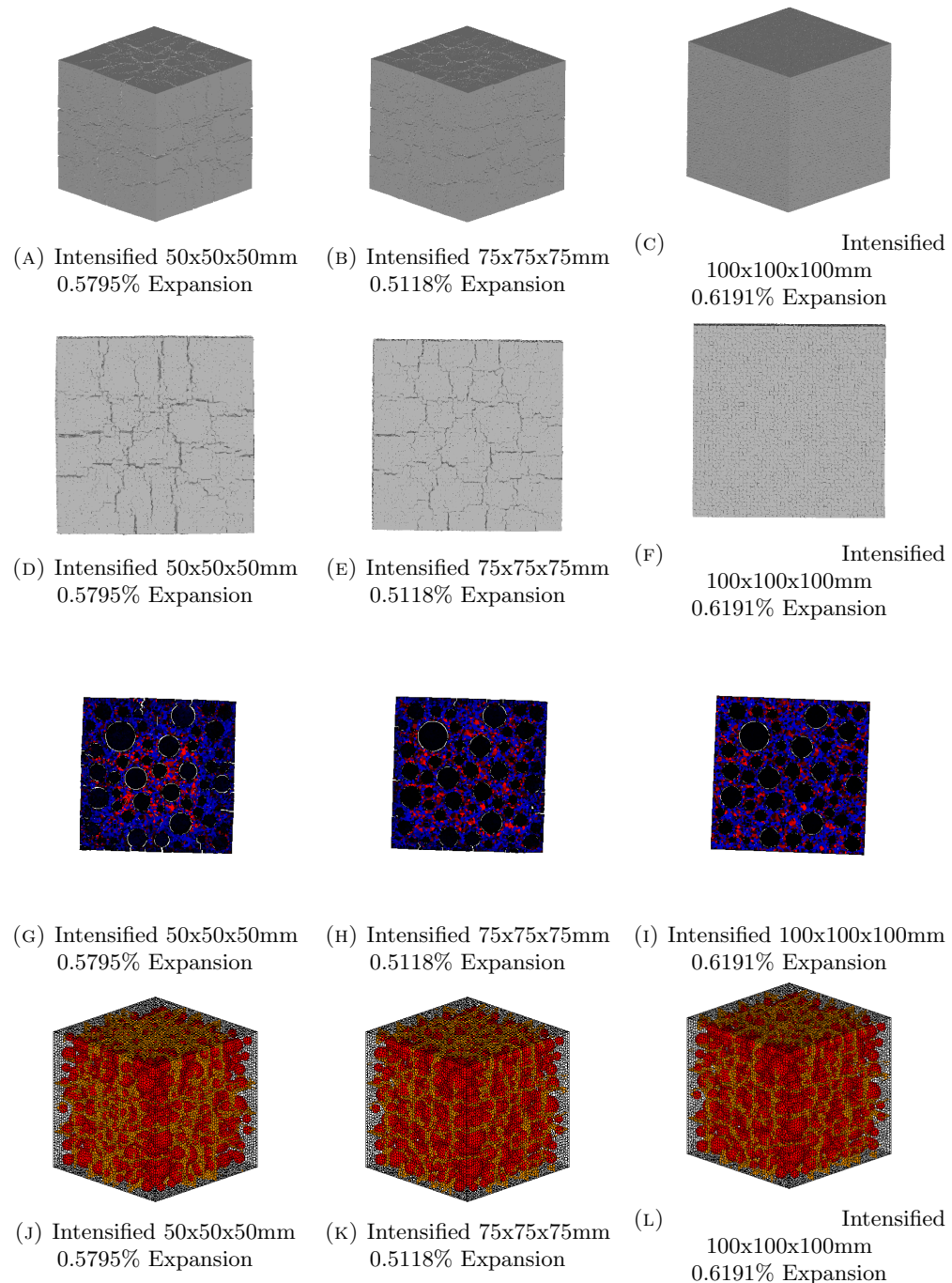


FIGURE 3.51: Comparing between different DEF Expansion Intensified Cases

3.4 Comparing Between ASR Expansion and DEF Expansion Simulation Result

Here the 2 expansion simulation results are compared to analysis the similarities and difference between ASR and DEF expansion.

For ASR, 100x100x100mm model with 30% aggregate is chosen, of which 75% of total aggregates are ASR reactive.

For DEF, same 100x100x100mm model with 30% aggregate is using, of which the 75x75x75mm at the center part is given intensified DEF expansion, and decreased gradually in the surrounding part.

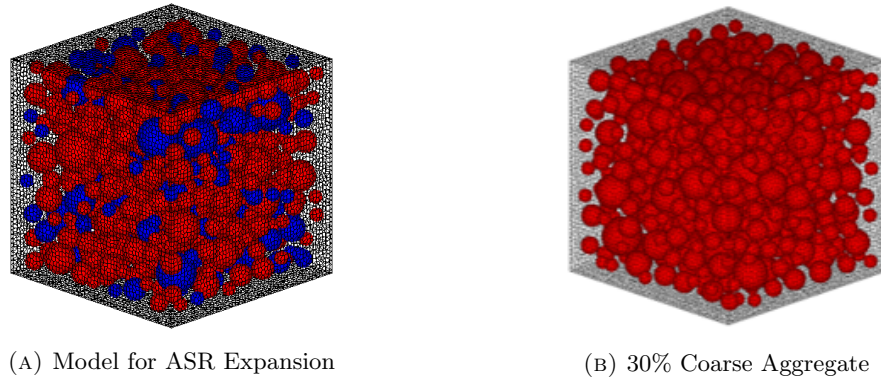


FIGURE 3.52: Model for DEF Expansion

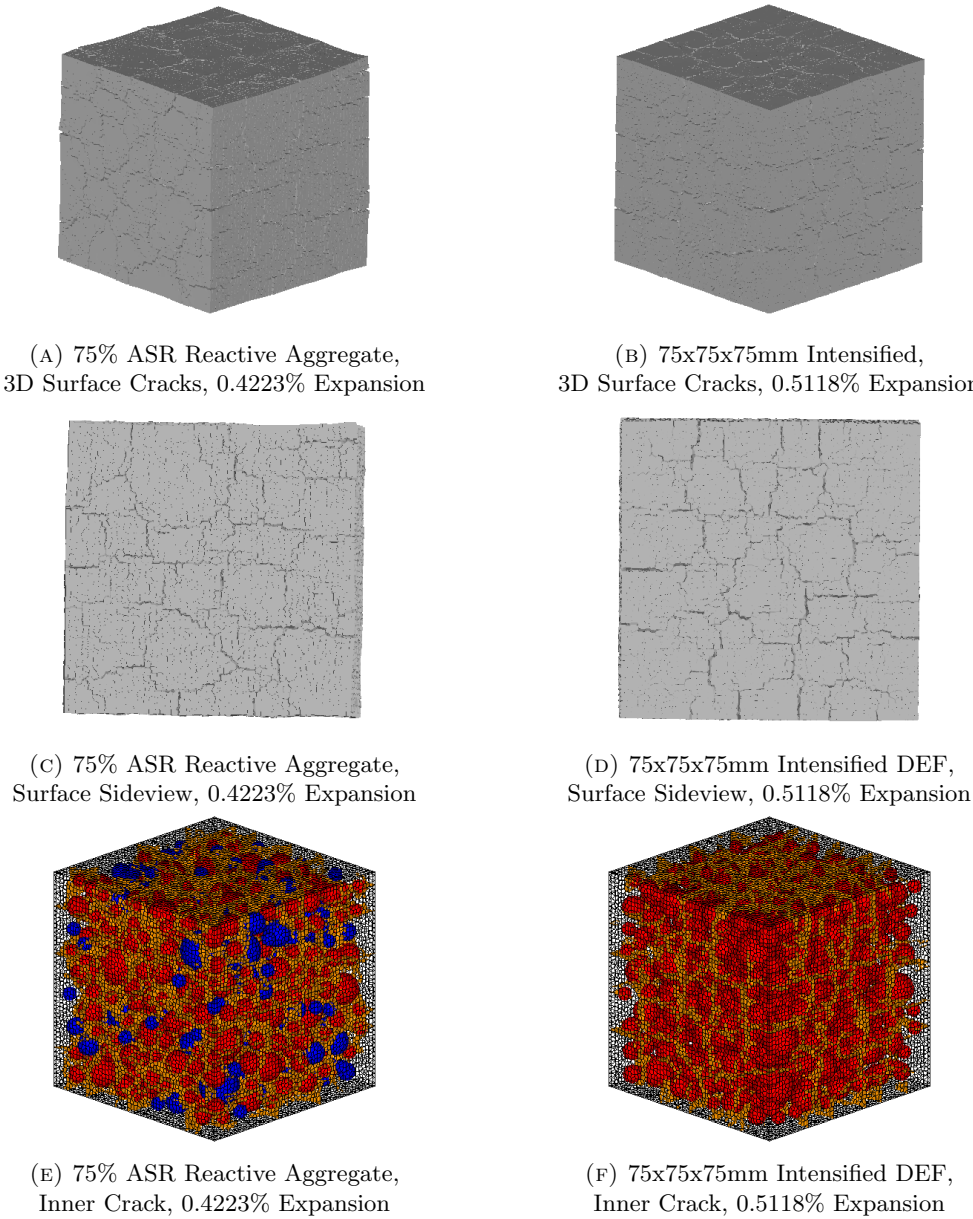


FIGURE 3.53: Cracks Compare Between ASR Expansion and DEF Expansion Simulation Result

From Figure it can be seen that at a relatively close global expansion ratio, the surface cracking pattern of ASR expansion and DEF expansion can be very close.

However, the inner crack distribute is not exactly the same in these 2 cases. Clear cross alike distribution can be seen in DEF expanded case but not in ASR case.

This can also be confirmed by the cross-section view (Figure 3.54), where in middle of each face of DEF expanded model concentration of crack perpendicular to surface is shown. Besides, for the DEF expansion, the inner part of the model is more integrated comparing to ASR case, with almost no crack inside.

This may indicate with similar outside cracking damage level, deterioration caused by DEF expansion is less severe compared with ASR expansion.

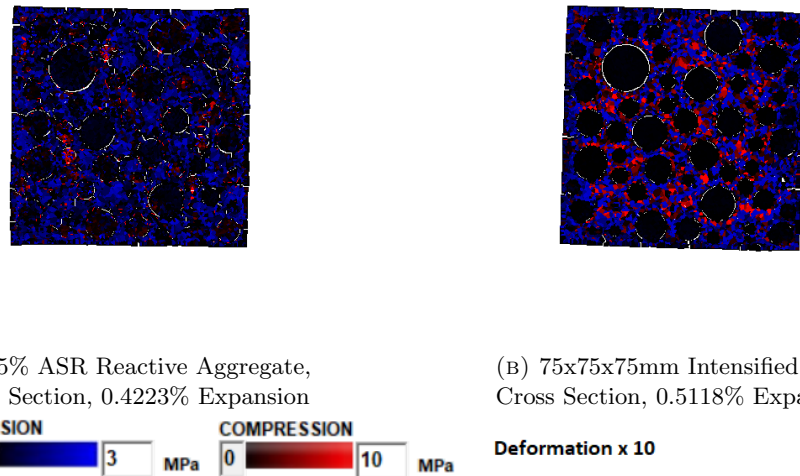


FIGURE 3.54: Cross Section Compare Between ASR Expansion and DEF Expansion Simulation Result (Deformation x 10)

Crack Width [mm]	ASR A30P75 0.4223% Expansion Total Cracked Interfaces	DEF A30I75 0.5118% Expansion Total Cracked Interfaces
0.00000 - 0.00005	316744	373019
0.00005 - 0.00010	286704	335814
0.00010 - 0.00020	263943	299690
0.00020 - 0.00050	234672	249242
0.00050 - 0.00100	183238	177030
0.00100 - 0.00300	131553	113350
0.00300 - 0.01000	42432	42207
0.01000 - 0.03000	275	240
0.03000 - 0.10000	0	0
0.1000+ 0	0	0

TABLE 3.15: Expansion in Each Step for A30 P75 Case 3

PLOT

When comparing the cracked interfaces grouped by the width of crack (Table 3.15), it also can be seen that comparing to ASR expansion, cracks in DEF expansion simulation result is more concentrated in smaller crack width, which is under 0.001mm in this comparison.

ASR and DEF expansion, though similar on their surface cracking, are different in their mechanism and inner condition. And the simulation used in this research can properly reproduce not only the similarities but also the difference between them.

Chapter 4

Simulation of Residual Mechanical Capabilities Of ASR and DEF Expanded Concrete

4.1 General

In this chapter, three-dimensional expanded concrete models are tested under uni-axial compression condition. The purpose of this study is for the prediction of the behavior and residual capacity of ASR or DEF expanded concrete, especially in uni-axial compression.

Displacement of loading boundary is controlled in this analysis. In each step of loading, the top boundary of the concrete model moves downwards 0.02mm.

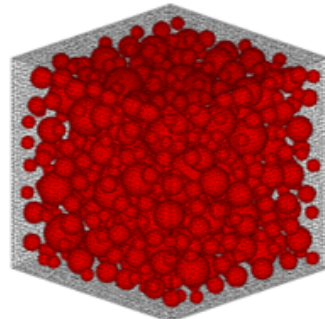


FIGURE 4.1: 30% Coarse Aggregate

Figure 4.2 and Figure 4.3 here presented the internal stress condition of 2 example cases for ASR and DEF loading of Fixed boundary condition, separately. In Figure , 100x100x100mm model with 30% coarse aggregate is used, of which 75% of all coarse aggregates are ASR reactivated. While for DEF, same 100x100x100mm model with 30%

coarse aggregate is used, of which the center 75x75x75mm part has been given intensified DEF expansion, and gradually decrease until reaching the surface of the model.

It can be seen that with the increasing of vertical displacement applied to the expansion damaged models, compressive force generated in the concrete model, and X shape cracking developed gradually until the failure of the structure is reached.

The internal stress reaction of ASR and DEF expanded concrete model is relatively close, but the maximum Compressive Strength and Elastic Modulus does show some of the differences.

And when considering free boundary condition loading, as presented in Figure H.1, the top and bottom of the concrete model can move freely in horizontal directions, thus the X-shape cracking pattern shown in fix boundary loading cases does now show up here.

Figure Free Loading Internal Stress

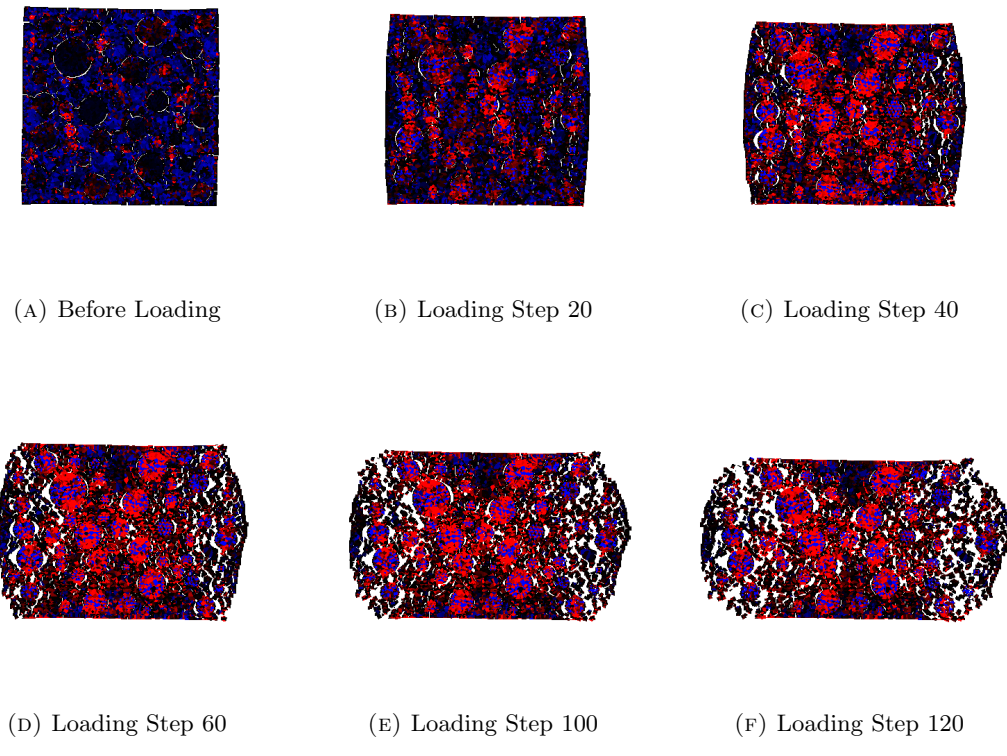


FIGURE 4.2: ASR Loading

As for the displacement change in each step, Compressive Strength is also recorded to show the residual mechanical properties of the expanded model. Besides, Elastic Modulus will also be calculated from the plotting of the load-displacement graph.

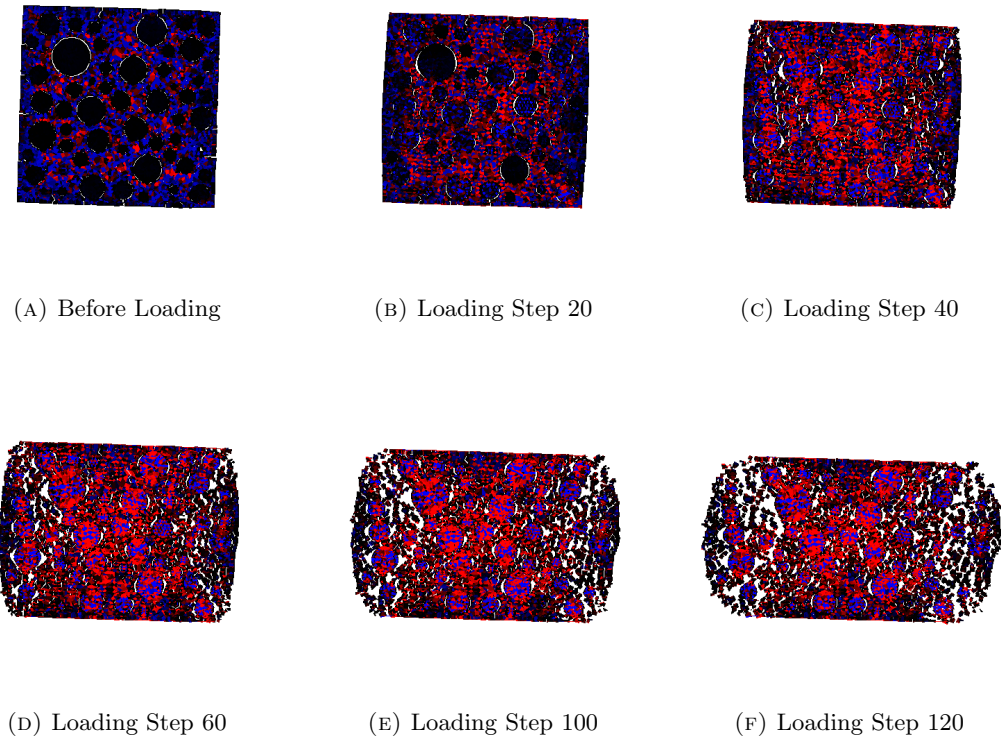


FIGURE 4.3: DEF Loading

4.1.1 Overview of Experimental Results of Residual Mechanical Properties After ASR Expansion

4.1.2 Overview of Experimental Results of Residual Mechanical Properties After DEF Expansion

4.2 Residual Capabilities after Pure ASR Expansion

Here the uni-axial compression test result for ASR expanded concrete model is summarised.

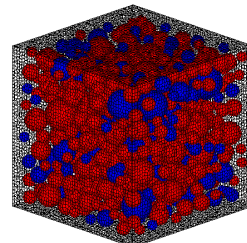


FIGURE 4.4: 30% Coarse Aggregate

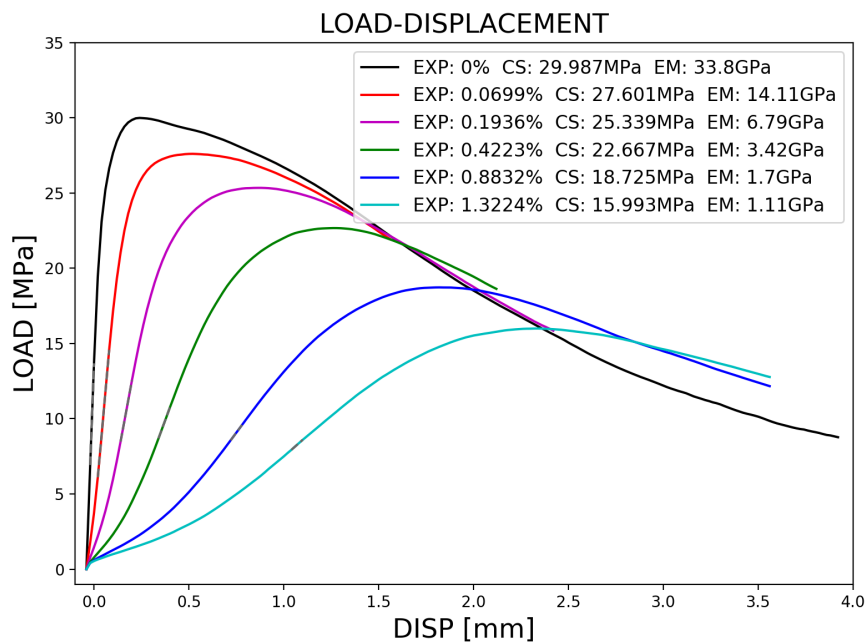


FIGURE 4.5: A30 P75 Fix Load-Displacement

Initial Strain (Each Step)	Expanding Steps	Final Expansion [%]	Maximum Compressive Strength in Fix Loading Condition [MPa]	Maximum Compressive Strength in Free Loading Condition [MPa]
0	0	0	29.987	19.897
0.0002	20	0.0699	27.601	13.889
0.0005	20	0.1936	25.339	9.8203
0.001	20	0.4223	22.667	7.4466
0.002	20	0.8832	18.725	5.8732
0.003	20	1.3224	15.993	

TABLE 4.1: One Dimensional Expansion Ratio in Single ASR Model Simulation

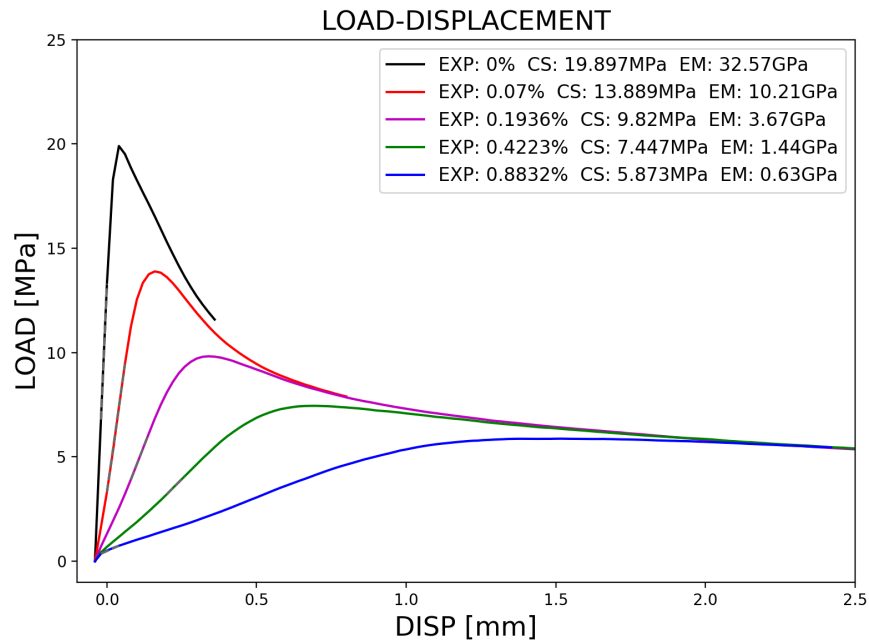


FIGURE 4.6: A30 P75 Free Load-Displacement

From the Figure 4.5 and Figure 4.6 it can be seen that with the increasing of given initial strain in each step, its global expansion ratio also increasing, and both maximum compressive strength in fix boundary condition and free boundary condition gradually decrease.

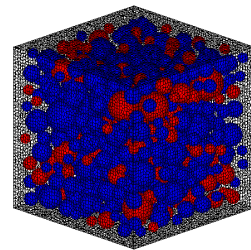


FIGURE 4.7: 30% Coarse Aggregate

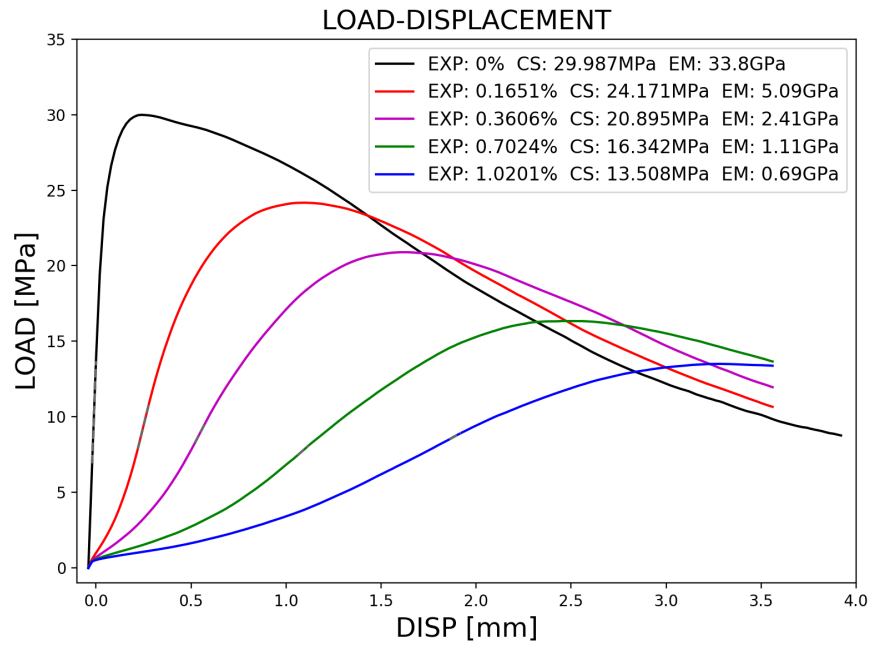


FIGURE 4.8: A30 P25 Fix Load-Displacement

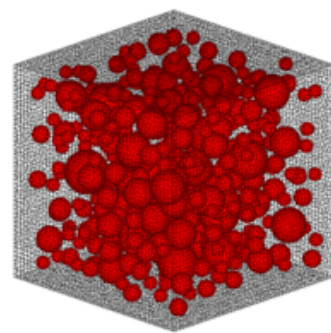


FIGURE 4.9: 15% Coarse Aggregate

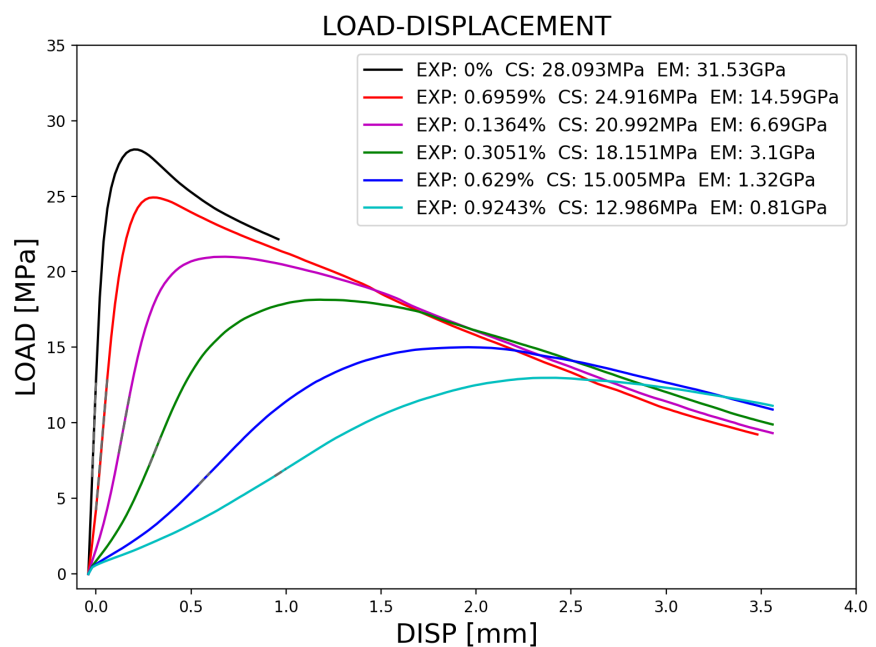


FIGURE 4.10: A15 P75 Fix Load-Displacement

4.3 Residual Capabilities after Pure DEF Expansion

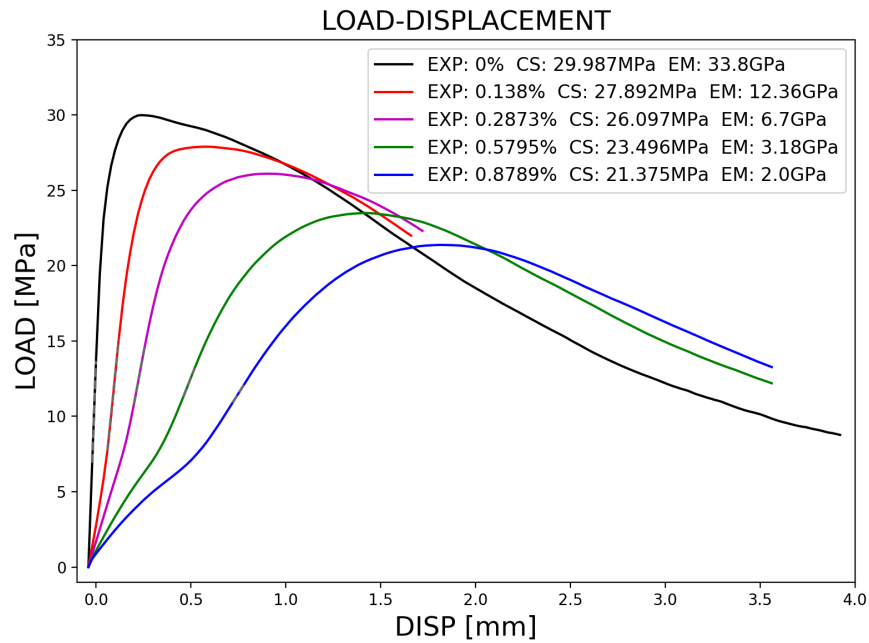


FIGURE 4.11: A30 I50 Fix Load-Displacement

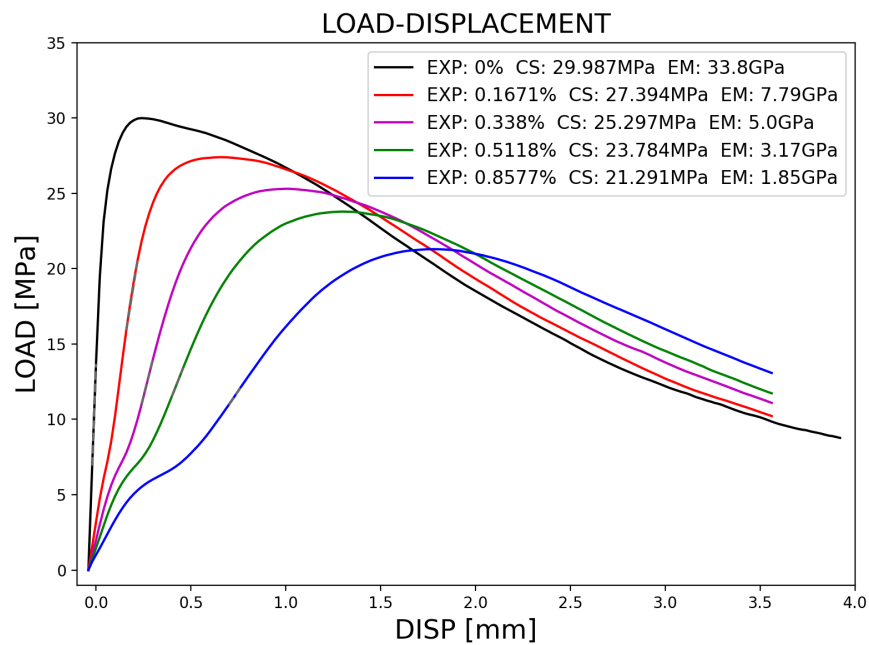


FIGURE 4.12: A30 I75 Fix Load-Displacement

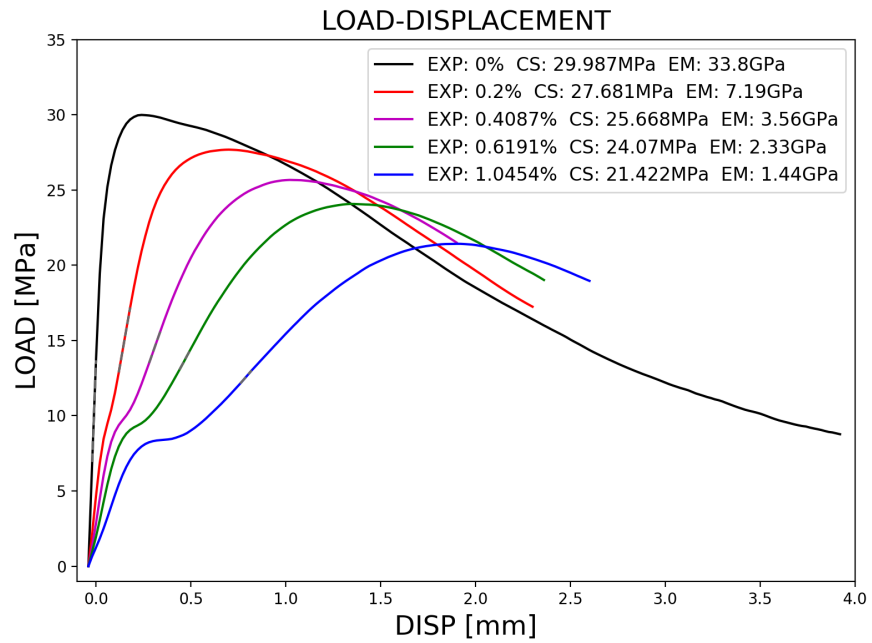


FIGURE 4.13: A15 I50 Fix Load-Displacement

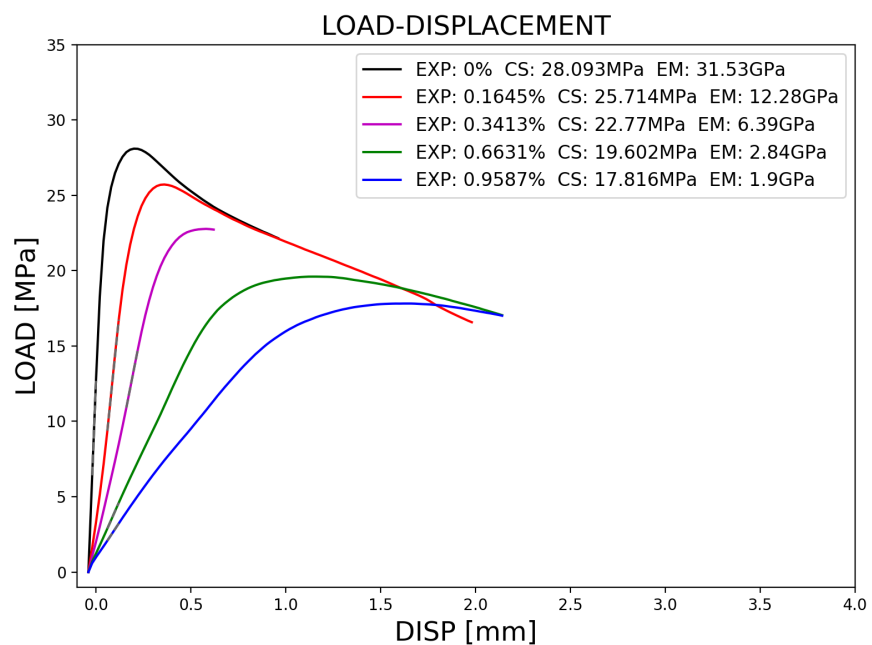


FIGURE 4.14: A15 I50 Fix Load-Displacement

4.3.1 Result And Discussion

In this section, the relationship between concrete's behavior of expansion and its losses on mechanical properties are discussed.

By RBSM, all information of the 3-dimensional cracking behavior can be recorded and analysis numerically. While it is with difficulties to summarized the behavior of expansion by the naked eye, all stress distribution and crack generation process are able to be analyzed numerically.

For example, in Figure 4.15, the relationship of total cracked interfaces and its relationship with residual compressive strength (in a ratio of the compressive strength of undamaged model) is presented.

It can be seen that as the total cracking interfaces number increase, the residual compressive strength decrease in all kinds of expansion applied.

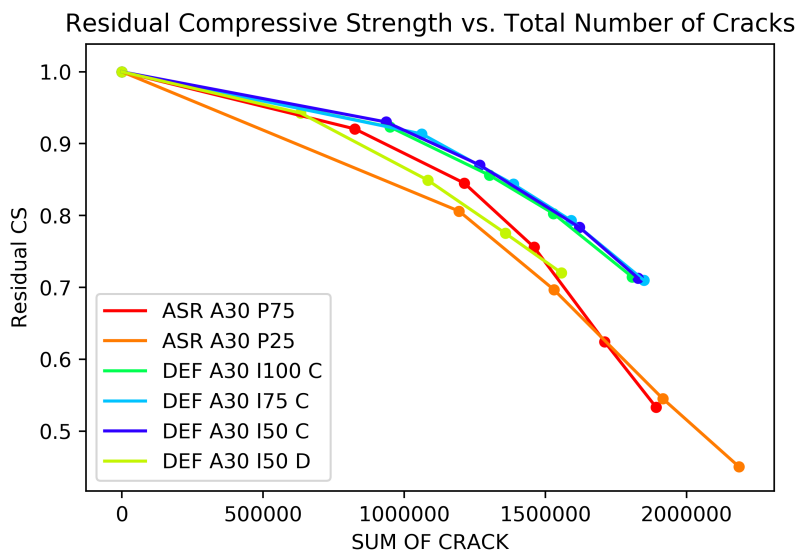


FIGURE 4.15: Residual Compressive Strength vs. Total Number of Cracks

While structually, larger crack in width do represent larger damage, especially in its mechanical properties, here in Figure 4.16 the relationship between total number of cracked interfaces larger than 0.0005mm and the residual compressive strength is plotted.

This time clear linear relationship between the number of cracks larger than 0.0005mm and the reducing in its compressive strength can be seen here, both in ASR expansion and DEF expansion.

This result implied that while the expansion mechanism and cracking pattern can be different in ASR and DEF expansion, the residual mechanical properties, for example,

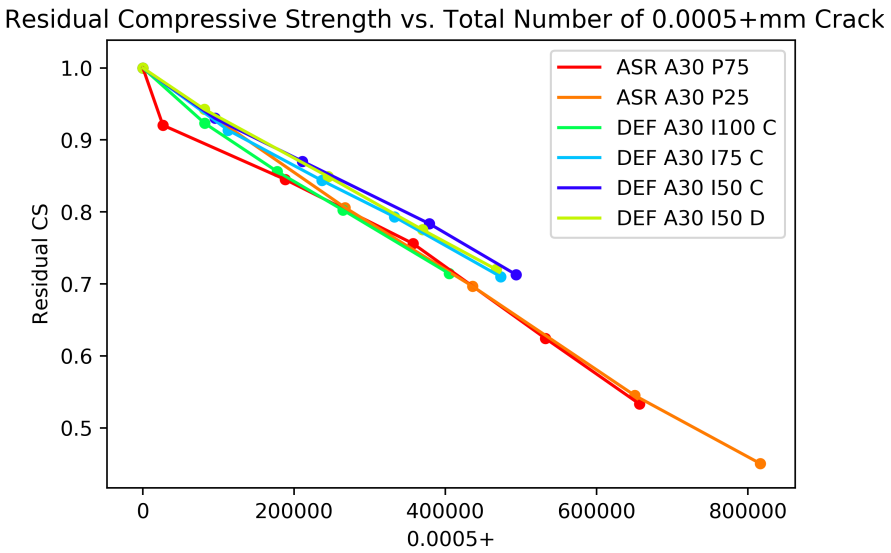


FIGURE 4.16: Residual Compressive Strength vs. Total Number of Cracks over 0.0005mm

the compressive strength, is determined by the existence of larger cracks (0.0005mm+ here). This may offer us a new direction in the analysis the residual capacity of the expanded concrete structure.

Case	Final Expansion	Number of cracked face over 0.0005mm	Residual Compressive Strength
ASR A30P75 Case 3	0.4223	357498	0.7559
DEF A30I50 Case 3	0.5795	379069	0.7835
ASR A30I75 Case 3	0.5118	332827	0.7931

TABLE 4.2: One Dimensional Expansion Ratio in Single ASR Model Simulation

4.4 Residual Capabilities after Combination of ASR and DEF Expansion

4.5 Conclusion

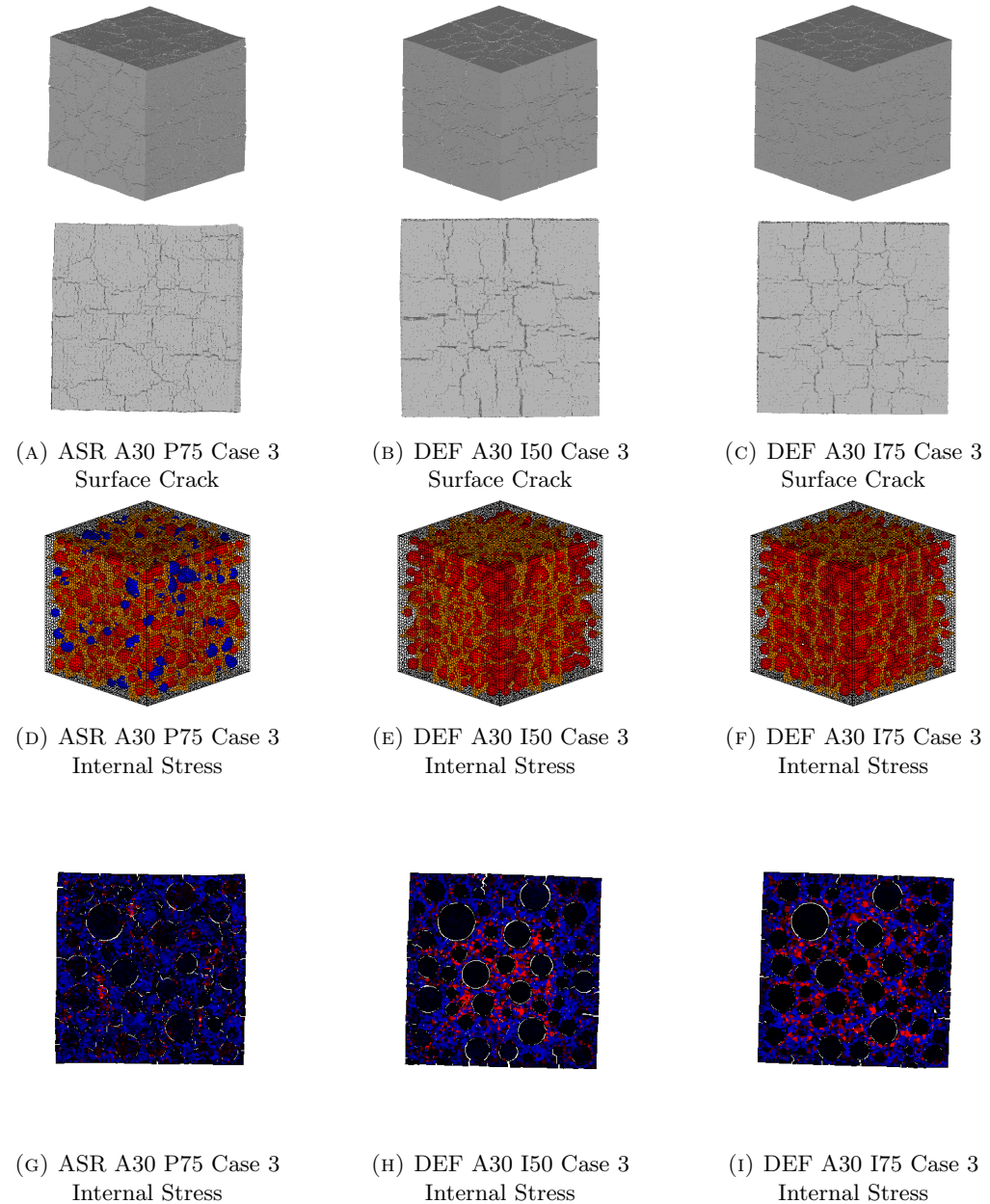


FIGURE 4.17: Cracking Pattern Compare

Chapter 5

Summary and Conclusions

Appendix A

ASR-A30-P25

Expansion [%]	0- 0.0001mm	0.0001- 0.001mm	0.001- 0.01mm	0.01- 0.1mm	0.1+mm	Sum
0.1651	537971	525011	130908	196	0	1194086
0.3606	608649	674893	239765	6584	0	1529891
0.7024	679994	832452	371687	31863	0	1915996
1.0201	723062	928882	457810	75617	0	2185371

TABLE A.1: Number of Cracked Faces in Different Crack Width

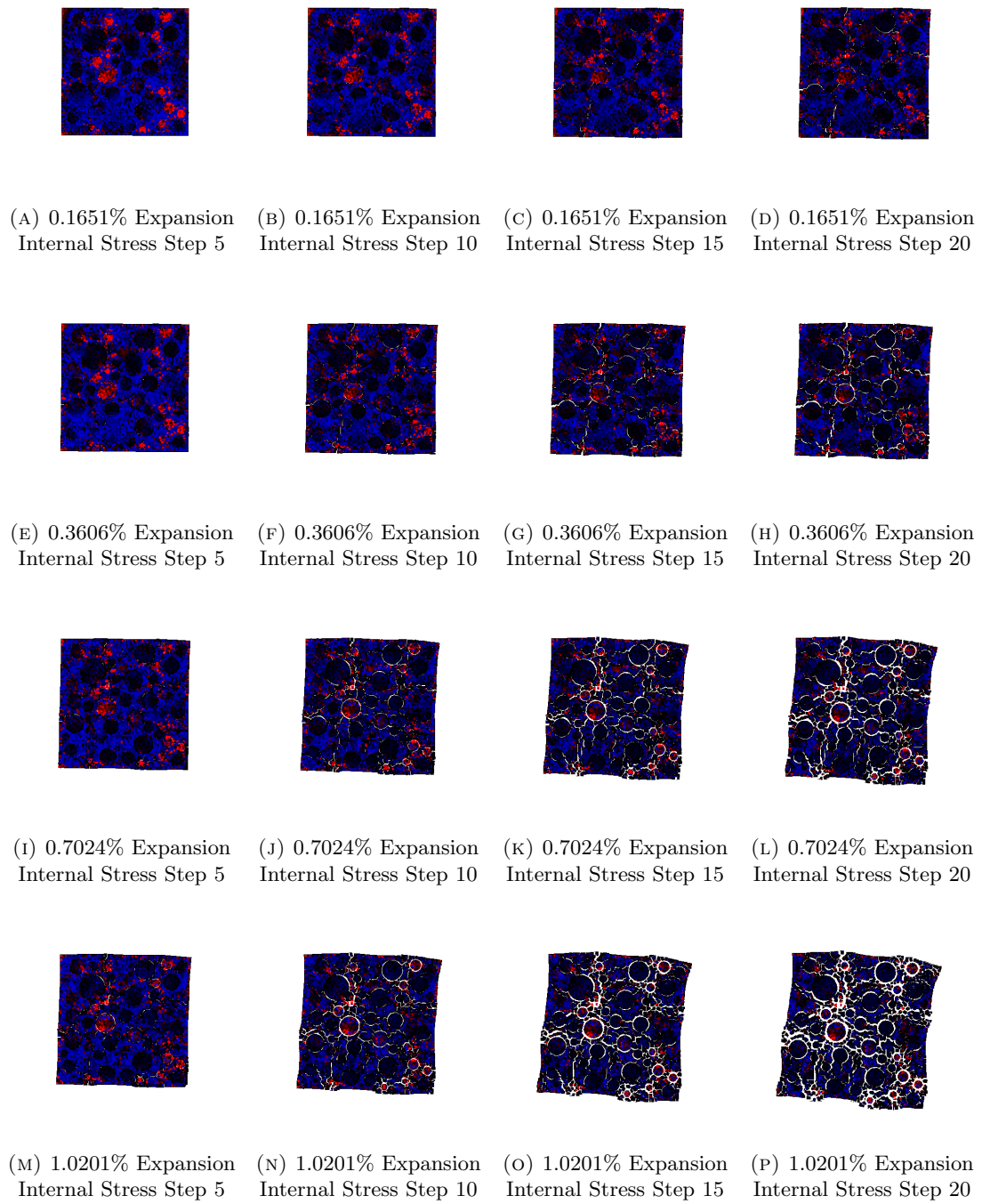


FIGURE A.1: Generation of Internal Stress for Expansion to Step 20(Final Expansion Step)

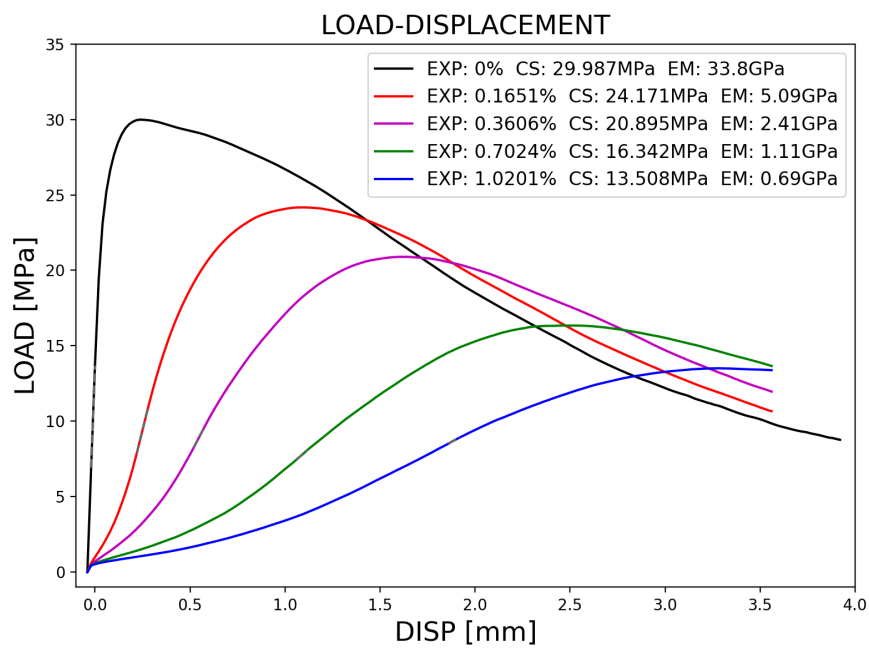


FIGURE A.2: LOAD-DISPLACEMENT(Fix Boundary Condition)

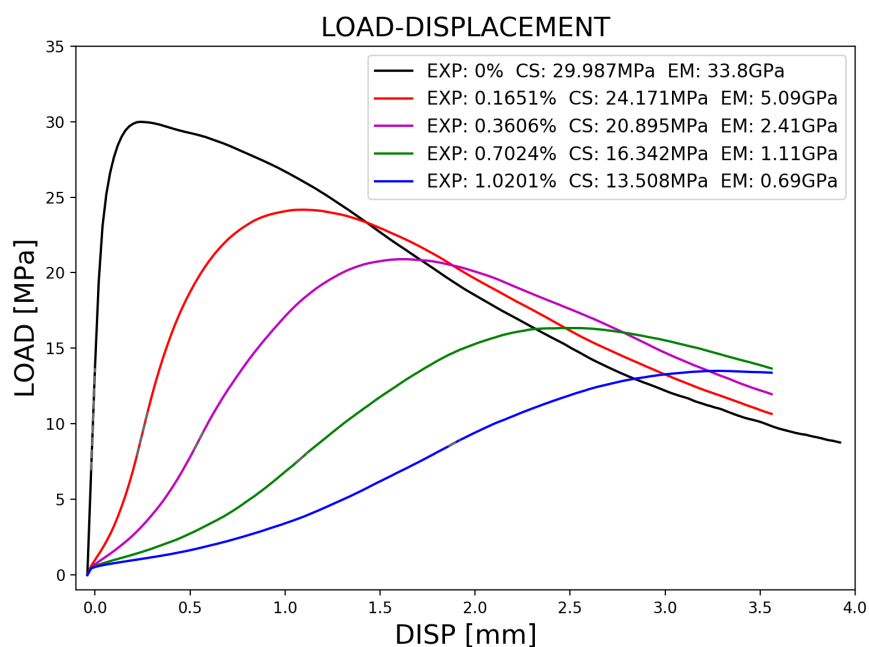


FIGURE A.3: LOAD-DISPLACEMENT(Fix Boundary Condition)

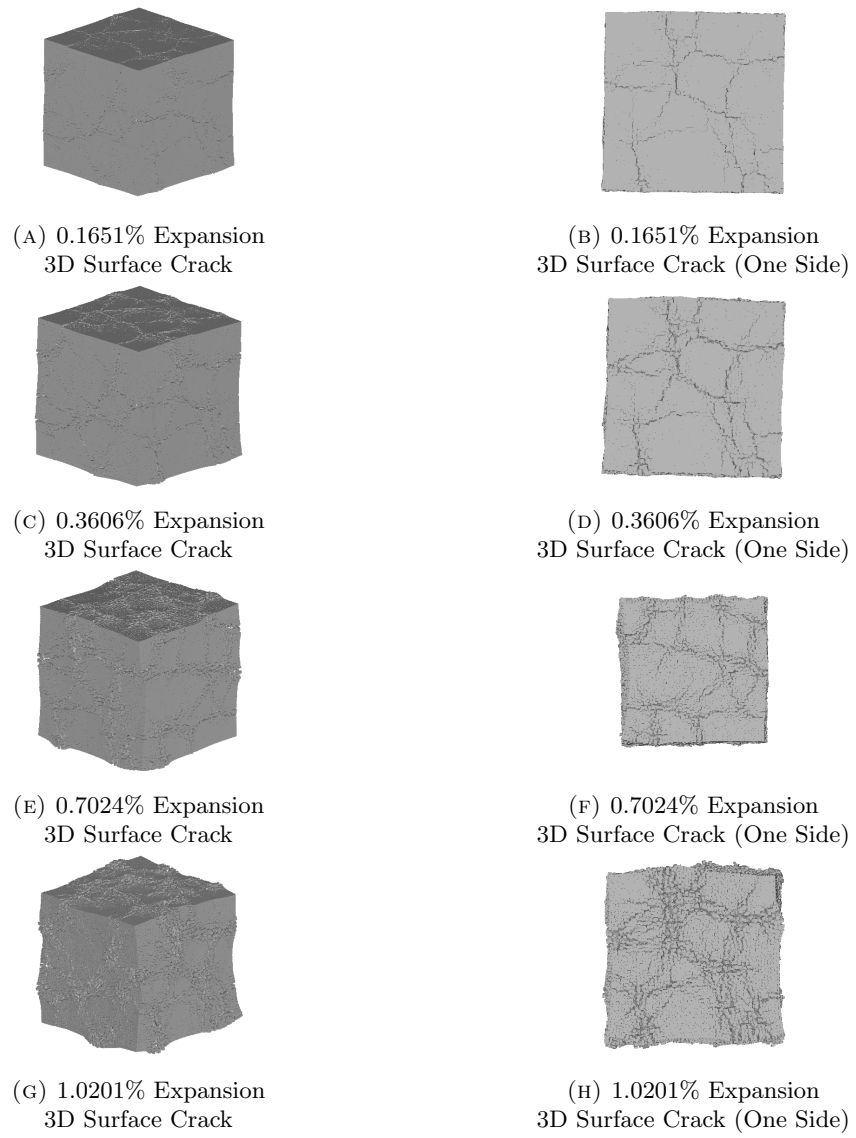


FIGURE A.4: 3D Surface Cracking Pattern

Appendix B

ASR-A30-P75

Expansion [%]	0- 0.0001mm	0.0001- 0.001mm	0.001- 0.01mm	0.01- 0.1mm	0.1+mm	Sum
0.0699	512896	310203	2118	0	0	825217
0.1936	579249	570671	62649	0	0	1212569
0.4223	603448	681853	173985	275	0	1459561
0.8832	629798	771779	299364	8393	0	1709334
1.3224	652189	833253	376456	29725	0	1891623

TABLE B.1: Number of Cracked Faces in Different Crack Width

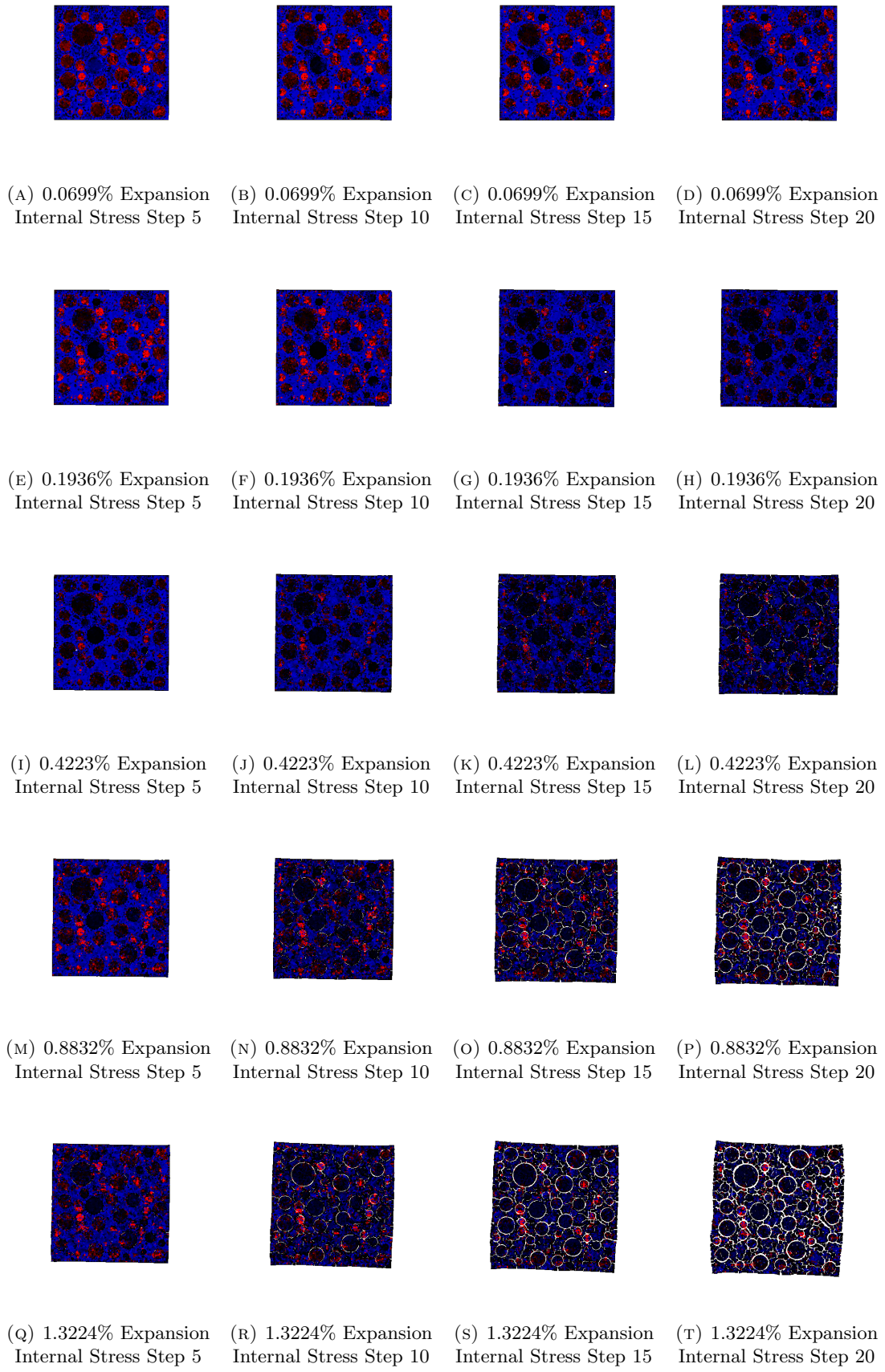


FIGURE B.1: Generation of Internal Stress for Expansion to Step 20(Final Expansion Step)

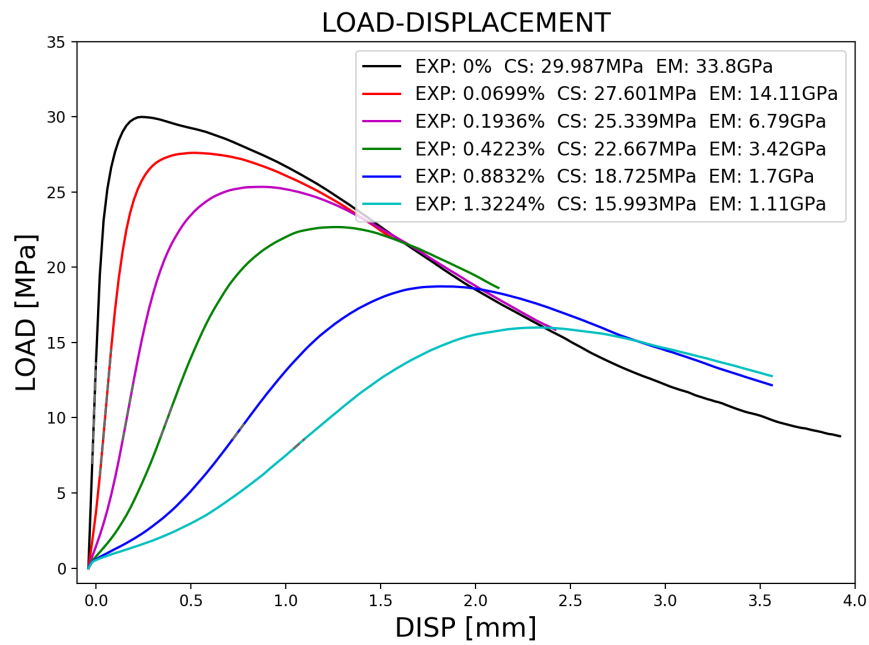


FIGURE B.2: LOAD-DISPLACEMENT(Fix Boundary Condition)

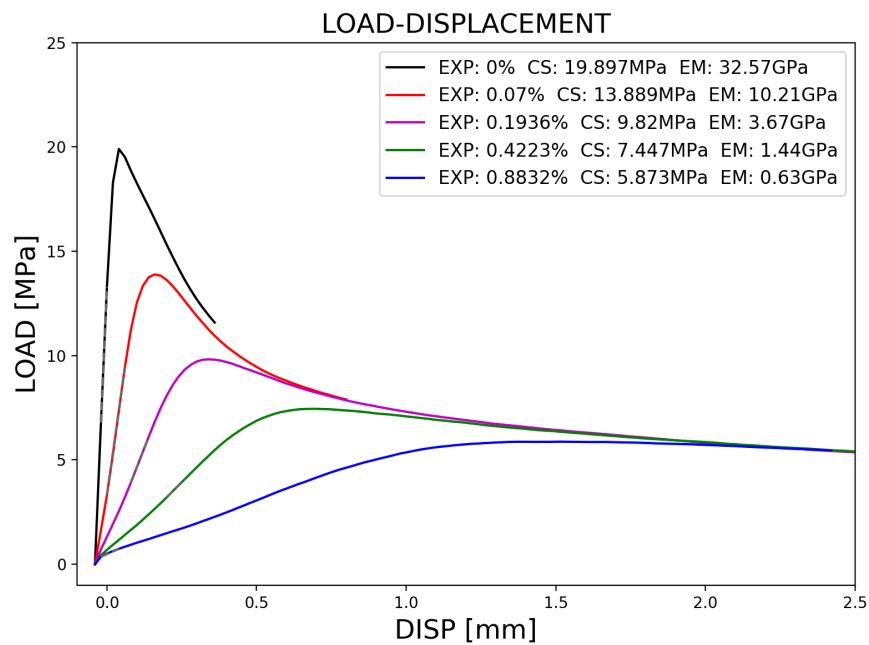


FIGURE B.3: LOAD-DISPLACEMENT(Free Boundary Condition)

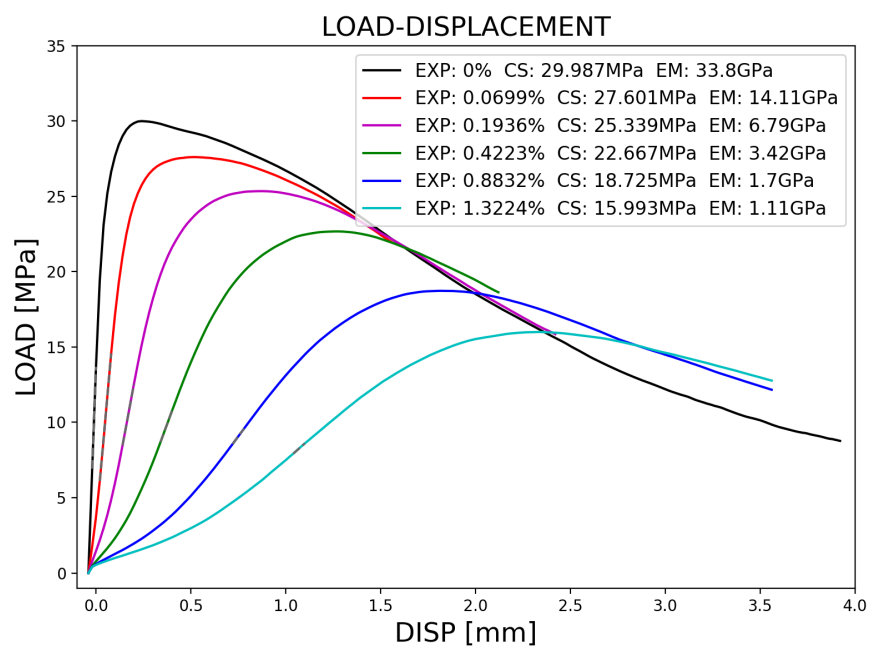


FIGURE B.4: LOAD-DISPLACEMENT(Fix Boundary Condition)

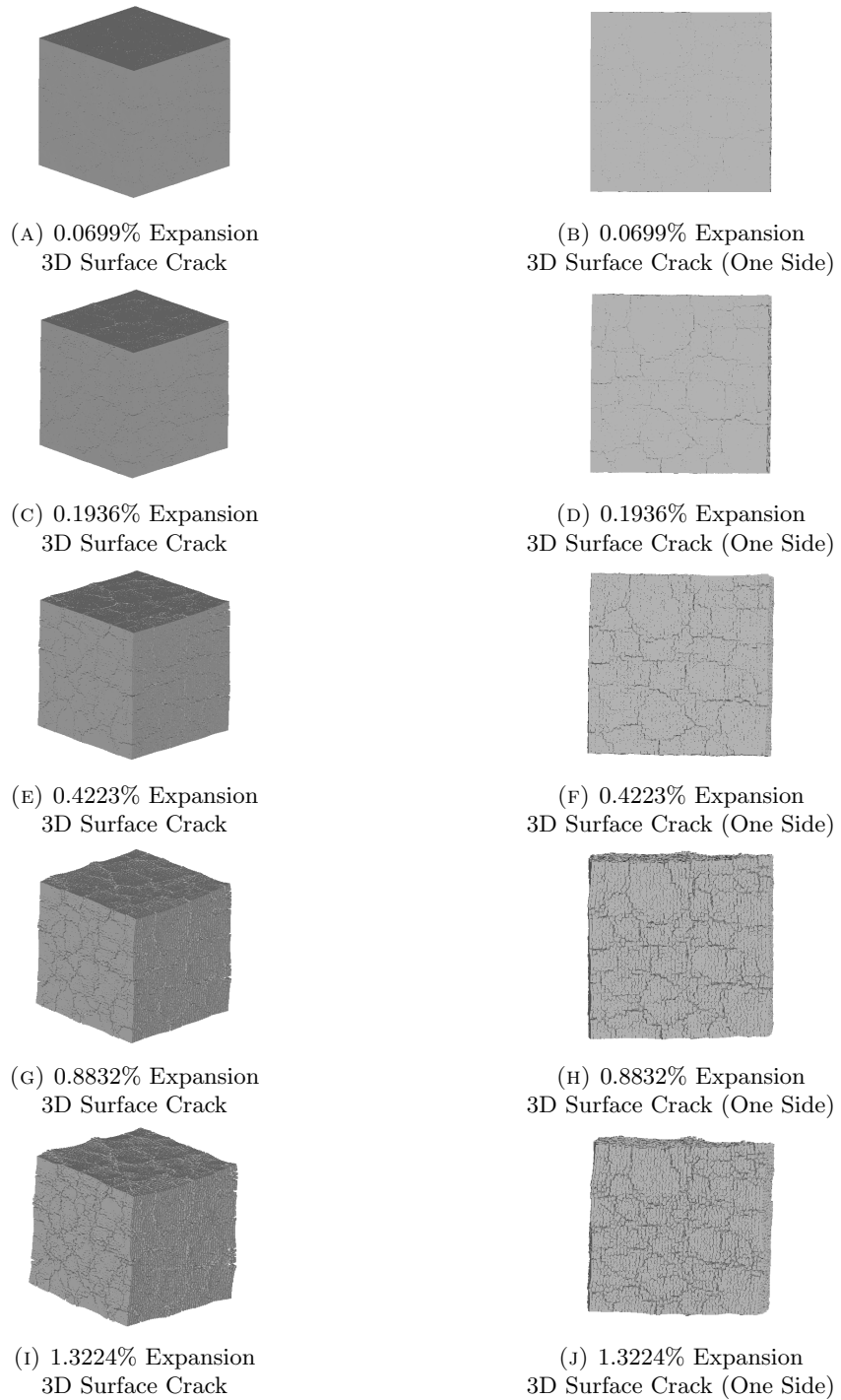


FIGURE B.5: 3D Surface Cracking Pattern

Appendix C

ASR-A15-P75

Expansion [%]	0- 0.0001mm	0.0001- 0.001mm	0.001- 0.01mm	0.01- 0.1mm	0.1+mm	Sum
0.0699	528243	254227	1498	0	0	783968
0.1364	640053	529840	57764	0	0	1227657
0.3051	667144	646747	163733	696	0	1478320
0.6290	706276	761149	280510	14006	0	1761941
0.9243	740875	850004	360338	37280	0	1988497

TABLE C.1: Number of Cracked Faces in Different Crack Width

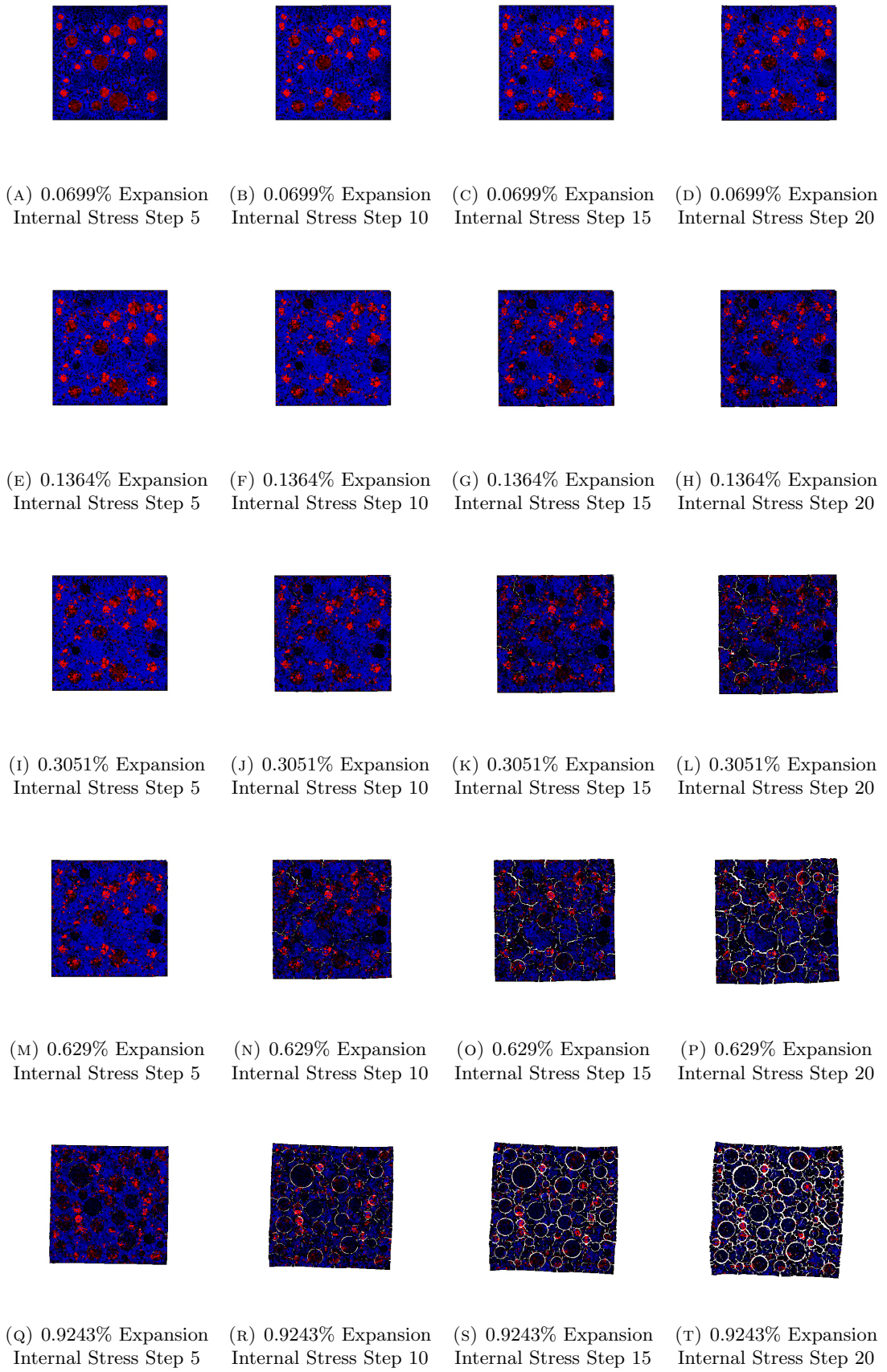


FIGURE C.1: Generation of Internal Stress for Expansion to Step 20(Final Expansion Step)

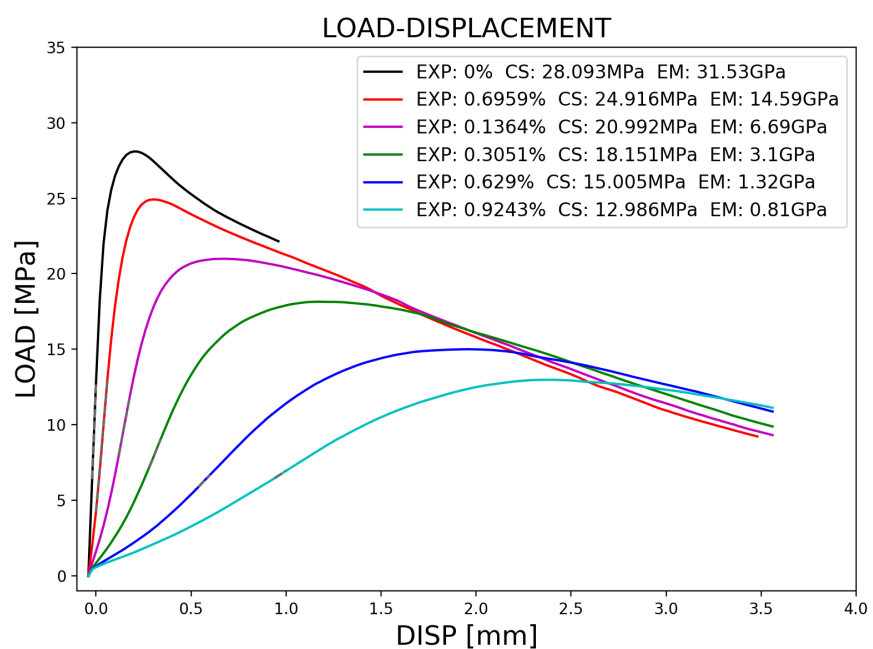


FIGURE C.2: LOAD-DISPLACEMENT(Fix Boundary Condition)

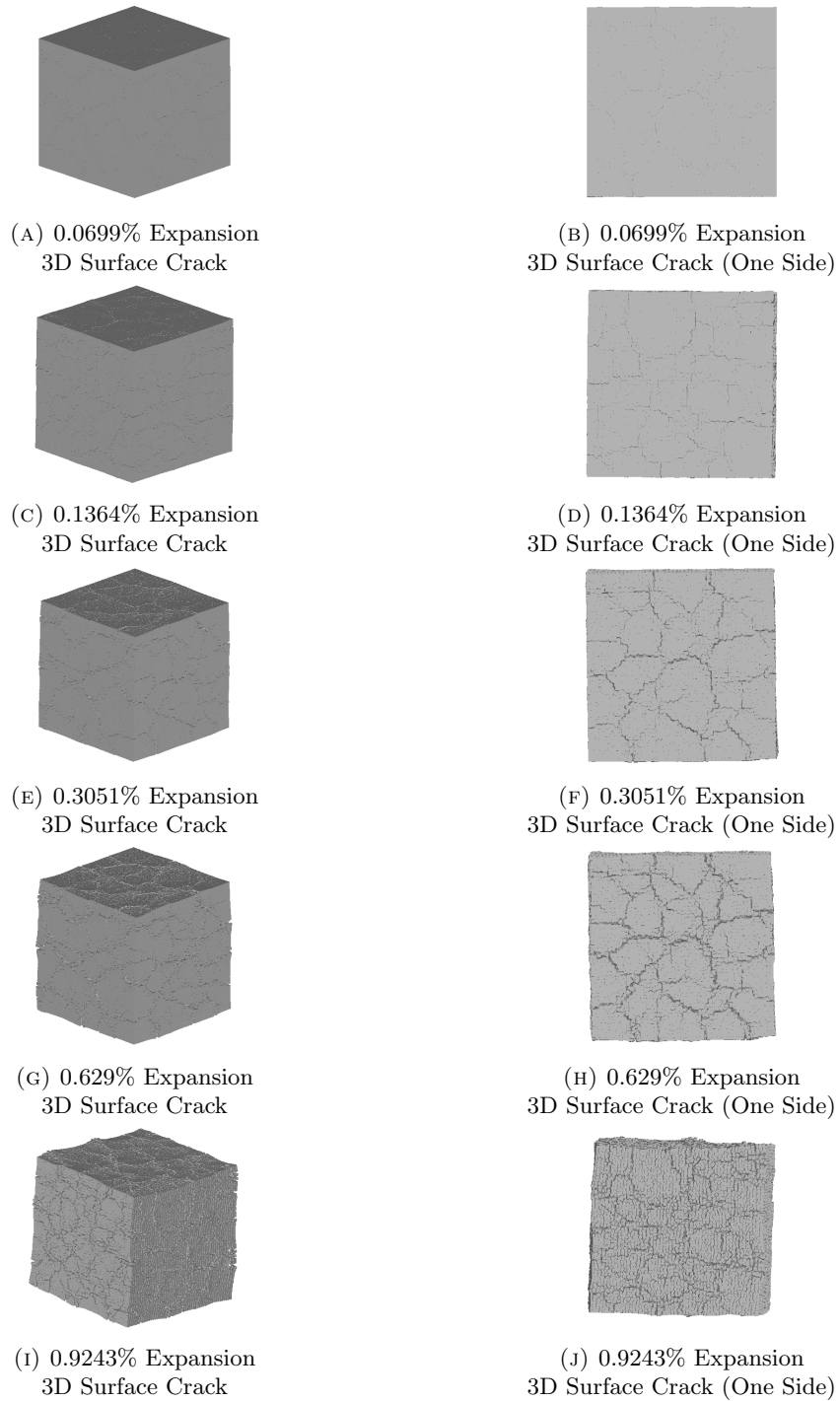


FIGURE C.3: 3D Surface Cracking Pattern

Appendix D

DEF-A30-X-1C

Expansion [%]	0- 0.0001mm	0.0001- 0.001mm	0.001- 0.01mm	0.01- 0.1mm	0.1+mm	Sum
0.2	546880	374968	27843	0	0	949691
0.4087	667896	566941	66911	0	0	1301748
0.6191	716595	704857	106738	0	0	1528190
1.0454	758236	854387	192851	1909	0	1807383

TABLE D.1: Number of Cracked Faces in Different Crack Width

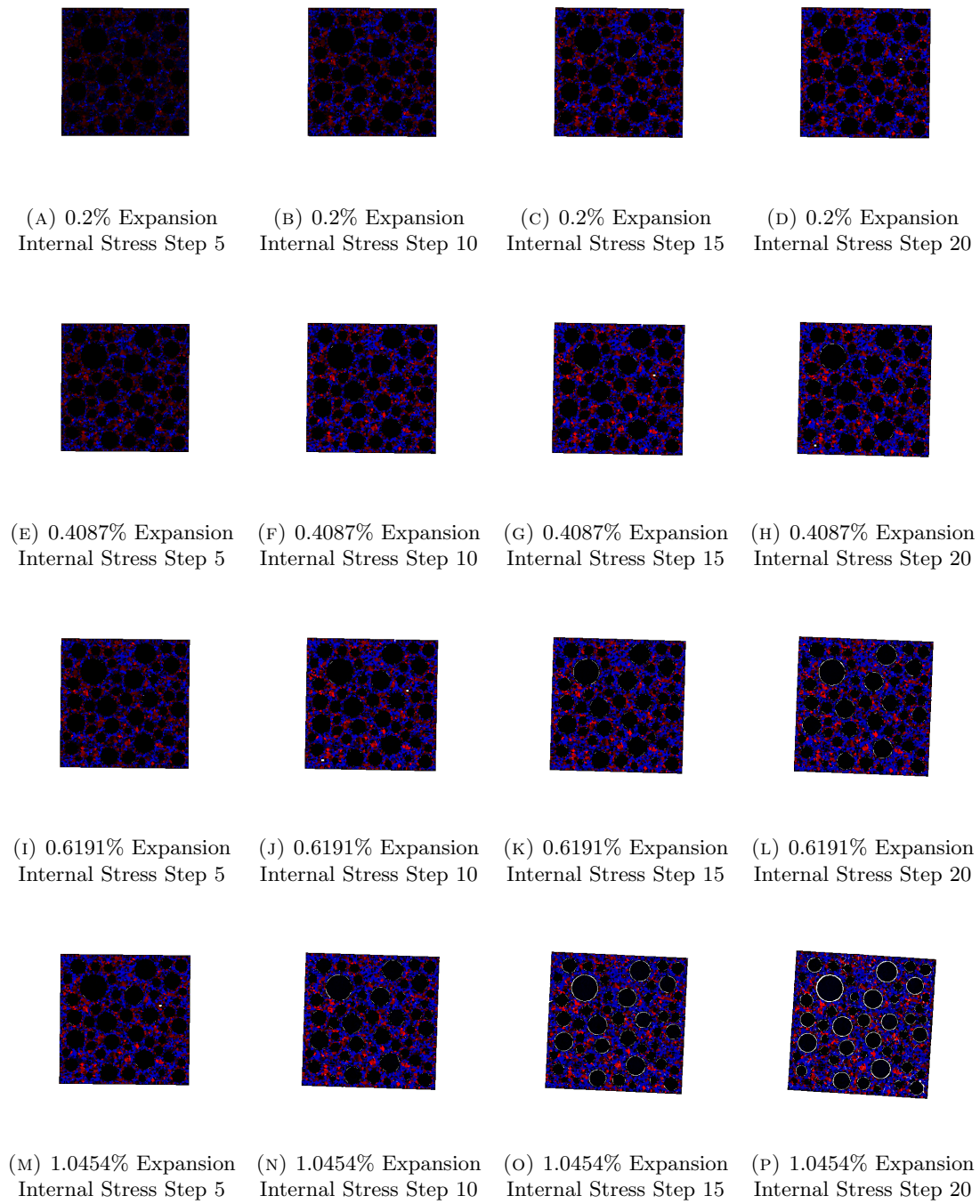


FIGURE D.1: Generation of Internal Stress for Expansion to Step 20(Final Expansion Step)

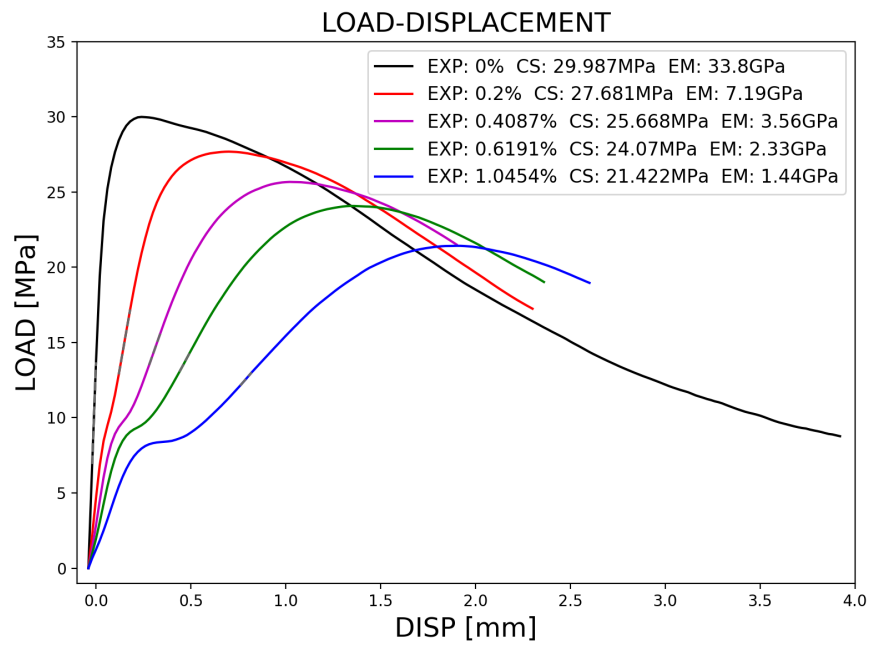


FIGURE D.2: LOAD-DISPLACEMENT(Fix Boundary Condition)

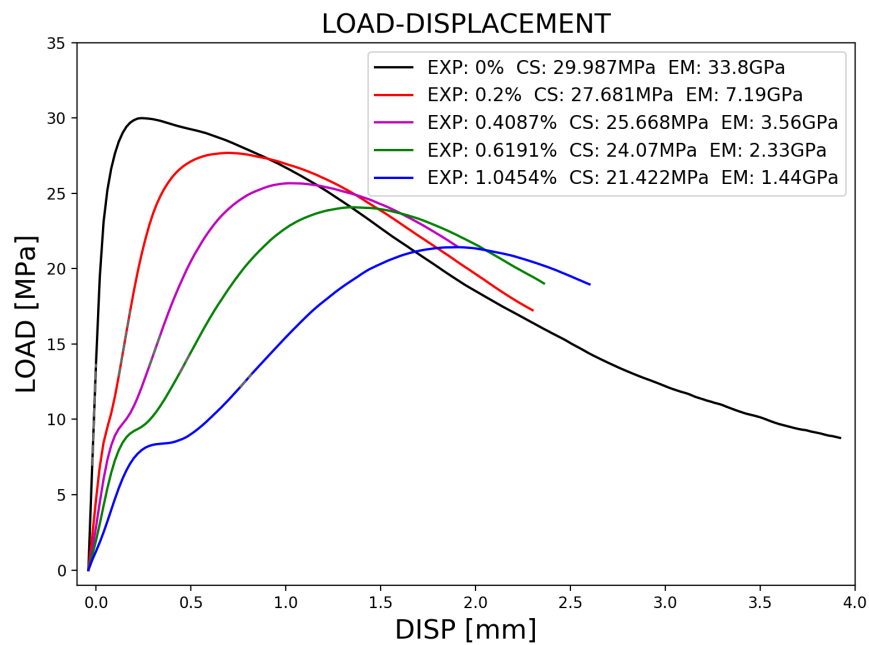


FIGURE D.3: LOAD-DISPLACEMENT(Fix Boundary Condition)

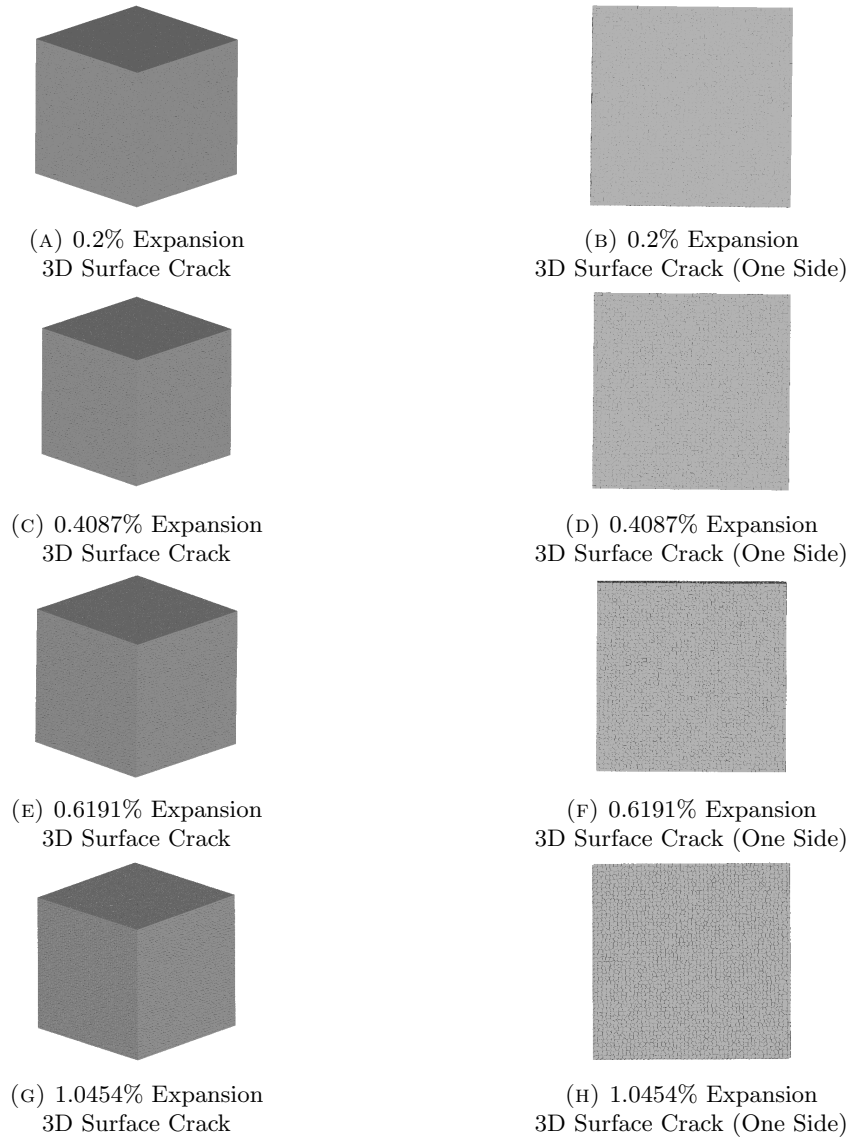


FIGURE D.4: 3D Surface Cracking Pattern

Appendix E

DEF-A30-X-5C

Expansion [%]	0- 0.0001mm	0.0001- 0.001mm	0.001- 0.01mm	0.01- 0.1mm	0.1+mm	Sum
0.1671	586017	439450	36561	0	0	1062028
0.3380	670005	616246	99949	5	0	1386205
0.5118	708833	725962	155557	240	0	1590592
0.8577	746251	853144	245537	3458	0	1848390

TABLE E.1: Number of Cracked Faces in Different Crack Width

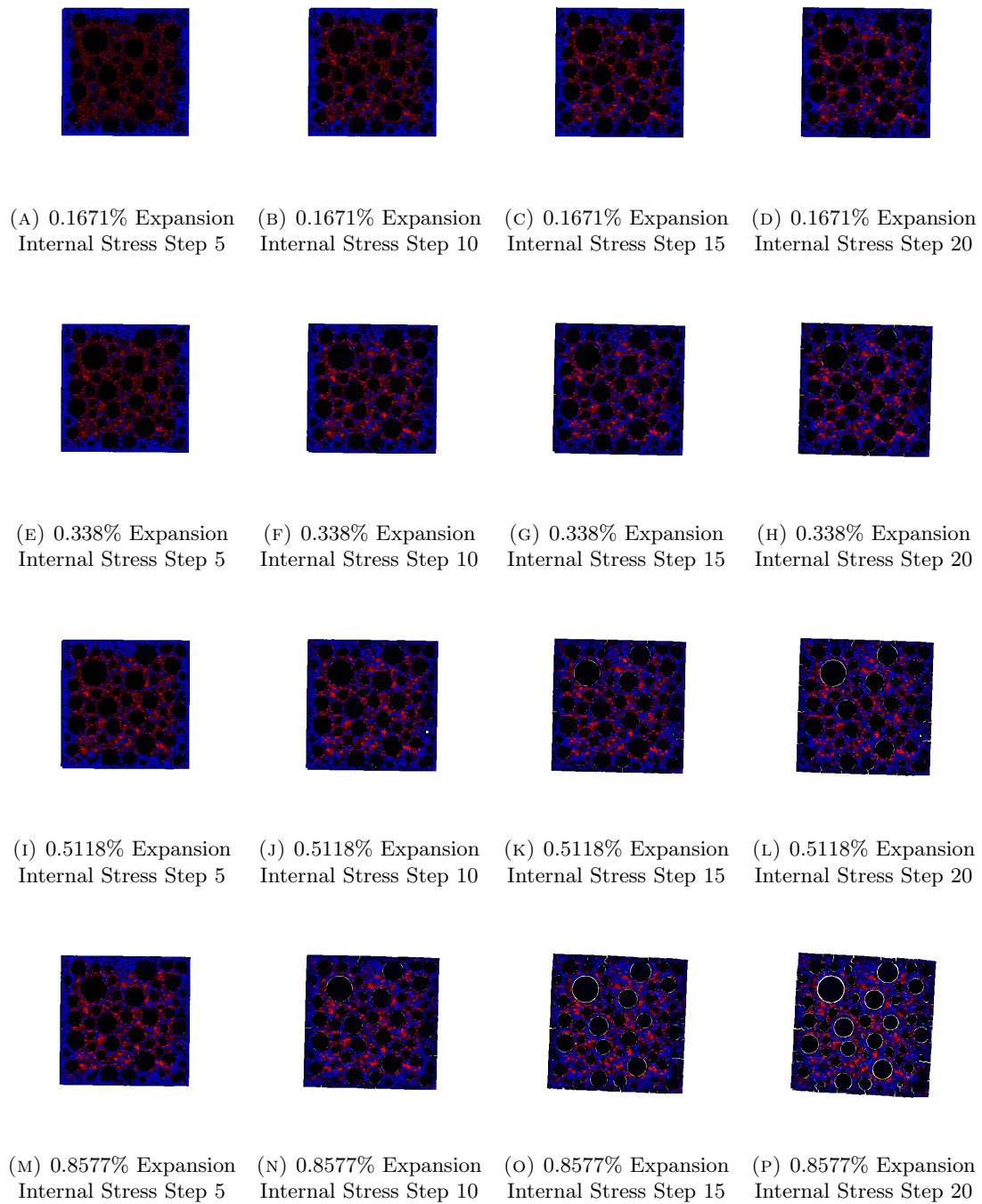


FIGURE E.1: Generation of Internal Stress for Expansion to Step 20(Final Expansion Step)

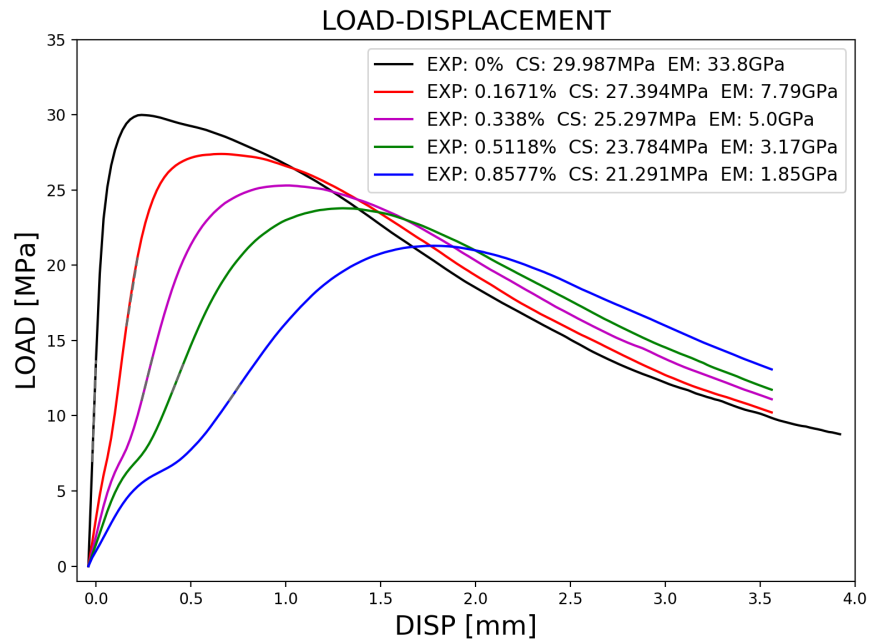


FIGURE E.2: LOAD-DISPLACEMENT(Fix Boundary Condition)

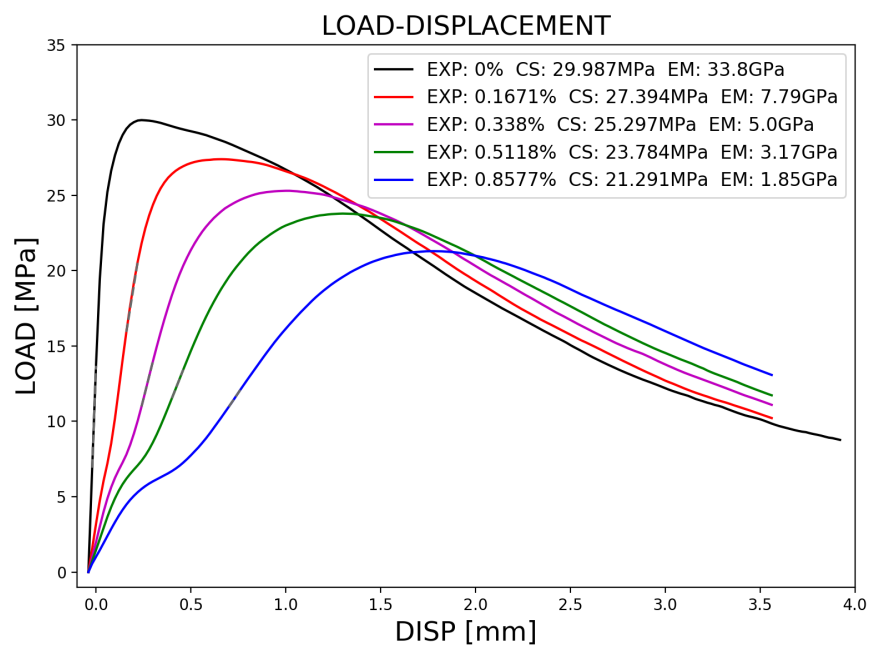


FIGURE E.3: LOAD-DISPLACEMENT(Fix Boundary Condition)

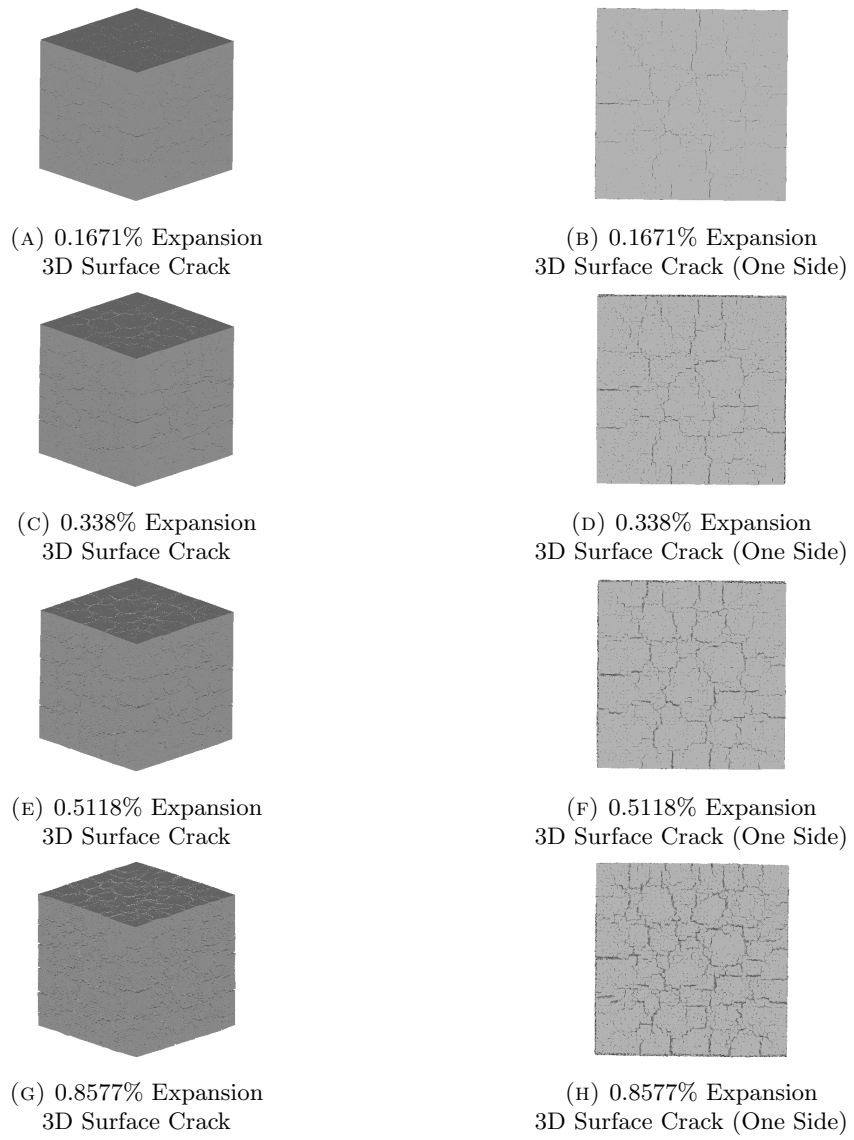


FIGURE E.4: 3D Surface Cracking Pattern

Appendix F

DEF-A30-X0C

Expansion [%]	0- 0.0001mm	0.0001- 0.001mm	0.001- 0.01mm	0.01- 0.1mm	0.1+mm	Sum
0.1379	537891	365522	32007	0	0	935420
0.2873	627417	549242	90200	151	0	1267010
0.5795	696009	731565	191275	1736	0	1620585
0.8789	728259	829503	262231	8098	0	1828091

TABLE F.1: Number of Cracked Faces in Different Crack Width

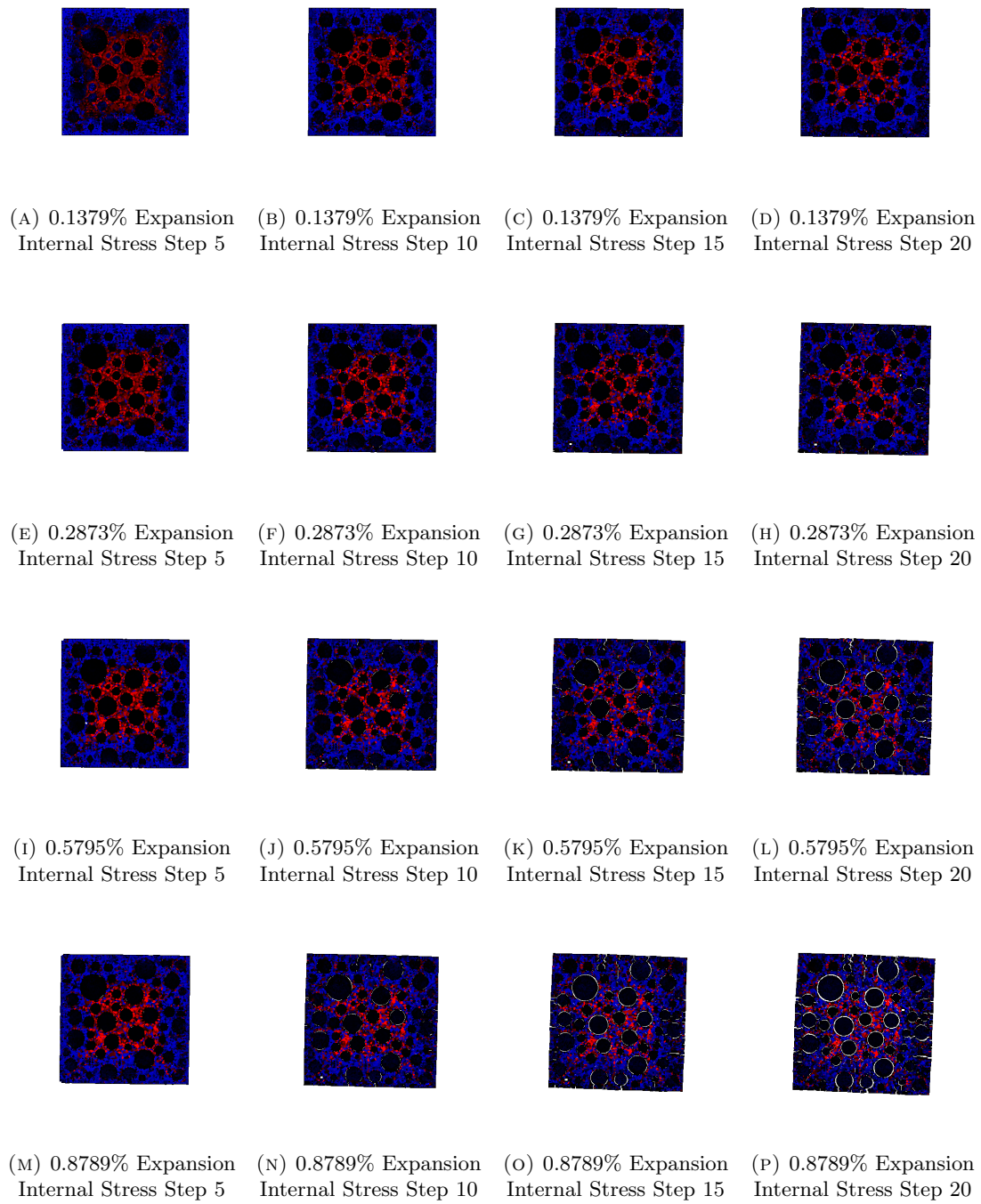


FIGURE F.1: Generation of Internal Stress for Expansion to Step 20(Final Expansion Step)

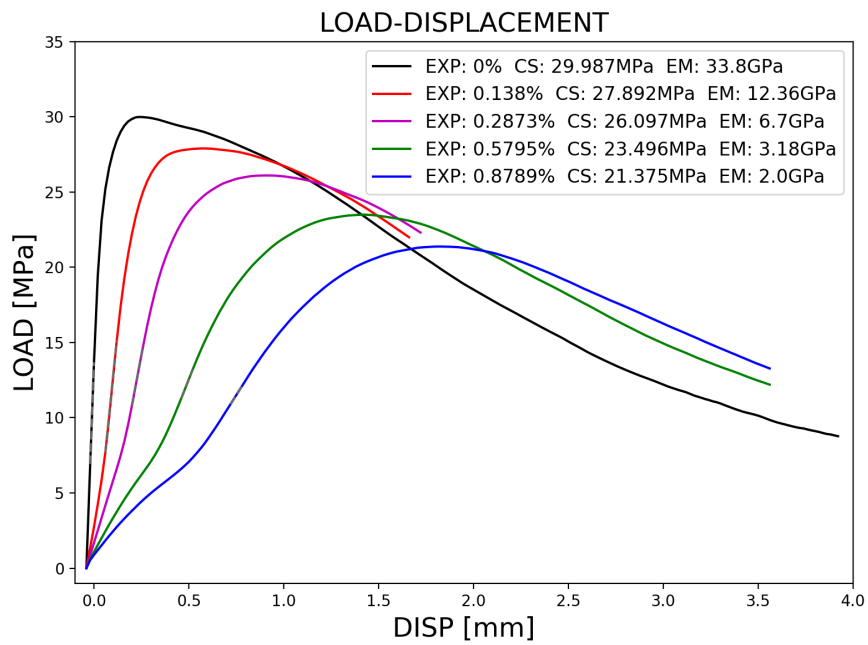


FIGURE F.2: LOAD-DISPLACEMENT(Fix Boundary Condition)

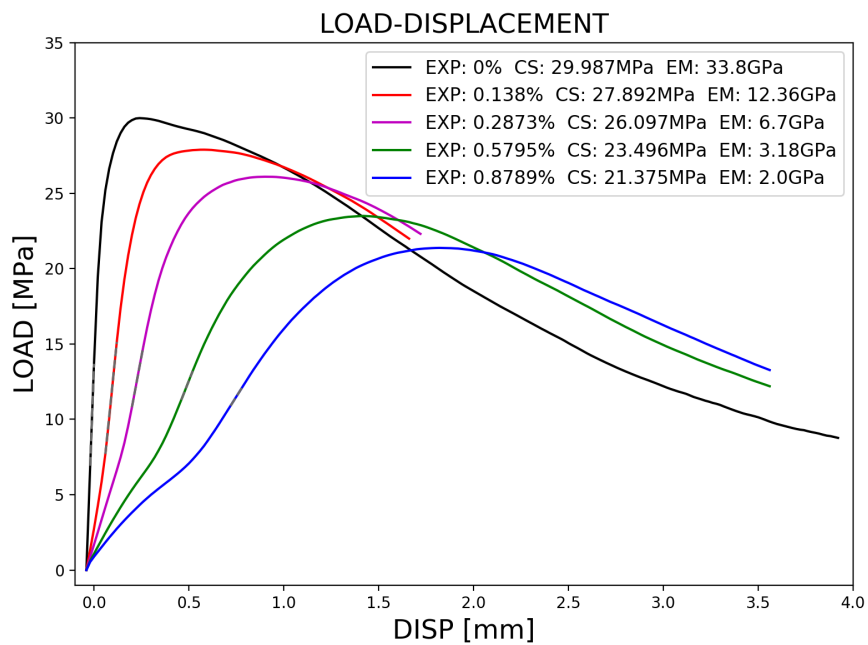


FIGURE F.3: LOAD-DISPLACEMENT(Fix Boundary Condition)

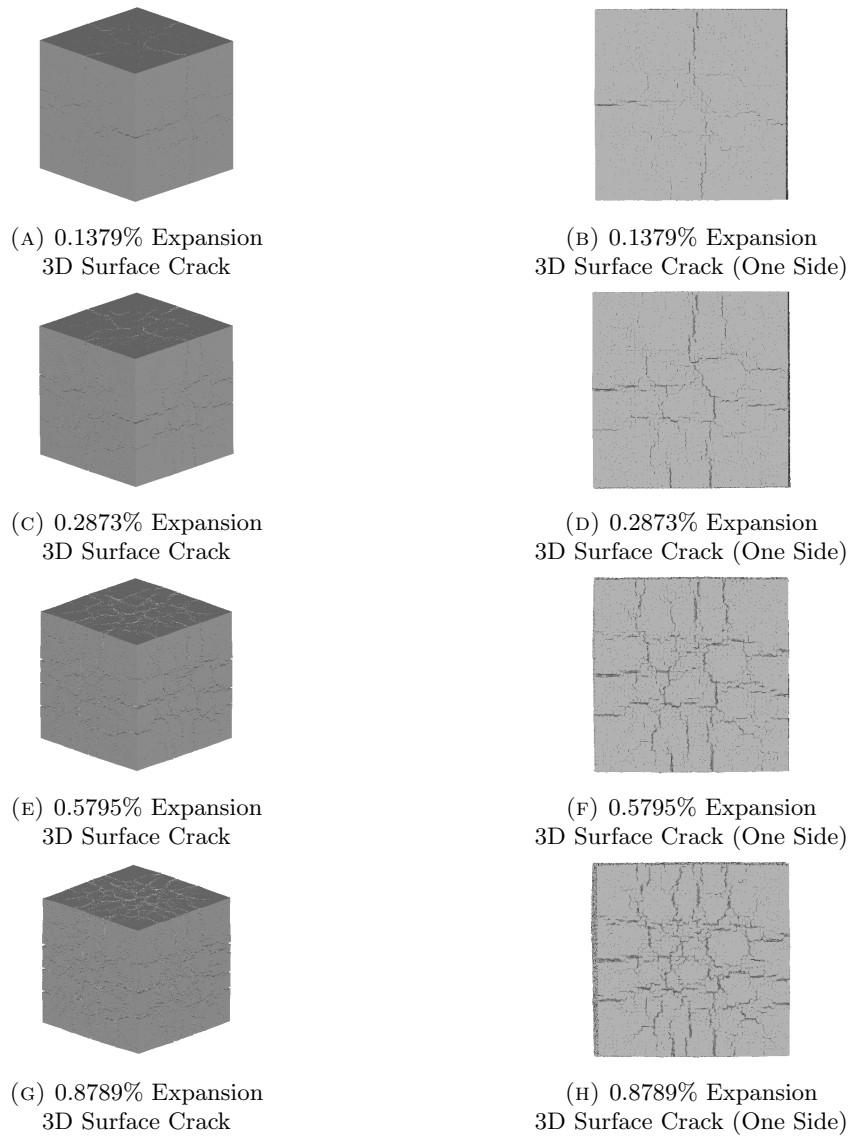


FIGURE F.4: 3D Surface Cracking Pattern

Appendix G

DEF-A30-X0D

Expansion [%]	0- 0.0001mm	0.0001- 0.001mm	0.001- 0.01mm	0.01- 0.1mm	0.1+mm	Sum
0.1175	364902	234151	33968	0	0	633022
0.3305	496948	459094	124777	2515	0	1083334
0.5335	560685	589143	200026	8188	0	1358042
0.7454	604521	677150	257933	17279	0	1556883

TABLE G.1: Number of Cracked Faces in Different Crack Width

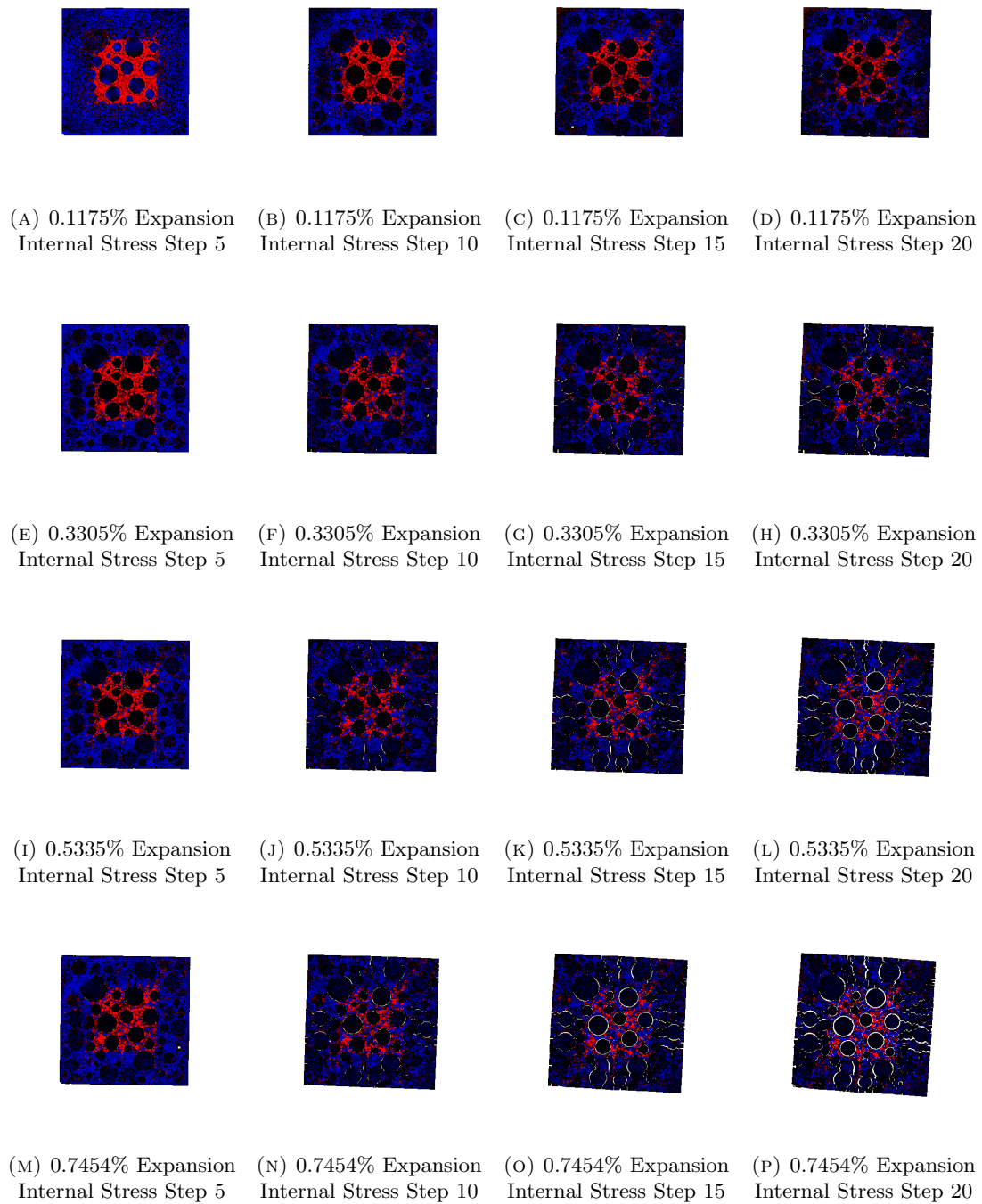


FIGURE G.1: Generation of Internal Stress for Expansion to Step 20(Final Expansion Step)

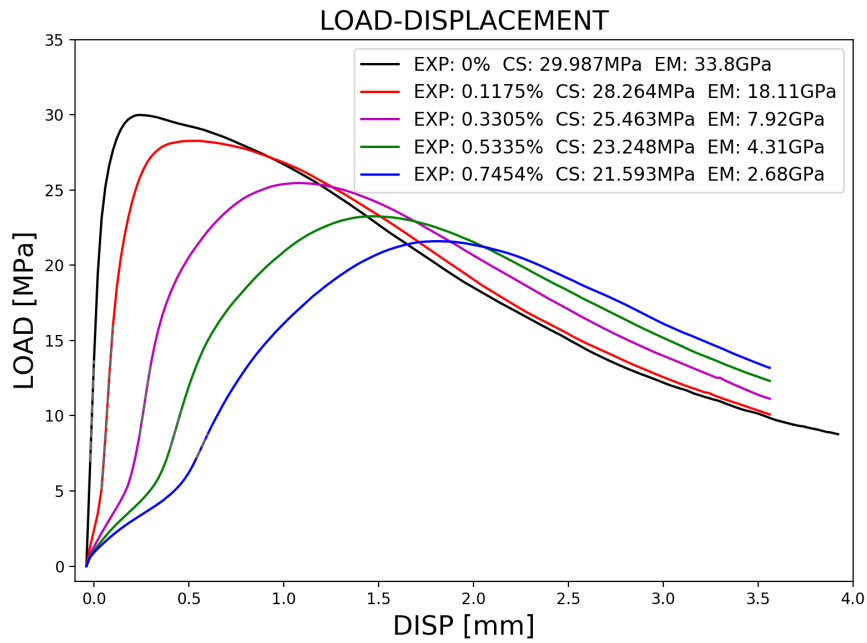


FIGURE G.2: LOAD-DISPLACEMENT(Fix Boundary Condition)

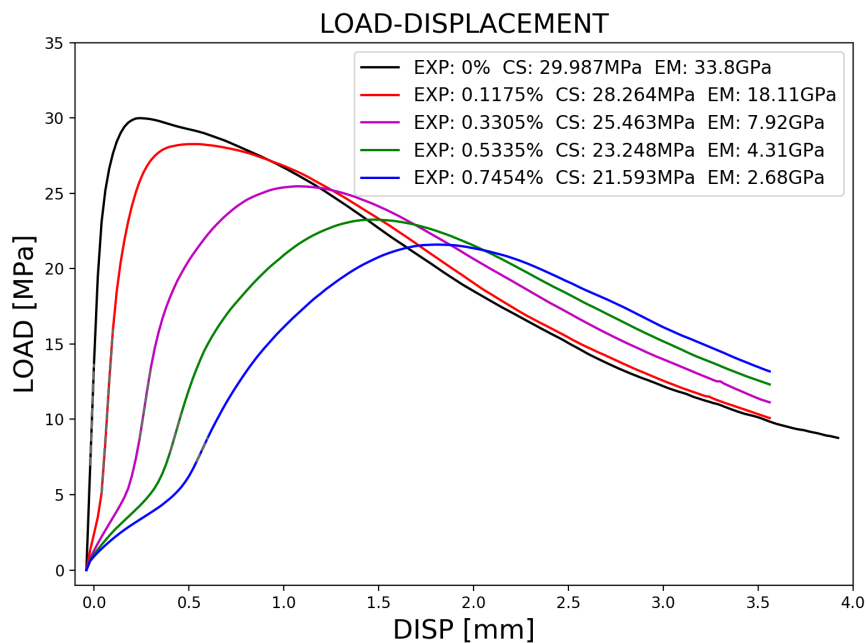


FIGURE G.3: LOAD-DISPLACEMENT(Fix Boundary Condition)

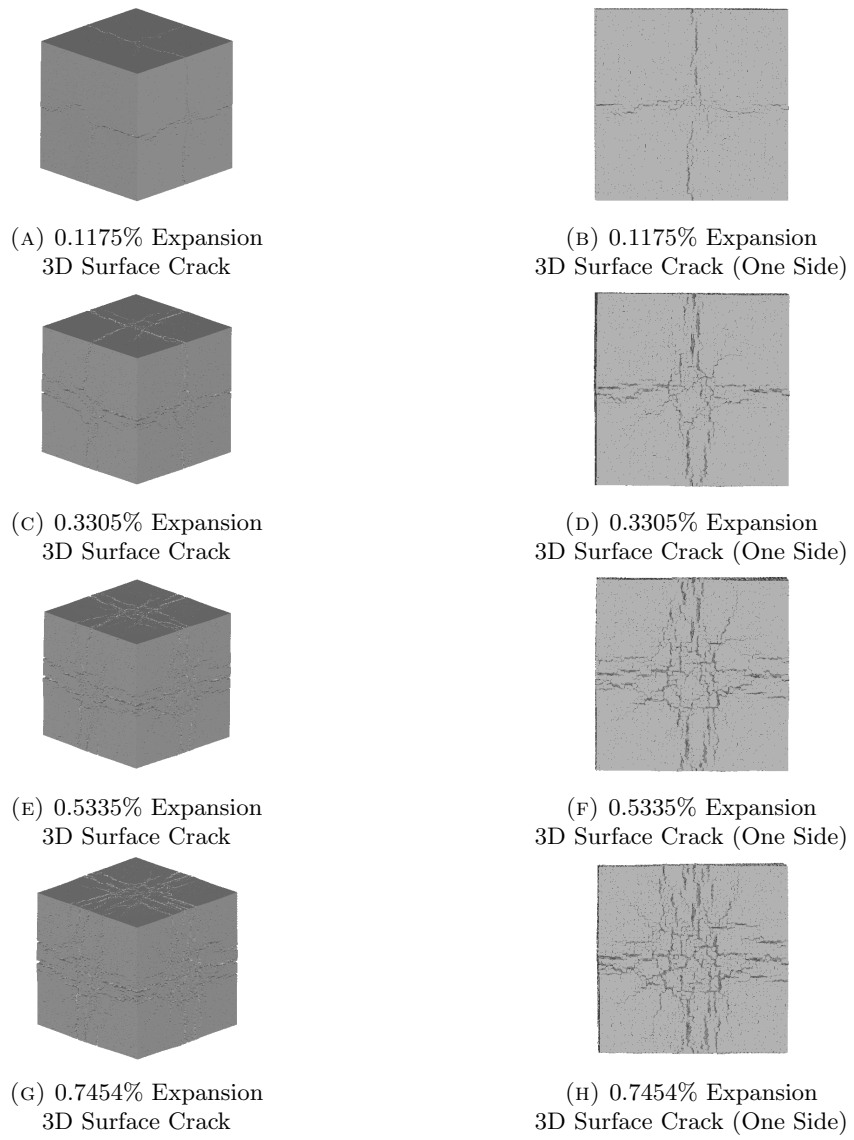


FIGURE G.4: 3D Surface Cracking Pattern

Appendix H

DEF-A15-X0C

Expansion [%]	0- 0.0001mm	0.0001- 0.001mm	0.001- 0.01mm	0.01- 0.1mm	0.1+mm	Sum
0.1645	536032	296576	29338	6	0	861952
0.3413	646687	467636	77288	639	0	1192250
0.6631	740972	678505	157160	3983	0	1580620
0.9587	787281	812412	219303	12047	0	1831043

TABLE H.1: Number of Cracked Faces in Different Crack Width

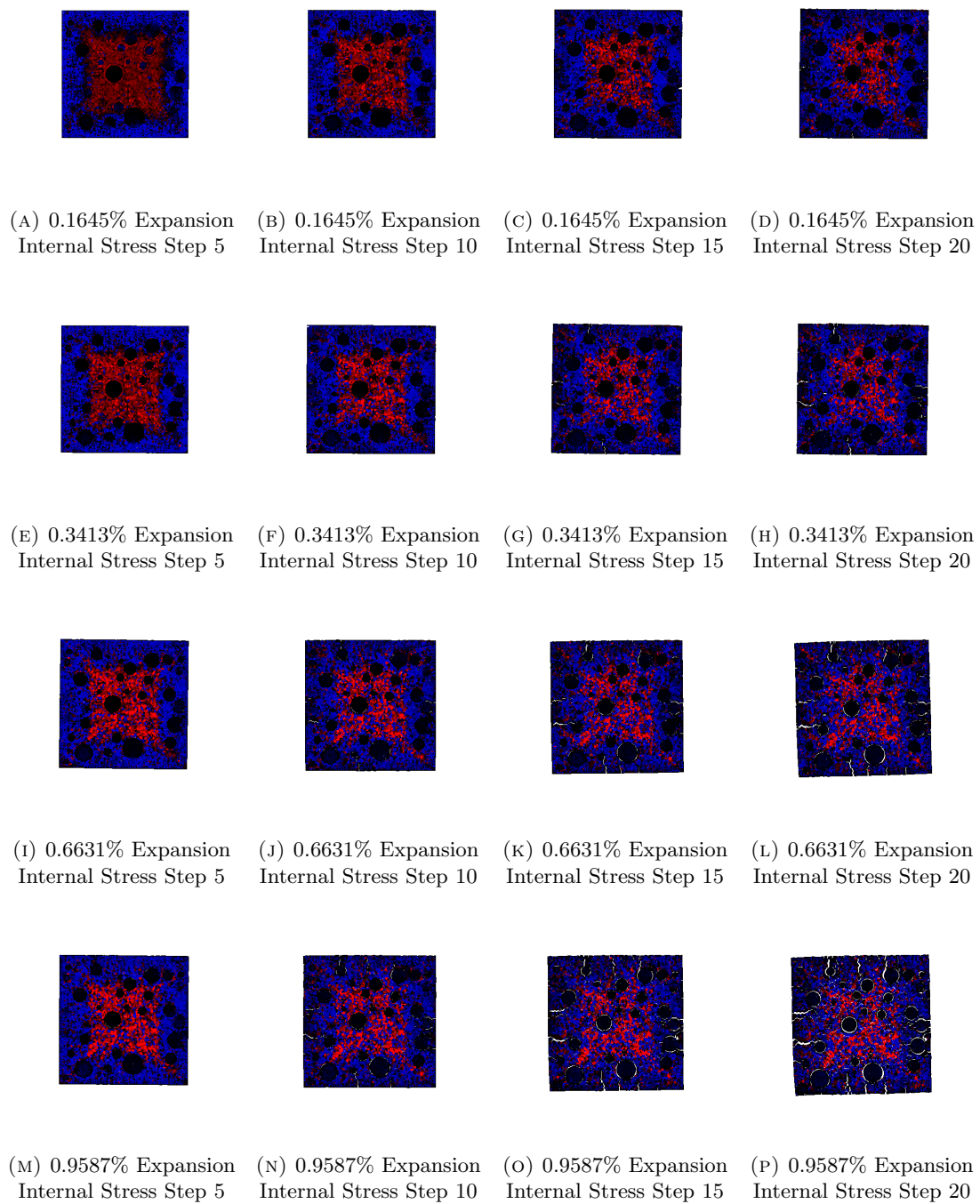


FIGURE H.1: Generation of Internal Stress for Expansion to Step 20(Final Expansion Step)

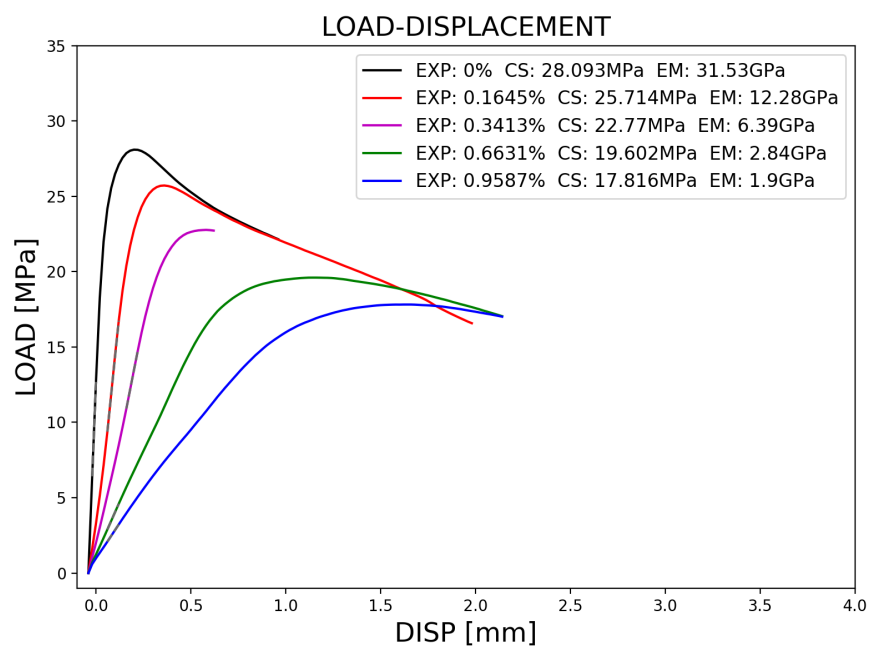


FIGURE H.2: LOAD-DISPLACEMENT(Fix Boundary Condition)